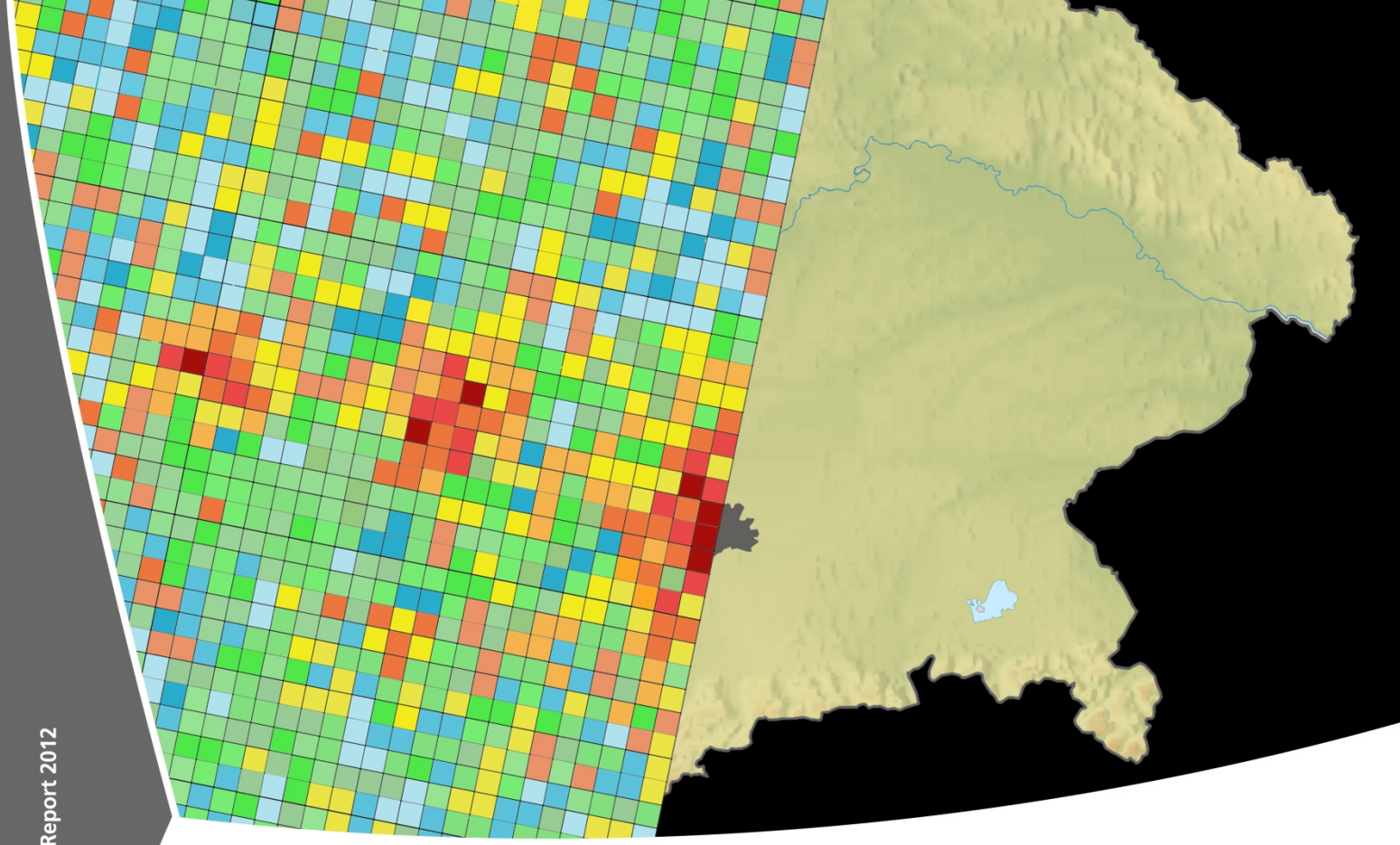

Annual Report 2012

2012 Annual Report Jahresbericht

Remote Sensing Technology Institute

Department
Atmospheric Processors

DLR

Published by **German Aerospace Center** (DLR)
A member of the Helmholtz Association

Remote Sensing Technology Institute
Institut für Methodik der Fernerkundung (MF)

Department
Atmospheric Processors (MF-ATP)

Department Head Prof. Dr. Thomas Trautmann

Editorial Team Prof. Dr. Thomas Trautmann
Dr. Manfred Gottwald
Brigitte Rüba

Layout Dr. Manfred Gottwald

Cover A simulated orbit segment from the Sentinel 5 Precursor mission over Bavaria illustrating the excellent spatial resolution which will permit to study atmospheric constituents on the scale of urban quarters.

Contents

1. Foreword

Early in 2012 one of the mishaps, demonstrating that space-borne remote sensing is still a challenging and complex undertaking with potential anomalies causing a highly successful story to end abruptly, had occurred. The loss of the ENVISAT platform in April 2012 marked the beginning of the end of the SCIAMACHY mission. SCIAMACHY was not only one of Germany's Earth Observation flagship enterprises but also occupied our department with many aspects of atmospheric remote sensing for a very long time – from the development of retrieval algorithms to planning the measurements and operating the instrument. Our contributions helped that the SCIAMACHY mission, an international collaboration between space agencies, industry and the science community, provided excellent insights into the changing Earth's atmosphere for 10 years, more than twice of the expected in-orbit lifetime. We hope that the mission providing agencies fully support our plans for the post in-orbit mission phase such that all information acquired by SCIAMACHY, i.e. science data and operations related information, is further analyzed and finally prepared for long-term data preservation.

In the view of the ENVISAT loss, maintaining the launch schedule for the next Earth Observation missions with relevance to the atmospheric domain, particularly the Sentinel 5 Precursor, is considered very important. This would ensure that the science data stream does not dry up and long-term studies could continue. Currently only the GOME-2 sensors aboard the MetOp platforms serve as our 'workhorses'.

The past year has again shown how interdisciplinary approaches become more and more important. While Earth Observation serves the needs for understanding our home planet, it is now obvious that without the knowledge gained in this field we would be unable to decrypt the information contained in the light acquired from exoplanets, own worlds light years away. Since the discovery of the first exoplanet in the mid-90s of the last century one of the prime scientific goals is the search for a 'second Earth'. Such an object will reveal its existence via biomarkers in the spectrum. Any light escaping its surface and finally reaching telescopes on Earth has to pass through the exoplanet's atmosphere, where the same interactions between photons and atmospheric constituents as in our own occur – absorption, re-emission, scattering and reflection. If we want to retrieve from the exoplanet's spectrum the footprints of a habitable environment we have to understand all aspects of radiative transfer. This is our asset we contribute to exoplanet studies. It is still a small niche in our department's portfolio, but begins delivering exciting results.

MF-ATP, October 2012

In October 2012 our department had spent a few days in the town of Freising to discuss future strategies and initiate new developments. We hope that the spirit, said to be present on both hills towering the city, the Domberg and Weihenstephan, will help us through successful years to come.

We thank all our staff for their efforts and achievements in 2012 and their contributions to this annual report.

Prof. Dr. Thomas Trautmann
Dr. Manfred Gottwald

2. Atmospheric Remote Sensing – Instrument Operation, Calibration and Measurement Techniques

2.1 SCIAMACHY Operations 2002-2012

M. Gottwald, E. Krieg (TwIG), K. Reissig (IBR), J. How (TwIG), S. Noël (IUP-IFE), K. Bramstedt (IUP-IFE), H. Bovensmann (IUP-IFE)

When the year 2012 started, the SCIAMACHY mission had already accomplished a successful in-orbit phase lasting almost 10 years. Operations were intended to continue until the end of 2013 with preparations for another extension in the 2014+ timeframe having started. The fatal ENVISAT anomaly, which occurred on 8 April 2012, stopped all these activities. Due to this failure all communications links with the ENVISAT platform were suddenly lost, i.e. no telemetry was received indicating the status of the spacecraft and the commands sent by ESOC to gain control of ENVISAT again were all unsuccessful. Immediate investigations by ESA came to the conclusion that the anomaly must have occurred in orbits 52867/52868 between 11:09 and 12:28 UTC. For about 9-10 hours the S-band carrier remained available, but only unmodulated. ENVISAT's status was summarized as follows:

- no sign of platform degradation before the failure
- ENVISAT remained intact as confirmed by ground (Fig. 2-1) and space-borne observations
- ENVISAT remained in nominal orbit
- ENVISAT was slowly rotating, i.e. nominal Safe Mode was not achieved

Two potential failure scenarios were finally suggested. Either a double-failure in the power subsystem or a failure in the Central Communication Unit, together with a Safe Mode anomaly could have caused the mishap. In both cases the chance for a recovery was almost non-existent. On 9 May 2012, ESA declared the end of the ENVISAT mission. Since then, ESA had continuously listened to any potential S-band carrier signal periodically until mid-December 2012 – but without success.

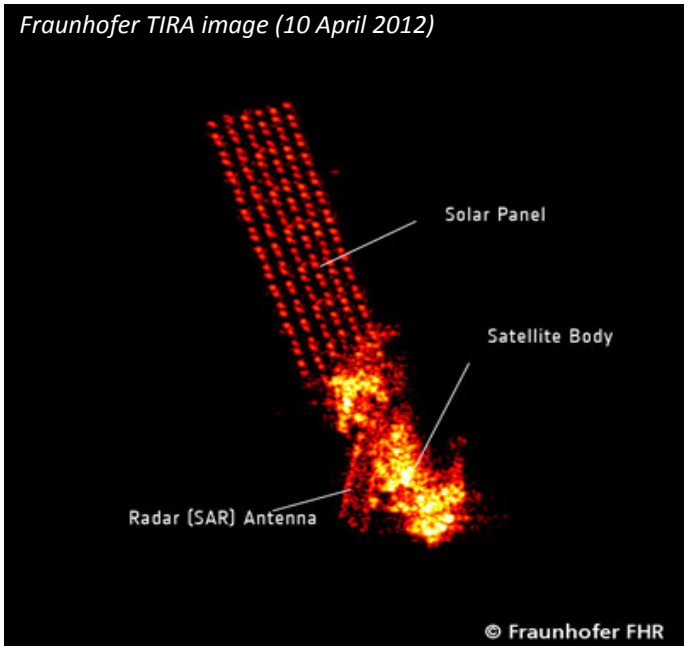

Fig. 2-1: ENVISAT as seen by the TIRA radar facility on 10 April 2012 (image: Fraunhofer FHR).

For the SCIAMACHY Operations Support Team (SOST) – formed by personnel from MF-ATP and IUP-IFE/University of Bremen – the ENVISAT anomaly and the associated sudden completion of the SCIAMACHY mission ended a more than 15 years long challenging period where, in cooperation with ESA (flight operations at ESOC, mission management and later post launch support at ESTEC and payload data segment at ESRIN), industry (EADS Astrium and Dutch Space), the Quality Working Group (SQWG) and the Science Advisory Group (SSAG), highly efficient instrument operations were developed, implemented and finally executed.

A summary of SCIAMACHY's in-orbit operations performance in the period 2002-2012 was compiled by SOST in the document *SCIAMACHY Preliminary In-Orbit Mission Report, PO-TN-DLR-SH-0033, Issue 1, Rev. 0, 31 July 2012*, which ESA had requested in support of ENVISAT mission closure activities. This TN provided a comprehensive overview by describing SCIAMACHY operations as requested by different mission operations phases and the corresponding instrument configurations. Mission planning was a separate item since the status of being an Announcement of Opportunity instrument required specific planning and scheduling interfaces. Of particular interest was how the availability of the instrument evolved with time in response to certain failures and anomalies. Finally the optical, thermal, LoS pointing

performance and Life Limited Items performance were elaborated illustrating the instrument's very good shape at the moment when ENVISAT and its payload 'disappeared' from the screens in orbit 52868.

Mission Operations Phases

SCIAMACHY mission phases consisted of the launch and early operation phase (LEOP), the switch-on and data acquisition phase (SODAP), the main validation phase with quasi-routine operations and finally, the routine operations phase (Table 2-1). All these phases were successfully accomplished. The ground segment functions for operating the instrument had been implemented and tested in time such that the planned engineering and measurement tasks could be achieved without delays.

Phase	Instrument Activity	Date	Orbit
LEOP	OFF-Leo mode	1-7 Mar 2002	
SODAP	first switch-on	11 Mar 2002	147
	AZACM cover released	3 Apr 2002	477
	SRC released	15 Apr 2002	653
	ELACM cover released	20 Jun 2002	1594
	end SODAP	2 Aug 2002	2204
Validation	start validation	2 Aug 2002	2204
	final flight states loaded	15 Dec 2002	4143
	timelines with final flight states loaded	16 Dec 2002	4151
Routine Operations	nominal measurement programme – start	6 Jan 2003	4457
	ENVISAT orbit change	24 Oct 2010	45222
	nominal measurement programme – end	8 Apr 2012	52868

Table 2-1: Main SCIAMACHY activities from launch to end of mission (for details see text).

Instrument Configurations

When SCIAMACHY was switched-on on 11 March 2002 it occurred using the primary chain of hardware, called *side A*. The instrument stayed on side A for the entire in-orbit mission lifetime. No need for activating any of the redundant hardware components arose. Even the number of s/w patches, required for curing individual instrument on-board control malfunctions, remained at a very low level with only two uploads. Throughout the Commissioning Phase the instrument underwent many configuration changes as required by the scheduled engineering and measurement tasks. In summary, at the end of the Commissioning Phase SCIAMACHY had successfully

- executed more than 21200 MCMDs,
- started almost 5500 timelines, which had
- triggered more than 78000 individual states, which had required
- upload of 5700 parameter tables and
- upload of 560 timelines.

In the routine phase SOST had taken over from industry responsibility for the definitions of the operations content. Changing instrument configuration was still required in response to

- platform operations modifications
- instrument degradation
- instrument anomalies
- science requirements updates
- calibration and characterization requirements updates.

Implementation occurred via changes in engineering parameters, measurement parameters or mission scenarios.

Updates of engineering parameters usually required the execution of flight operation procedures (FOP) at FOCC. The parameter content of the FOP was specified by SOST according to rules and requirements outlined in the corresponding applicable documents, particularly the IOM. Transfer of this information occurred using the *SCIAMACHY Operations Request (SOR)* interface.

Most of the engineering parameter related configuration changes dealt with adjustments of the Thermal Control (TC) system for maintaining detector temperatures. It happened mainly in the first part of the mission. Later, calibration and characterization had progressed such that detector temperatures outside the assigned limits were found acceptable. Overall, the SOR interface proved to be rather efficient. It was operated only via manual interaction without the need of automatic processing of information. Therefore even short-notice SORs could be implemented successfully.

With the start of routine operations the final flight status of the measurement configuration had to be established. It consisted of the applicable mission scenarios, the complement of 70 states and a timeline set (63 timelines stored on-board, > 63 timelines specified on-ground and exchanged as specified in mission planning).

Contrary to engineering parameters, measurement parameters and timelines were always updated via MCMD. Whenever needed, parameter tables with modified parameter settings or new timelines were translated by SOST to the CTI (Configurable Table Item) format and submitted to FOCC for inclusion into the corresponding command databases or further transfer to ESRIN.

Since SOST kept final flight configurations under strict configuration control, the formal process of an *Operation Change Request (OCR)* was necessary whenever changes to either the mission scenario, state or timeline final flight configuration had to be made. This applied to both temporary and permanent changes. OCR implementation was a sequential process between the author of the OCR, the SSAG approving/disapproving the OCR from a science point of view, SOST analysing and finally implementing the OCR and the AOP agency giving the formal approval. During the mission the OCR mechanism had proven rather successful permitting the handling of rather different requests – from changing only a single measurement parameter to achieve better retrieval results to complex modifications such as adapting SCIAMACHY to measurements from a lower ENVISAT orbit or even observing an extraterrestrial target such as planet Venus. In total 50 OCRs had been successfully implemented between January 2003 and April 2012.

Since 4 April 2002 (orbit 486) the ENVISAT orbit had remained unchanged with mean orbital parameters as listed in Table 2-2 (second column). These parameters were applicable in the specified 5-years mission lifetime and the first phase of the mission extension lasting well into 2010. For extending the mission up to 2013 ESA had selected an approach which required lowering the orbit and introducing drifting parameters from end of October 2010 on (Table 2-2 third column).

For SCIAMACHY as an instrument with multi-viewing capabilities the modification of the ENVISAT orbit had major impacts on operations. The Line-of-Sight (LoS) pointing knowledge required an adaption of orbit-related engineering and measurement parameters. In a common approach, and owing to the share of responsibilities, SOST and EADS Astrium prepared the instrument for the extension phase with a modified orbit. Particularly challenging was maintaining the matching of the geolocation of limb states with associated nadir states, a major scientific requirement for SCIAMACHY operations. Both its orbit dependent across-track and an along-track component had to be adjusted. A thorough verification phase in November 2010 confirmed the successful modification of the SCIAMACHY configuration in response of the ENVISAT orbit manoeuvre. Only small adjustments were needed for a few measurement parameters subsequently.

	Nominal Orbit	Mission Extension Orbit (October 2010)	Remark (Mission Extension Orbit)
Semi-major Axis	7159.496 km	7142.146 km	drifting with a rate of -64 m/year
Orbital Period	6035.928 sec	6014.036 sec	drifting with a rate of -0.087 sec/year
Inclination	98.549°	98.537°	drifting with a rate of -0.46 mdeg/year
Repeat Cycle	35 days / 501 orbits	30 days / 431 orbits	n.a.
MLST	22:00:00	21:59:39	drifting (max: 22:07, min 21:55)

Table 2-2: ENVISAT orbit parameters in the nominal and the mission extension orbit (as originally planned).

Mission Planning

Mission planning was a joint undertaking with SOST preparing the measurement plan (Orbit Sequence Definition File – OSDF) while ESRIN verified and integrated this plan into the overall ENVISAT plan (Reference Operations Plan using the ROP Generation Tool – RGT). Finally FOCC generated the ENVISAT schedule (Detailed Mission Operations Plan – DMOP). It included all platform and payload activities which were executed via MCMD. SOST extracted from the ENVISAT schedule the SCIAMACHY specific part (SCIAMACHY DMOP – SDMOP). For having full insight into the scheduling, SOST operated its own scheduler. It was developed applying the same scheduling rules as the ENVISAT MPS, but was limited to timeline start/stop and high data rate on/off. Orbit propagation and Sun/Moon target visibility utilized CFI results based on the reference orbit. Each OSDF was processed with SOST's scheduler before submission to ESRIN to form the simulated SDMOP (SIM_SDMOP), a schedule identical in format to the SDMOP. The difference in times between the SDMOP and the SIM_SDMOP was smaller than 1 sec as long as ENVISAT's orbit followed the stable 35 days / 501 orbits repeat cycle. Even when the ENVISAT orbit parameters started drifting in the modified mission extension orbit, the accuracy of the SIM_SDMOP still amounted to better than 1.5 sec on average.

In the Commissioning Phase the SIM_SDMOP was a prerequisite for executing the challenging engineering and measurement sequences. It was always available as soon as the OSDF existed, i.e. much earlier than the FOCC provided SDMOP. This permitted preparation of the FOP inputs by industry and SOST with sufficient time margin, even when short-notice replanning was required.

Additional output of the SOST scheduler comprised, for each orbit, a list of states with start/stop times, a list of all nadir states with geolocation of the ground pixel – given in longitude and latitude – at start/stop of the state and the same list for all limb states where the geolocation of the ground pixel was defined by the longitude/latitude of the tangent point at state start/stop. The nadir and limb ground pixels also appeared as separate orbital maps. This scheduler functionality was particularly useful for validation campaigns when the exact time of an ENVISAT overpass at a validation site, within the accuracy of the reference orbit, was required for preparing the validation instruments.

Instrument Availability

The measurement programme as planned in an OSDF was occasionally interrupted either due to anomalies on various levels or particular scheduled activities. This included

- instrument anomalies
- platform anomalies
- ground segment anomalies
- orbit control manoeuvres (OCM)
- platform maintenance
- instrument maintenance.

In all cases the goal for SCIAMACHY operations was to keep the instrument unavailability period as short as possible without introducing unnecessary risks when recovering back to the nominal measurement status.

Over the entire in-orbit mission lifetime (Commissioning Phase plus routine operations phase), a total of 133[1] engineering activities / measurement interrupts had occurred. They are illustrated in SCIAMACHY's availability record (Fig. 2-2). The period from first switch-on of the instrument in orbit 147 until the loss of the platform in orbit 52868 covered 52722 orbits in total. Only 2660 orbits (5%) could not be used for engineering activities / measurements. For only the routine operations phase, the number of unavailable orbits is reduced to 2000 orbits, i.e. 4.1%.

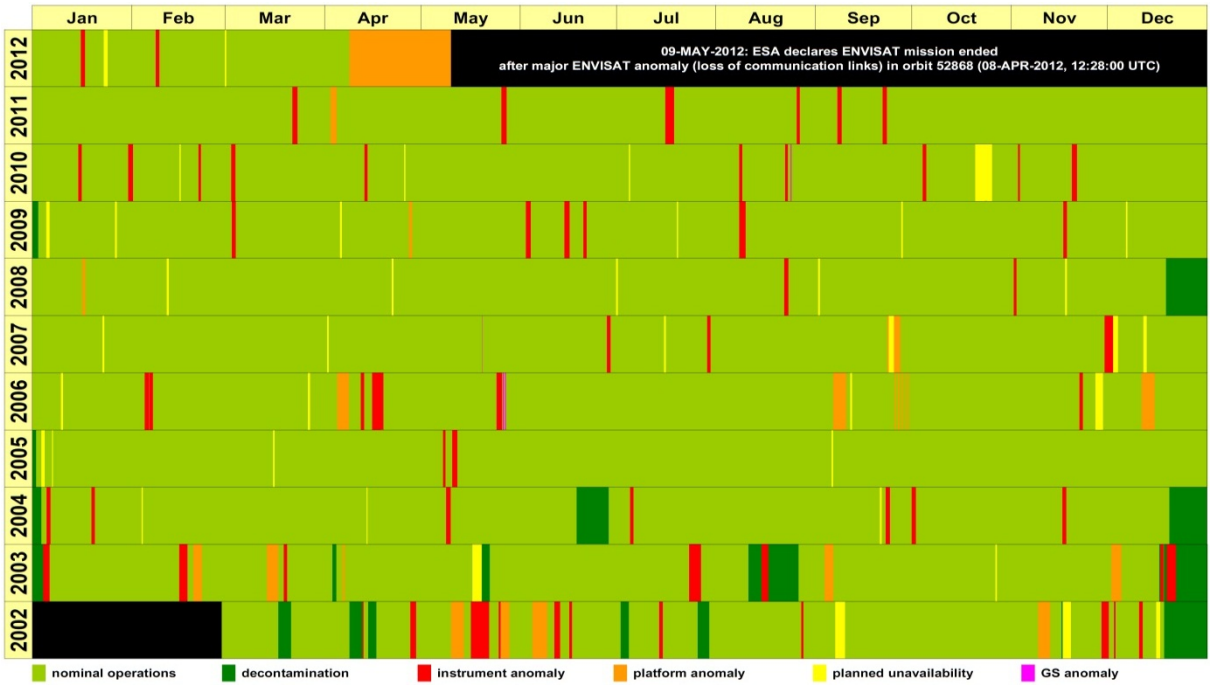

Fig. 2-2: SCIAMACHY availability 2002-2012.

All severe instrument anomalies sent the instrument to a safe state with the need for verifying the underlying failure and, after successful analysis, initiating recovery back to the MEASUREMENT mode. They defined four groups:

- parameter mismatches
- CCA MCMD Check Error
- Single Event Upsets (SEU)
- unidentified (all cases which could not be attributed to any of the other three types).

The occurrence of the CCA MCMD Check Errors, SEU induced events and anomalies with unidentified cause over the in-orbit mission lifetime did not indicate an increasing anomaly rate (Fig. 2-3). They followed a linear trend with a rate of 1.3 per year for the CCA MCMD Check Error (not counting SODAP), 1.0 per year for SEU anomalies and 3.0 per year for the unidentified cases.

[1] This number only includes cases where SCIAMACHY was transferred to a mode lower than MEASUREMENT TIMELINE for a complete orbit. Anomalies causing loss of individual states, e.g. blocking of the subsolar window by the Ka-band antenna, are not addressed.

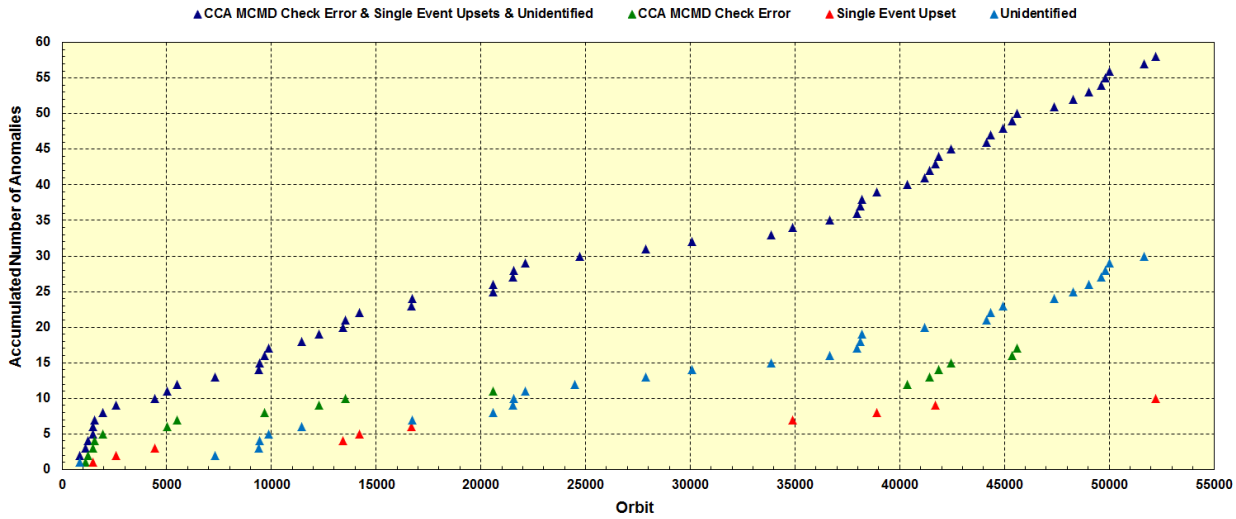

Fig. 2-3: Accumulated number of instrument anomalies (CCA MCMD Check Error, SEUs and unidentified failures).

Instrument Performance Evolution

Although degradation did exist, as is always the case in the harsh in-orbit environment, the overall performance of the instrument exceeded expectations. Only water as the major contaminant hampered the usefulness of the IR channels 7 and 8 from an operations point of view[2].

- **Optical throughput**: The optical throughput of the instrument was decreasing with time due to degradation of optical components, e.g. build-up of contaminants on optical surfaces. Its overall behaviour was best illustrated by the channel averages. Although the results for the various light paths differed slightly, all results provided a consistent view of the optical performance (Fig. 2-4).
- **Thermal performance – ATC**: The orbital mean OBM temperature derived in the regular monitoring was maintained at the specified value with high stability. This indicated that the ATC control loops functioned well. The degradation of the ATC, which had been predicted before launch, was compensated well. Only a single adjustment of ATC parameters had been required in October 2008 in the entire in-orbit mission phase.
- **Thermal performance – TC**: TC settings for routine operations had been uploaded in June 2002. Since then infrequent TC adjustments have occurred. Early in the mission a TC adjustment occurred whenever a detector temperature limit was exceeded. Later they were omitted since high quality retrieval could also be achieved with measurement data acquired under thermal conditions slightly out-of-spec.
- **Thermal performance – decontaminations**: Already early in the mission it became obvious that the infrared channels 7 and 8 began to show a significant loss of radiance response. Investigations indicated that an ice layer growing in the light path detectors was responsible for this. It affected only channels 7 and 8 because these were the detectors operated at lowest temperatures. By adopting the specified decontamination procedure (Non-nominal decontamination – NNDEC) appropriately, i.e. invoking a second cold trap in both detectors, stable conditions could be achieved for most of the in-orbit mission lifetime.

[2] Note that shortly after launch a light leak became apparent in channel 7. It made generation of useful retrieval results from channel 7 impossible.

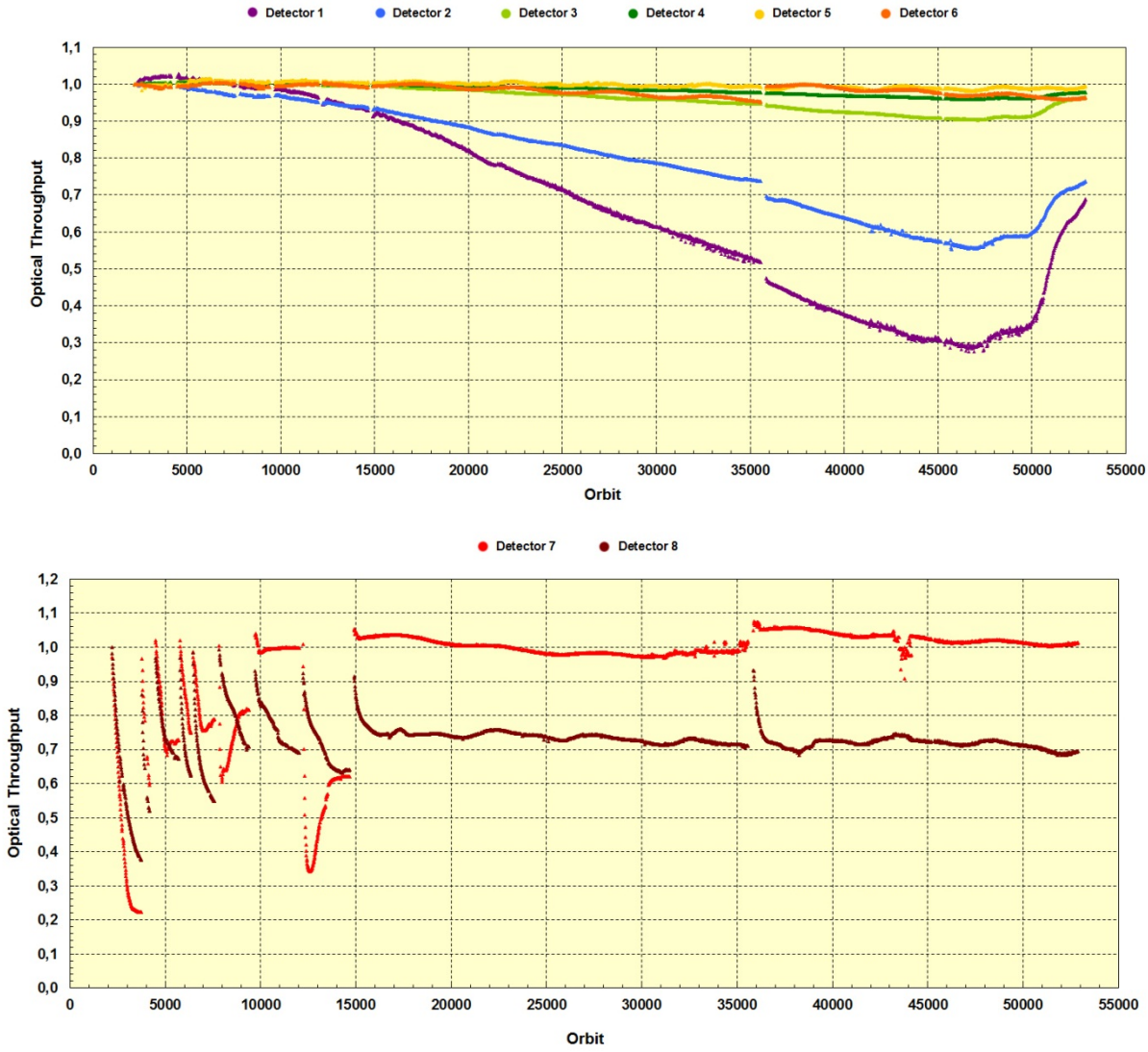

Fig. 2-4: Degradation of the SCIAMACHY throughput relative to August 2002 in channels 1-6 (top) and 7 and 8 (bottom) in the limb light path (based on SOST-IUP/IFE monitoring).

- **Line-of-Sight (LoS) Pointing Performance:** Knowledge of the LoS was a key parameter in retrieving correct and reliable geolocation information. Particularly for SCIAMACHY's limb mode a necessity for obtaining useful measurements was the accuracy of reconstructing altitudes in general and tangent heights in particular from elevation and azimuth angles. After correcting a state vector related bug on platform level, SCIAMACHY's limb tangent heights displayed a less variable behavior. However a stable bias of 1.5 km persisted. When using small irregularities in ESM/ASM readings during certain solar states, extra mispointing angles in roll, pitch and yaw could be determined. They amounted to about 20 mdeg for pitch and roll. Once applied, the retrieved limb tangent heights no longer showed an offset with an achieved accuracy of ± 150-200 m (Fig. 2-5).
- **Life Limited Items – LLI**: The LLI complement consisted of Aperture Stop Mechanism (APSM), Neutral Density Filter Mechanism (NDFM), Nadir Calibration Window Mechanism (NCWM), White Light Source (WLS), Spectral Line Source (SLS) and Cryogenic Heatpipe. Each LLI had a specified total budget. By considering the on-ground usage during test campaigns in phase C/D, the maximum allowed in-flight budget, i.e. the End-of-Life (EOL) budgets could be derived. Fig. 2-6 displays how the usage of individual LLIs evolved with time. In the routine operations phase the trend was linear. Only for the NCWM a change occurred mid 2006 when the rate of subsolar measurements was reduced from 1 per day to 1 every 3 days. In January 2012 this was reversed and the subsolar rate was back to 1 per day. The usage of the Cryo Heatpipe accumulated stepwise early in the mission because of the frequently occurring decontaminations. Later, only a single NNDEC had been added.

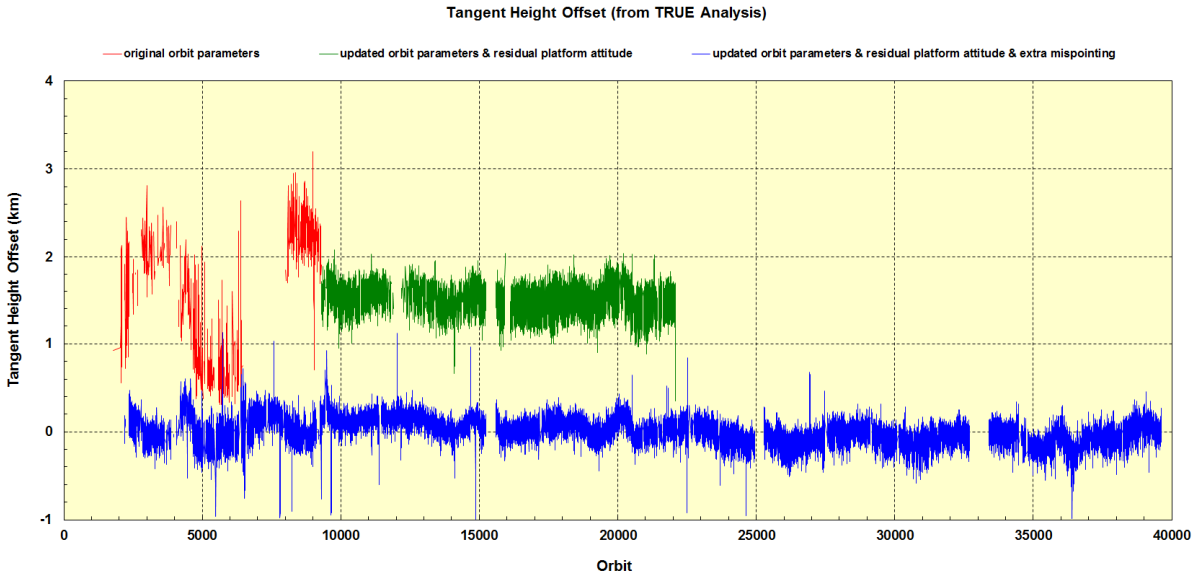

Fig. 2-5: Tangent height offsets as determined from operational data products and TRUE retrieved profile information (based on IUP-IFE analysis). Prior to December 2003, the bias had a strong harmonic variation (red). After the update of the on-board propagator model and including residual platform mispointing, the variation was reduced but a constant offset persisted (green). When the extra mispointing was introduced in geolocation retrieval this offset vanished (blue).

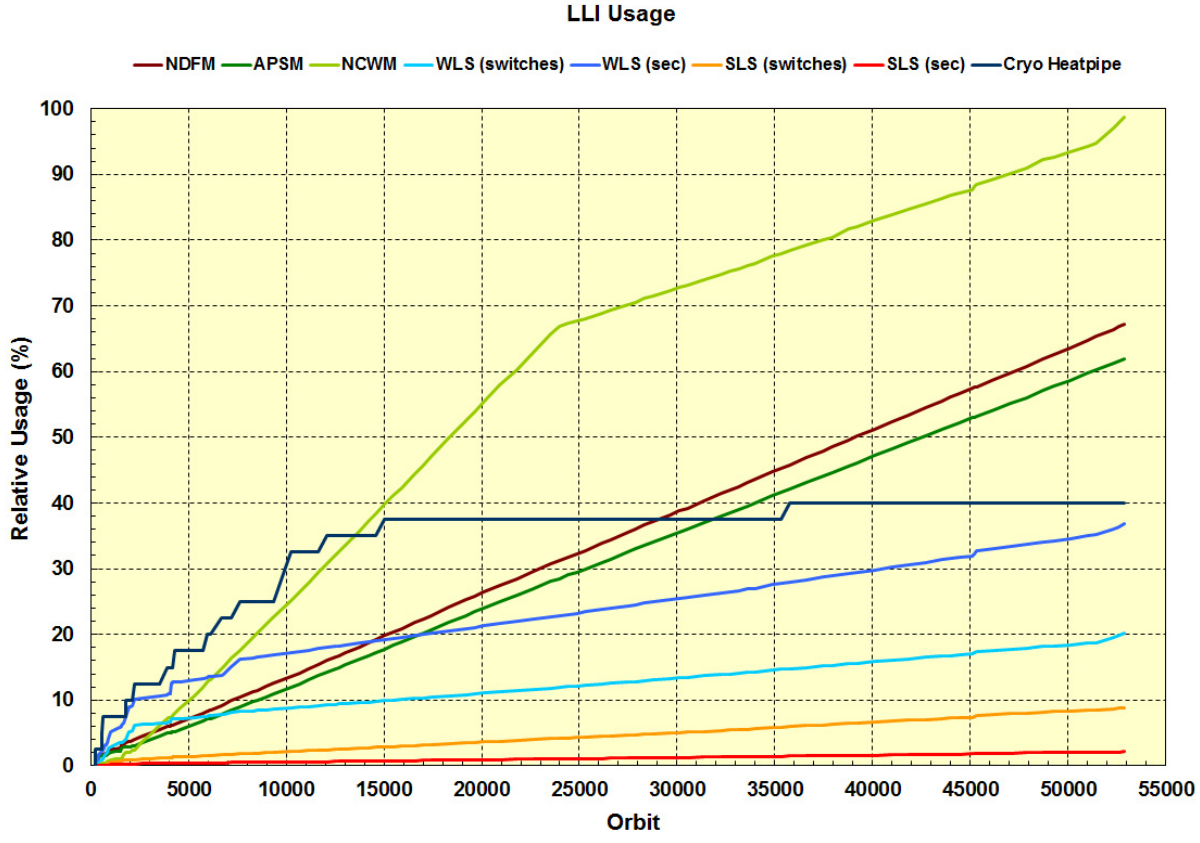

Fig. 2-6: Evolution of LLI usage with time.

2.2 The SCIAMACHY Consolidated Level 0 Archive 2002-2012

M. Gottwald, E. Krieg (TwIG), K. Reissig (IBR), J. How (TwIG), G. Brizzi (Serco S.p.A.)

The SCIAMACHY consolidated level 0 (cL0) products refer to absolute orbit numbers in the same way as measurement operations planning and execution. Each consolidated product starts at the time when ENVISAT crossed a particular ANX and ends when this occurs for ANX+1. Therefore, the consolidated products are expected to contain all measurements for a specific orbit. Since SCIAMACHY executes timelines almost continuously from several minutes before sunrise to shortly before the end of eclipse, consolidated products must usually cover a complete orbital period. Only in cases of instrument unavailability, either triggered by a planned switch-off or an unexpected platform or instrument anomaly, the consolidated product does not exist or may deviate from planning.

Consolidated Product Consistency Checking

The delivery of SCIAMACHY consolidated level 0 (cL0) data to the AOP is one of the AOP specific data interfaces in the Payload Data Segment (PDS). This interface has been technically implemented via an electronic link between the D-PAC and the Data Information Management System (DIMS) of the German Remote Sensing Data Center (DFD) at DLR. The transfer from D-PAC to DIMS generated, over the mission lifetime, a complete data set of SCIAMACHY cL0 products serving as a cL0 master data set. The SCIAMACHY Operation Support Team (SOST) established and maintains this cL0 archive in the DIMS environment for the purpose of instrument performance monitoring.

Consolidated products have been generated at LRAC and delivered to D-PAC since mid 2002. With the beginning of cL0 delivery, several inconsistencies had been observed. These included:

- Orbits were not covered by cL0 products although SCIAMACHY was operational.
- Orbits were covered by cL0 products but the product duration did not comply with the actually planned and executed instrument operations in that particular orbit.
- For one orbit there could be more than one cL0 product. These products were identical or different in content (disregarding the product type file counter).
- cL0 products exhibited corrupt data (e.g. exceeding Reed Solomon correction threshold, sync bit errors). The occurrence of such products was non-uniform.

A pre-condition for a cL0 master data set was to identify and reject cL0 files transferred from LRAC to D-PAC containing any of the above listed inconsistencies. Therefore, prior to sending a data file from D-PAC to DIMS, SOST developed and operated a filter mechanism ensuring the consistency of each product. It performed a sequence of error checks. Only files passing each check were finally transferred to DIMS. All others were rejected. The consistency check was based on information retrieved from

- filename
- Main Product Header (MPH)
- Secondary Product Header (SPH)
- data format: all data is read and format checked
- product size.

Applying this verification scheme yielded more than 46700 fully consolidated level 0 orbits in the master archive. About 780 orbits were only partially consolidated but showed no other anomaly. Finally, in about 1010 orbits the quality of the consolidated level 0 data was not acceptable or the data, although acquired, was not available at all (ground segment unavailable or data lost). Overall, between 97%-98% of the orbits with SCIAMACHY operating in MEASUREMENT TIMELINE mode could be processed in consolidated form (Fig. 2-7).

Meanwhile the cL0 master archive has become a repository for SCIAMACHY level 0 related information in the entire ENVISAT PDS. ESA has adopted a similar approach for the cL0 products archived in the D-PAC environment. It has meanwhile turned out that a thoroughly verified, bug-free cL0 repository is a pre-requisite for generating unambiguous and flawless higher level products. Therefore the cL0 master archive plays a major role whenever level 0-1b and level 1b-2 reprocessing campaigns are in preparation.

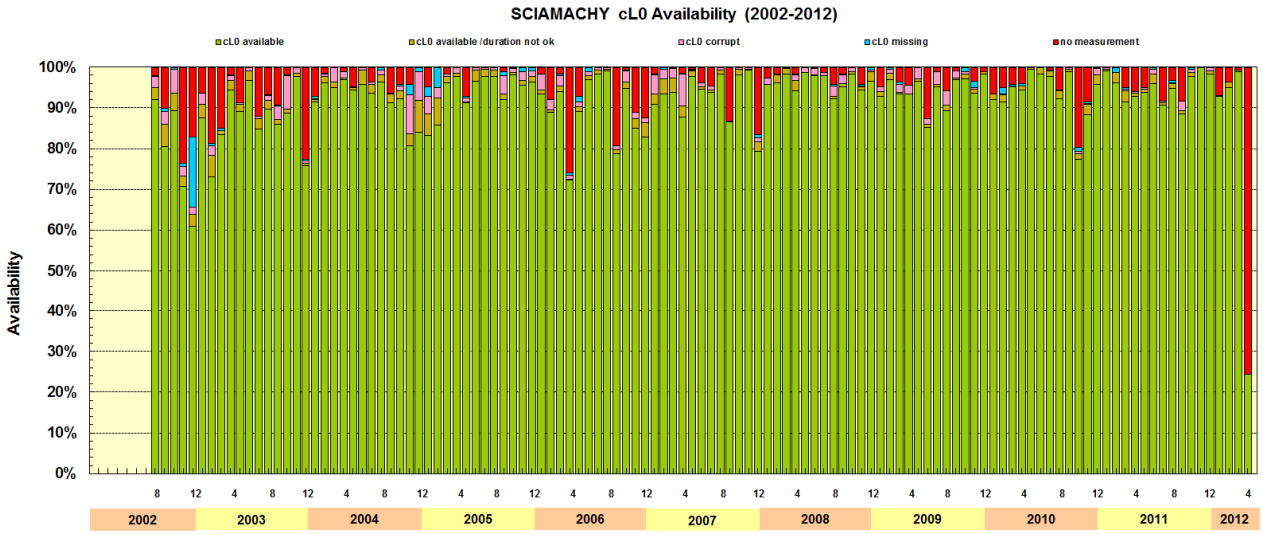

Fig. 2-7: cL0 availability on a monthly basis between August 2002 and April 2012.

Consolidated Level 0 Classes

Consolidated orbits form several classes. These differ by state content, cL0 product duration and product size. They include

- **Completely consolidated orbits**: They form two clusters with product durations of 5700 sec and 6000 sec and product volumes of 220-230 MB.
- **Completely consolidated orbits with limb_mesosphere_lower_thermosphere measurements**: As the completely consolidated orbits but with sequences of limb_mesosphere_lower_thermosphere states replacing all limb states.
- **Incompletely consolidated orbits**: Orbits where data are missing although they had been generated on-board (either not received on-ground and/or unused in the level 0 consolidation process).
- **Monthly calibration orbits**: Orbits with the state/timeline sequences for monthly calibration orbits.
- **Orbits where an instrument unavailability started**: Whenever an instrument unavailability had occurred, either triggered by an instrument or platform anomaly, measurements had stopped in an orbit and the scheduled measurement programme for this particular orbit was not entirely executed. Productwise it resembled incompletely consolidated orbits.
- **Orbits where an instrument unavailability ended**: As for the unavailability 'starting' case, the content of cL0 products depends on when SCIAMACHY resumed measurements after an unavailability, i.e. how much of the particular orbit could be recovered.
- **Orbits introduced by mission planning due to an OCR**: OCRs implemented operational changes which modified state or timeline definitions or even required modified mission scenarios. Certain OCRs resulted in a considerably different data content.

All cL0 products from the master archive are displayed in Fig. 2-8 and 2-9. The individual classes listed above can be clearly distinguished. For most of them the obvious relation is as expected. Where deviations exist, additional analyses are required.

In the framework of long-term data preservation, the goal of SOST is to improve the cL0 master archive even further. In close collaboration with ESRIN we intend to recover as much as possible of the still incompletely consolidated or entirely missing orbits. This will require re-consolidation runs at LRAC. One can even consider a re-consolidation of the complete level 0 data set. Although SCIAMACHY's in-orbit mission phase had unexpectedly ended with ENVISAT's fatal anomaly, there is still considerable work to be done before the cL0 data archive can be regarded of being 'complete' and 'finished'.

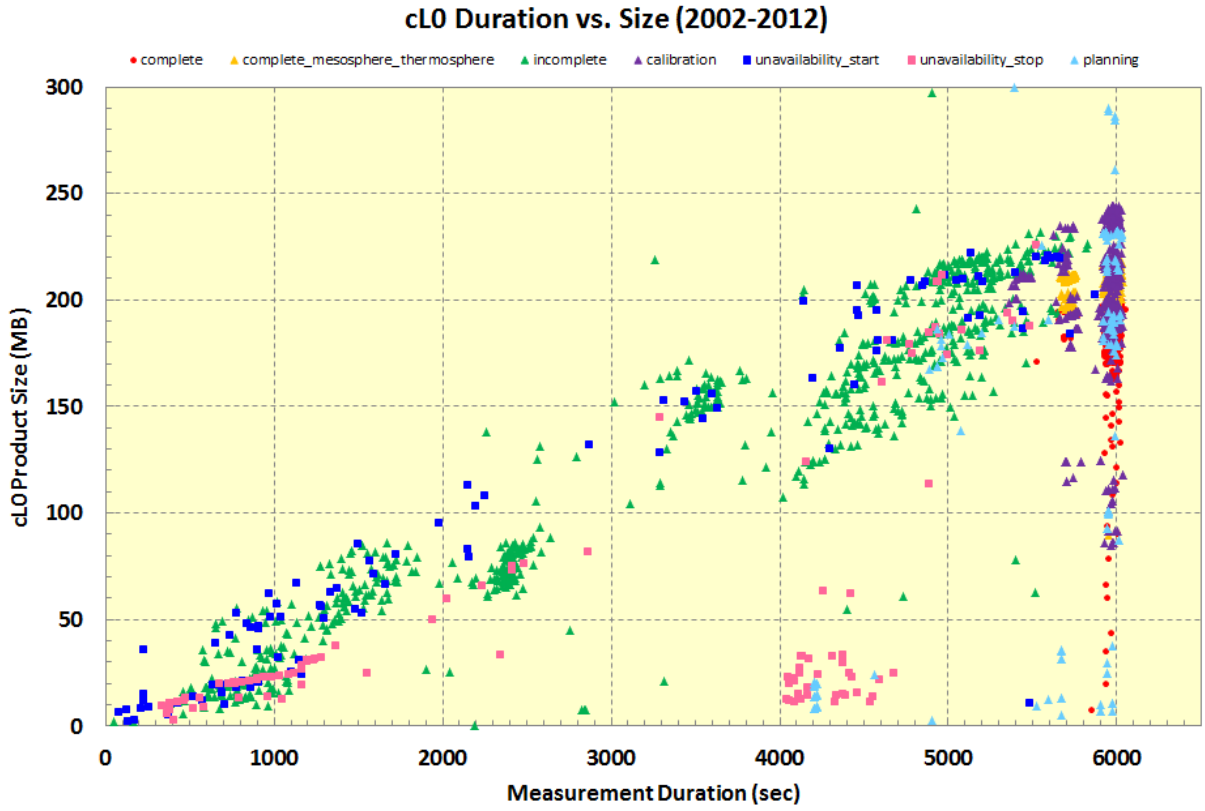

Fig. 2-8: Product duration / product size relation for the cL0 products of 2002-2012.

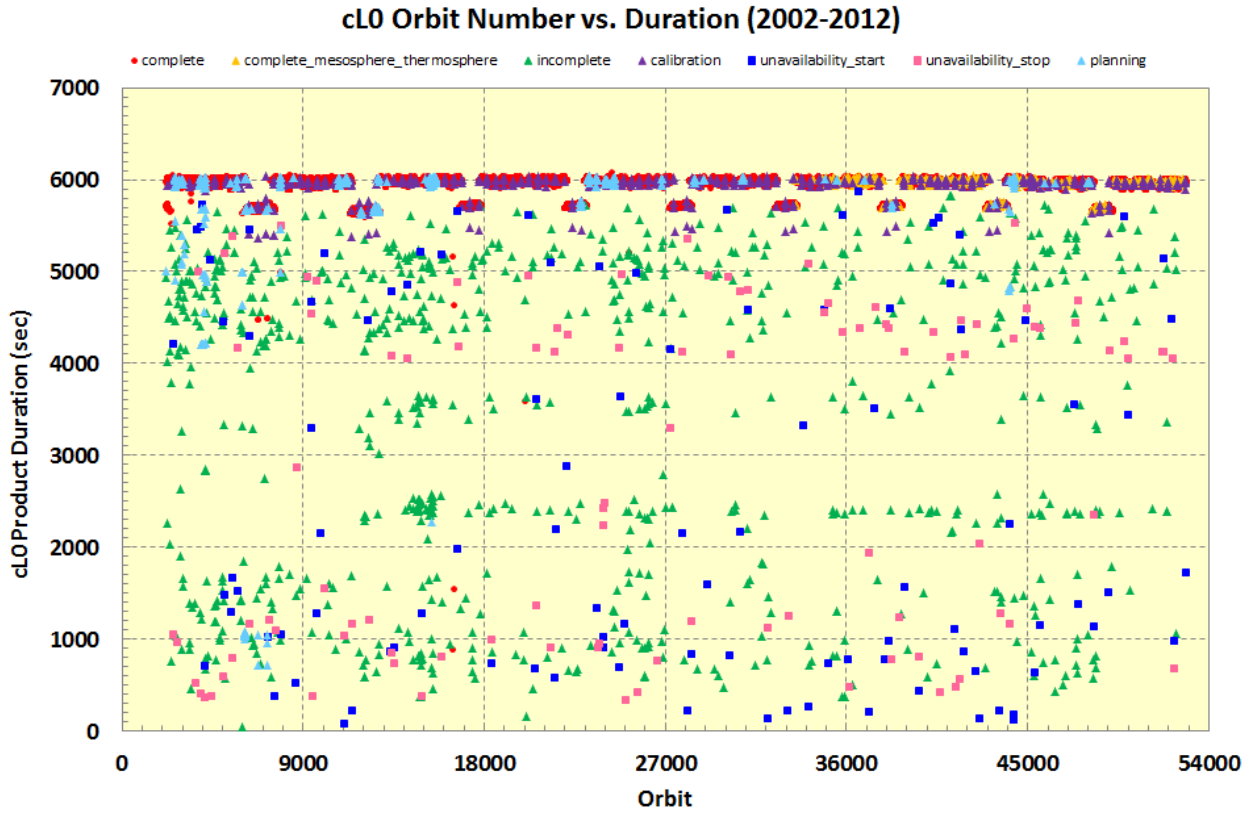

Fig. 2-9: Product duration as a function of orbit number for the period 2002-2012.

2.3 SCIAMACHY Processors and Products

G. Lichtenberg, B. Aberle, A. Doicu, S. Gimeno García, S. Hrechanyy, M. Meringer, F. Schreier, D. Scherbakov, S. Slijkhuis

Last year's loss of the ENVISAT platform with the entire payload, including SCIAMACHY (see chapter 2.1), was a major blow for our space-borne atmospheric remote sensing activities. However, other than instrument operations, algorithm development and processor implementation for the next version of the level 1 and level 2 products was less impacted.

With a delivery date for the prototypes end of 2012, the majority of the implementation work had already been finished in April 2012. Therefore, in spite of the platform loss, it was decided to deliver these versions as planned such that several improvements will become operational. For level 0-1 it includes a scan mirror model leading to a scan angle dependent degradation correction. The operational processor will be based on the new generic level 0-1 processor C++ framework which was developed by MF-ATP in the last year. The direct implementation has the advantage that prototype and operational processor are code identical thus facilitating the integration in the ground segment and subsequent maintenance. The new level 2 processor will have additional nadir products and an extension of the limb ozone profiles to larger altitudes. For mid 2013 it is further planned to integrate the first limb-nadir matching algorithm to retrieve tropospheric NO_2.

Level 0-1 Processing – a Short History

The first version of the level 0-1 prototype was specified and programmed in 2001, one year before the launch of ENVISAT. It used the IDL language in order to be able to easily debug the algorithms and to visualize intermediate results. The prototype was the basis of the operational processor that was built by industry. Once in orbit with the Commissioning Phase successfully accomplished it became clear that in some aspects the calibrated spectra were not of the expected quality. The reasons were two-fold:

- deficiencies in the calibration data (so-called *Key Data*) which serve as an input for the processor
- unexpected effects like nonlinearity, a different memory effect or ice forming on the SWIR detectors and the degradation of detector pixels in flight (Fig. 2-10).

While deficiencies in the calibration data did not necessarily lead to processor changes, the new effects had to be reflected in modified or completely new algorithms. In addition to processing changes triggered by instrument behaviour, there were also changes requested by the users to improve the data quality of the level 2 product. One example is the (optional) switching between the usage of standard dark measurements for the dark correction of limb data to the usage of limb darks that are measured at the end of each limb sequence.

Apart from such instrument and instrument calibration related issues, the method how the calibration & monitoring data were originally processed in the operational ground segment, was the source of another major re-design of the processor. In the early phase of the mission this occurred in the Instrument and Engineering Calibration Facility (IECF), an ESA developed s/w package with own calibration algorithms using level 1b data as input. Therefore each re-processing of the level 0 data set required two more processing steps:

- produce level 1b data for the IECF
- from the level 1b data produced by the IECF, generate degradation correction factors
- with the full calibration and degradation correction factor set, generate the final level 1b products ready for the users.

In order to minimize the effort for re-processing and at the same time make all data consistent, the SciCal facility was developed. It calculates all calibration data and uses level 0 as input. SciCal is based on the level 0-1 prototype, i.e. all data are processed with the same algorithms.

Today, the processing chain from level 0 data (uncalibrated, time ordered downlinked raw data) to level 1c (calibrated radiance and irradiance spectra) consists of three elements:

- **Level 0-1b Processor**: This processor takes level 0 as input (i.e. time ordered raw data from the instrument) and produces level 1b data. Level 1b data contain all data needed to produce calibrated Earthshine radiances.
- **SciCal**: The SciCal tool collects all calibration measurements, calibrates them using the level 0-1b prototype processor and saves them to auxiliary files that are later picked up by the level 0-1b processor and used in the calibration of Earthshine data.
- **Scial1c**: User tool to extract and calibrate data from the level 1b product and write them to a level 1c product. Filters enable the user to extract only data of interest based on geolocation, measurement category, time etc. It uses the same s/w code as the level1b-2 processor for applying the calibrations to the level 1b data. Therefore the consistency of the whole processing chain from level 0 to level 2 is ensured.

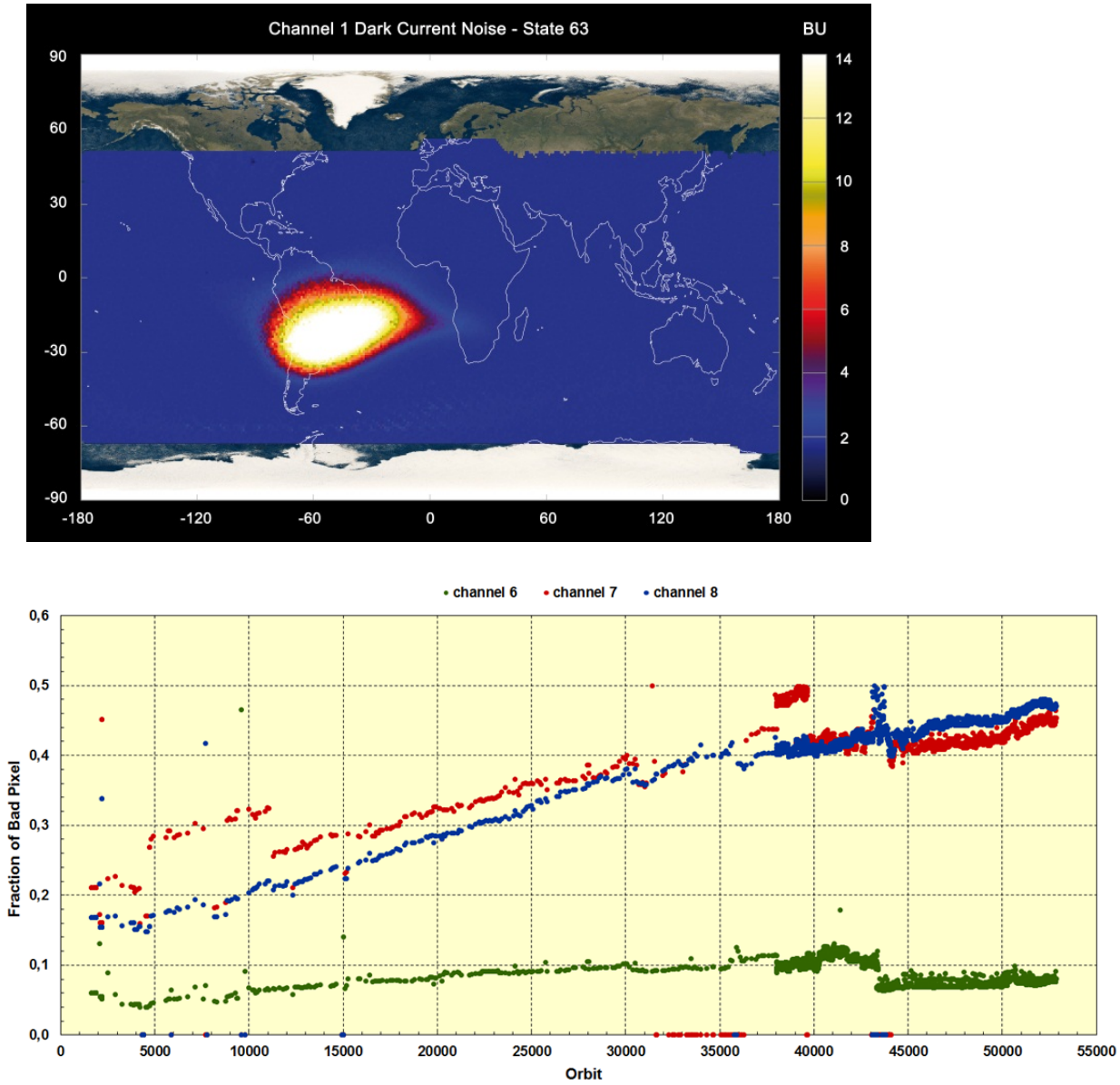

Fig. 2-10: Southern Atlantic Anomaly (SAA) as derived by dark noise in SCIAMACHY data (top). Development of the fraction of bad pixels over time in channels 6, 7 and 8 (bottom). Most of the pixels get bad when they are hit by protons in the SAA.

Year	Implemented Features
2001	First version of the prototype delivered to ESA
2003	End of last commissioning measurements of SCIAMACHY, adjustment and improvement of algorithms based on first in-flight experience
2004	Prototype for IPF Version 5 implemented
2005	Development of the SciCal tool to be used for the calculation of calibration data
2006/2007	Prototype for version 6 of the IPF • introduction of dynamic bad and dead pixel mask • introduction of new memory effect correction and non-linearity correction • measurements for dark correction now taken from same orbit • new stray light correction channel 1 • mispointing correction
2008	Prototype for version 7 of the IPF • Stray Light Matrix for channel 2 • correction geolocation for onboard software error • bug fixing
2012	Prototype for version 8 of the processor, see below

Table 2-3: Overview of important steps in the Level 0-1b processor development.

The history of how the SCIAMACHY level 0-1b processor had evolved over time demonstrates well that its continuous development is as important as that for the level 1b-2 processor.

New Level 0-1b Processor

The largest update of the processor concerns the degradation correction. To measure nadir and limb radiances, SCIAMACHY uses mirrors, which scan the total clear field of view of the instrument. The different viewing directions have different angles of incidence on the mirror. In the current version of the processor, the degradation of the instrument is treated as scan angle independent. For some products (especially those that need absolute radiances as inputs) this leads to a scan angle dependent bias which changes with the life time of the instrument. To correct the measurements, SRON had developed a scan mirror model that models the (two) mirror surfaces, a decontamination layer on the mirrors and the optical bench. Mathematically, the model uses the Mueller-Matrix approach to model the transformation of the light by the mirrors and the optical bench:

$$S_{det} = \left(M_1^{OBM} \;\; M_2^{OBM} \;\; M_3^{OBM} \;\; M_4^{OBM}\right) \cdot \begin{pmatrix} M_{11}^{sc} & M_{12}^{sc} & M_{13}^{sc} & M_{14}^{sc} \\ M_{21}^{sc} & M_{22}^{sc} & M_{23}^{sc} & M_{24}^{sc} \\ M_{31}^{sc} & M_{32}^{sc} & M_{33}^{sc} & M_{34}^{sc} \\ M_{41}^{sc} & M_{42}^{sc} & M_{43}^{sc} & M_{44}^{sc} \end{pmatrix} \cdot \begin{pmatrix} I \\ Q \\ U \\ V \end{pmatrix}$$

The scan mirror model was successfully implemented and verified. In addition, the following changes were made to the processor:

- introduction of matrix stray light correction for channels 3-8
- improvement of memory effect correction for Limb measurements
- better nonlinearity scaling for co-added measurements
- improvement of hot pixel correction for limb measurements
- possibility to choose individual measurement states for the dark correction.

Level 0-1b Phase F Activities

Plans exist to evolve the existing algorithms and processors in the post-operations phase F even further. The 'phase F processor' would take advantage of the fact that it is no longer restricted by the need of near-realtime delivery and forward processing: all inputs are known already before the processing.

Additionally, in this phase the data must be prepared for long-term archiving. Preliminary plans for phase F activities include

- analysis of all calibration data using the parameter database
- characterization of the quality of individual detector pixels in the retrieval windows
- consolidation of the errors of the level 1b product
- consolidation of all documentation
- transfer of products to a standard data format.

Level 1b-2 Processor

After abandoning the level 2 NRT processor in 2006, the offline processor developed at MF-ATP is used for the generation of all level 2 products. Although the number of products has steadily increased and the algorithms got more sophisticated, the computation time per orbit could be held more or less constant with 15-25 minutes. This led to the decision that the offline processor was also used for the so-called *Fast Delivery Service (FD)* that aimed to deliver products within 24 hours of sensing (see annual report 2010). After the loss of ENVISAT the FD service is no longer required. The pace of the development of the offline processor however did not change. The new processor (version 6) will add 4 new nadir products, one new limb product and several improvements. Table 2-4 gives an overview of the development of the processor since the establishment of the SCIAMACHY Quality Working group.

	V 3.01	(V 4)	V 5/5.02	V 6
Nadir				
O_3	improved[1]	improved	maintenance	maintenance
NO_2	improved	improved	maintenance	maintenance
AAIA	improved	new algorithm[3]	maintenance	improved
CTH	improved	maintenance[2]	maintenance	maintenance
CFR	improved	maintenance	improved	improved
SO_2		new[4] (SCD)	improved (VCD)	improved
BrO		new (SCD)	improved (VCD)	maintenance
OClO			new (SCD)	improved
H_2O			new	maintenance
CO			new	improved
CHOCHO				new
HCHO				new
CH_4				new
Limb				
O_3	improved	improved	improved	improved
NO_2	improved	improved	maintenance	maintenance
BrO			new	maintenance
Cloud			new	improved
Limb/Nadir				
Tropospheric NO_2				(new)

1 improved: Algorithm/entries of product were improved.
2 maintenance: Algorithms was checked versus validation and bugs
3 new algorithm: Newly implemented algorithm, same product
4 new: New product (SCD or VCD marks the introduction of the vertical or slant column density)

Table 2-4: Product improvements in the level 1b-2 processor since establishment of the SQWG. The algorithms are developed together with BIRA, IUP Bremen, KNMI and SRON. Tropospheric NO_2 will occur in version 6 or 7 depending on the maturity of the operational algorithm. Version 4 was delivered to ESA, but was not implemented in the ground segment due to delays in the ground segment migration to Linux.

It is planned to deliver version 6 of the processor in March 2013. Compared to the previous version it has the following changes:

- the Aerosol Absorbing Index Algorithm (AAIA) now uses the measured O_3 column instead of a modeled one to derive the aerosol index from modeling
- the cloud fraction algorithm takes into account the degradation of the instrument and has an additional cloud/snow separation based on the SPICI algorithm from SRON
- several improvements in the nadir SO_2 and OClO retrievals
- the CO retrieval takes into account the changing wavelength calibration of the channel
- new nadir products CHOCHO, HCHO and CH_4
- extension of the O_3 profile to 60 km
- improvements of the limb cloud algorithm.

Depending on the progress of the limb/nadir matching algorithm, tropospheric NO_2 could also be added to the next version of the processor.

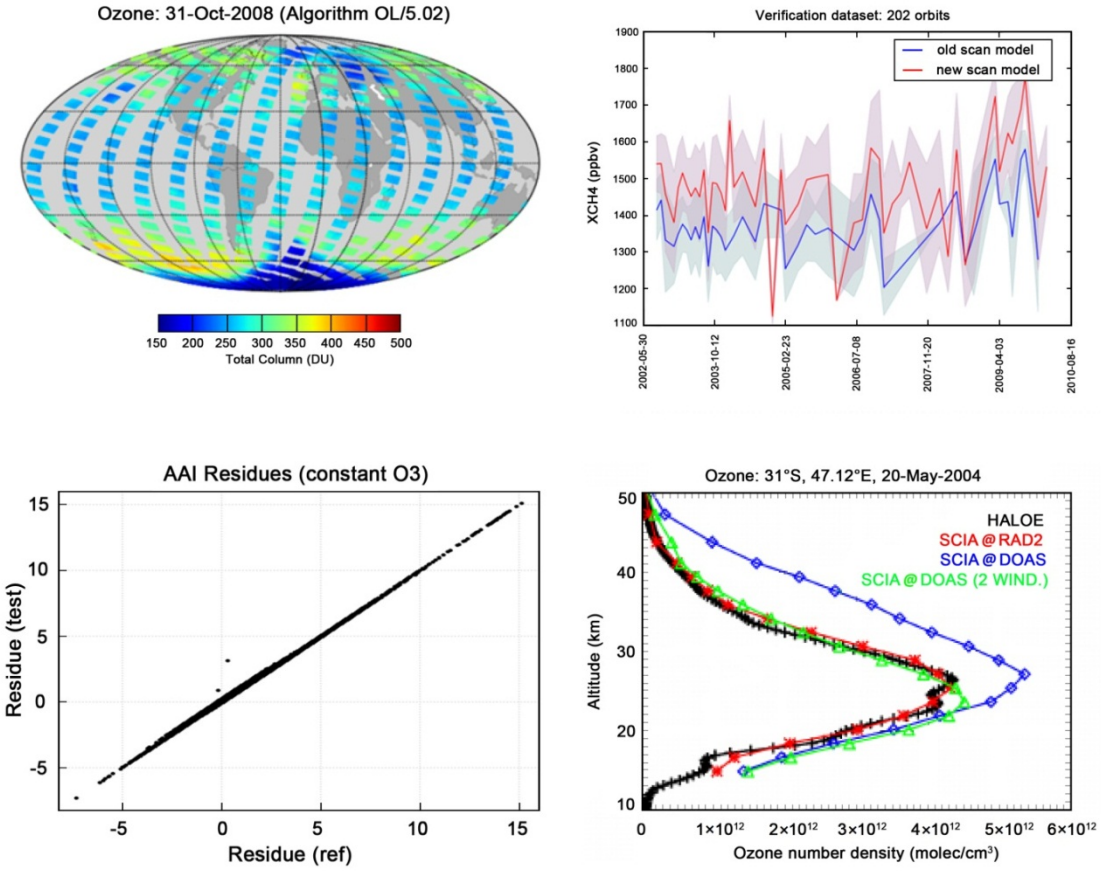

Fig. 2-11: Some Results of the level 1b-2 processor. Clockwise from top left: One day of O_3 measurements (V. 5.02), comparison of CH_4 column with and without the new scan mirror model in level 1b, AAIA verification for the version 6 processor, test of different implementations for the height extension of the Limb O_3 profile in comparison to a HALOE profile.

Apart from improvements in the product algorithms themselves, several modifications in the underlying structure of the processor and its ability to ingest data were implemented over time. In version 5 the possibility to select calibration options was added together with the application of radiometric degradation correction in the internal level 1b-c step (the level 2 processor performs the calibration of the level 1b data). In version 5.02 we migrated the processor to 64-bit architecture and the latest gcc compiler. For version 6 the build system was changed from the commercial Sniff to a more flexible combination of `Cmake` and subversion. These changes ensured that the processor can be maintained for the foreseeable future.

2.4 The Sentinel 5 Precursor Mission

D. Loyola, M. Gottwald, T. Trautmann

The Sentinel 5 Precursor (S5P) mission is an integral part of the space component of the European GMES (Global Monitoring of Environment and Security) initiative. Together with Sentinel 4 (S4) and 5 (S5) it contributes to retrieving knowledge about the state of the Earth's atmosphere. Since the launch of both Sentinels has to await the end of this decade (2019 – S4 and 2020 – S5), ESA and The Netherlands had agreed to develop and operate the S5P mission for bridging the gap between now and S4 and S5. It carries the absorption spectrometer TROPOMI, the Tropospheric Monitoring Instrument, which is a joint development of The Netherlands and ESA. TROPOMI is heritage of SCIAMACHY aboard ENVISAT and the Dutch OMI instrument aboard NASA's EOS-Aura mission. TROPOMI covers spectral bands in the ultraviolet (UV), the visible (VIS), the near-infrared (NIR) and the shortwave infrared (SWIR), see (Table 2-5).

	UV	UVIS	NIR	SWIR
Wavelength (nm)	270-320	320-490	710-775	2305-2385
Spectral resolution	0.5	0.5	0.5	0.25
Ground pixels per second	72-260	260	260-512	256

Table 2-5: TROPOMI spectral and spatial capabilities

One of TROPOMI's big assets is the excellent spatial resolution in the range of only a few kilometers (7 x 7 at nadir) with a daily global coverage (swath 2600 km). This is a real improvement when compared with the GOME-2 sensors onboard the MetOp series of satellites or SCIAMACHY on ENVISAT. It will permit retrieving trace gas maps with unprecedented spatial accuracy. In urban areas, local sinks and sources shall be detectable even on quarter level (Fig. 2-12). Very high spatial resolution can only be achieved when large amounts of data, i.e. absorption spectra over the full wavelength range, are acquired by the instrument, downlinked and processed on-ground. This turns out to be a real challenge for ground segment facilities. For a 7-year in-orbit operation lifetime estimates range up to about 2-3 PByte of acquired data (for comparison: SCIAMACHY captured, over 10 years, about 1% of this value). Therefore the amount of data from TROPOMI is comparable to the national TanDEM-X radar mission. A further big challenge is the very short schedule, since the S5P launch is planned for June 2015 already.

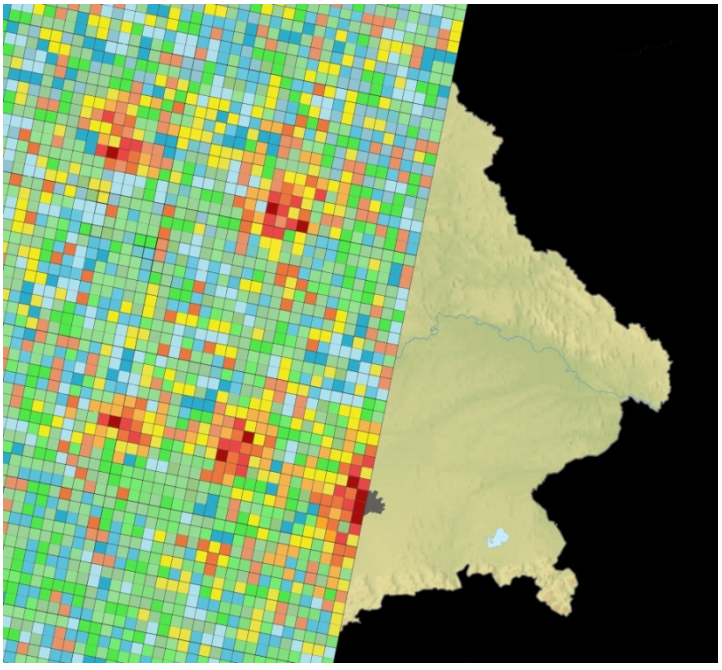

Fig. 2-12: A simulated S5P orbit over Bavaria with an orbit illustrating 7 km × 7 km ground pixels.

DLR-EOC Involvement in S5P

Participating in the S5P mission has always been considered important at EOC as a preparation for the future S4 and S5 undertakings. With the sudden loss of ENVISAT, including its atmospheric payload, in April 2012 (see chapter 2.1), the need for providing significant contributions has become an even bigger concern since otherwise a long data gap from European atmospheric missions could have developed

with UV/VIS/NIR measurements being only available from the GOME-2 sensors onboard the MetOp-A and MetOp-B satellites.

The previous year 2012 was particularly successful for EOC because two major involvements in operational S5P domains could be accomplished:

- **S5P Payload Data Ground Segment (PDGS)**: The German Remote Sensing Data Center (DFD) together with MF shall provide the functionalities for S5P data processing (level 0-1-2), archiving and product dissemination together with corresponding quality monitoring tasks. Due to the current financial restrictions, the ESA contract covers only a 'basic' PDGS version that will ensure 25% data throughput at a reduced rate for the Commissioning Phase (up to 6 months) with the option for upgrading to the full system afterwards including the NRT capabilities.
- **S5P Level 2 project (S5P L2)**: It comprises the generation of priority 1 GMES products in collaboration with IUP-IFE, University Bremen, KNMI, IASB-BIRA, SRON, Rutherford Appleton Laboratory (RAL) and the Max-Planck-Institute for Chemistry (MPIC). MF-ATP became responsible for various functions in level 2 algorithm and processor development (Table 2-6). It reflects our expertise developed over the past two decades with GOME, SCIAMACHY and GOME-2. The S5P L2 project is funded via complementary ESA contracts, grants from Bavaria, and DLR internal financing.

The development of the S5P L2 project is organized in three core activities:

- **Algorithm prototyping**: Retrieval algorithms for all S5P target species to be used/integrated in the operational L2 processors,
- **Independent verification**: Independent retrieval algorithms for verification of the algorithm prototypes, and
- **Operational processor**: Operational L2 processors, including their configuration, to be integrated into the S5P PDGS.

All development, verification, testing, operational and management tasks are organized in line with these core activities with the overall coordination being shared between three institutes.

Product / Processor Component	**Development**		**Operational Processor**
	Algorithm Prototyping	**Independent Verification**	
	KNMI	**IUP-IFE**	**DLR-MF**
Mandatory Products			
O_3 total column	DLR-MF, BIRA	KNMI	DLR-MF
O_3 profiles (incl. troposphere)	KNMI	RAL, IUP-IFE	KNMI
O_3 tropospheric column	IUP-IFE, DLR-MF	KNMI	DLR-MF
NO_2 total & tropospheric column	KNMI	IUP-IFE, DLR-MF, MPIC	KNMI
SO_2	BIRA	MPIC, DLR-MF	DLR-MF
HCHO	BIRA	IUP-IFE	DLR-MF
CO	SRON	IUP-IFE	KNMI
CH_4	SRON	IUP-IFE	KNMI
Clouds	DLR-MF	KNMI, MPIC, IUP-IFE	DLR-MF
Aerosols	KNMI	MPIC, IUP-IFE	KNMI
External Auxiliary Data			
Cloud data from NPP	RAL	n.a.	RAL

Table 2-6: Sentinel 5 Precursor level 1-2 development responsibilities.

The *Level 2 Working Group (L2-WG)*, chaired by ESA, manages the overall project organization by ensuring that the appropriate coordination between the various development teams is maintained throughout all development phases. The L2-WG is organized as indicated in Figure 2-13.

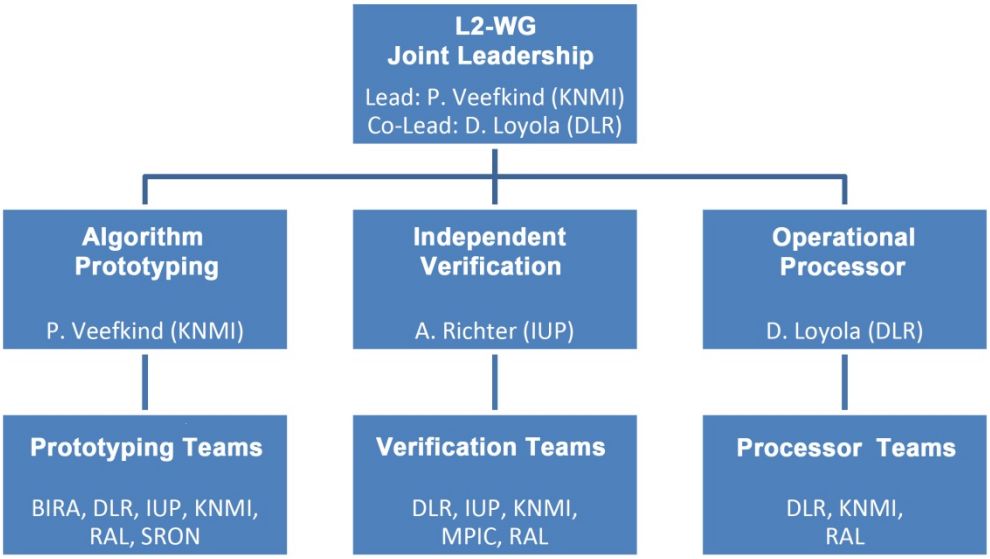

Fig. 2-13: S5P Level 2 Working Group Organization.

With the improved quality of the products from the S5P portfolio listed in Table 2-6 various prospects become possible. They comprise themes like, e.g., the GMES atmospheric core service MACC and the ESA Climate Change Initiative for space-borne exploration of global atmospheric change, air quality monitoring with subsequently issuing warnings, even on the level of urban quarters or monitoring volcanic eruptions in support of aviation safety.

3. Atmospheric Remote Sensing – Retrieval Methods

3.1 Operational O3M-SAF Trace Gas Column Products from GOME-2 on MetOp-A & B

P. Valks, N. Hao, M. Grossi, P. Hedelt, D. Loyola, and W. Zimmer

The GOME-2 trace gas column products have been developed by MF-ATP in the framework of EUMETSAT's Satellite Application Facility on Ozone and Atmospheric Chemistry Monitoring (O3M-SAF). The current GOME-2 trace gas products of the O3M-SAF include total ozone, total and tropospheric NO_2, SO_2, BrO, formaldehyde and water vapour. The O3M-SAF trace gas column products are generated operationally at DLR using the GOME Data Processor (GDP) version 4.5 (*Valks et al. 2012*). In February 2012, the Continuous Development and Operation Phase 2 of the O3M-SAF started, which will cover the period until 2017. The focus of the CDOP-2 will be on the development of new and better products, on new dissemination methods and on improved user services. New GOME-2 trace gas column products planned for the CDOP-2 are: total OClO, tropospheric O_3, BrO and glyoxal, and climate products for NO_2 and water vapor.

New Tropospheric O_3 Product

The tropospheric ozone column for the (sub)-tropical region is a new O3M-SAF product being developed within the CDOP-2. The retrieval algorithm for the tropical tropospheric ozone column is based on the convective-cloud-differential (CCD) method (*Valks et al. 2003*), and uses both ozone column and cloud measurements from GOME-2. In March 2012, a Product Consolidation Review of the new GOME-2 tropospheric ozone product was carried out successfully.

BrO Product Improvement

Inorganic bromine (Br_y) is the second most important halogen that affects stratospheric ozone. In the troposphere large emissions of inorganic bromine taking place during polar springtime period result in Ozone Depletion Events (ODEs). BrO is the only compound within the Br_y family to be measured routinely. The BrO slant column retrieval with the DOAS method has been improved for GOME-2 by using a larger fit window (332-359 nm) in the UV. This reduces the noise in the retrieved BrO columns and the interference with other absorbers in this wavelength region, such as formaldehyde. Early 2012, the algorithm improvement for BrO has been implemented in the operational GOME-2 processor.

SO_2 Product in Near-realtime

Atmospheric SO_2 is an important indicator for volcanic eruptions and volcanic activity like passive degassing. Furthermore, it is produced anthropogenically in power plants, refineries, metal smelting and the burning of fossil fuels. The GOME-2 SO_2 column is retrieved with the DOAS method in the UV wavelength region 315-326 nm, and includes a background correction for the interference of O_3 and SO_2 absorption features. The volcanic air mass factors are a function of plume height and SO_2 load, and a cloud correction is applied. The operational dissemination of the GOME-2 SO_2 product started in 2009. Since the end of 2012, the GOME-2 SO_2 product is also provided in near-realtime via EUMETCast (and FTP). This is especially of importance for early warning services related to volcanic hazards, such as the Support to Aviation Control Service (SACS) of ESA and the GMES European Volcano Observatory Space Services (EVOSS – see chapter 4.2).

GOME-2 on MetOp-B

The second GOME-2 instruments was launched on MetOp-B from Baikonur, Kazakhstan, on 17 September 2012. MetOp-B makes it possible to continue the supply of operational GOME-2 products for at least the coming 5 years. In December 2012, EUMETSAT initiated the regular delivery of GOME-2/MetOp-B level-1 products via EUMETCast and first retrievals of trace gas columns from GOME-2/B were performed at MF-ATP. An example of the total NO_2 columns from GOME-2/B is shown in Fig. 3-1 for December 2012. Clearly visible are the high tropospheric NO_2 concentrations above large urban and industrial areas, such as Eastern China (*Valks et al. 2011*). Fig. 3-2 shows an example of the enhanced SO_2 columns from the eruption of the Copahue volcano on the Chile/Argentina border as measured by

GOME-2/B on 24 December 2012. The eruption started two days earlier, and the SO_2 cloud has already been transported to the east over the Southern Atlantic Ocean.

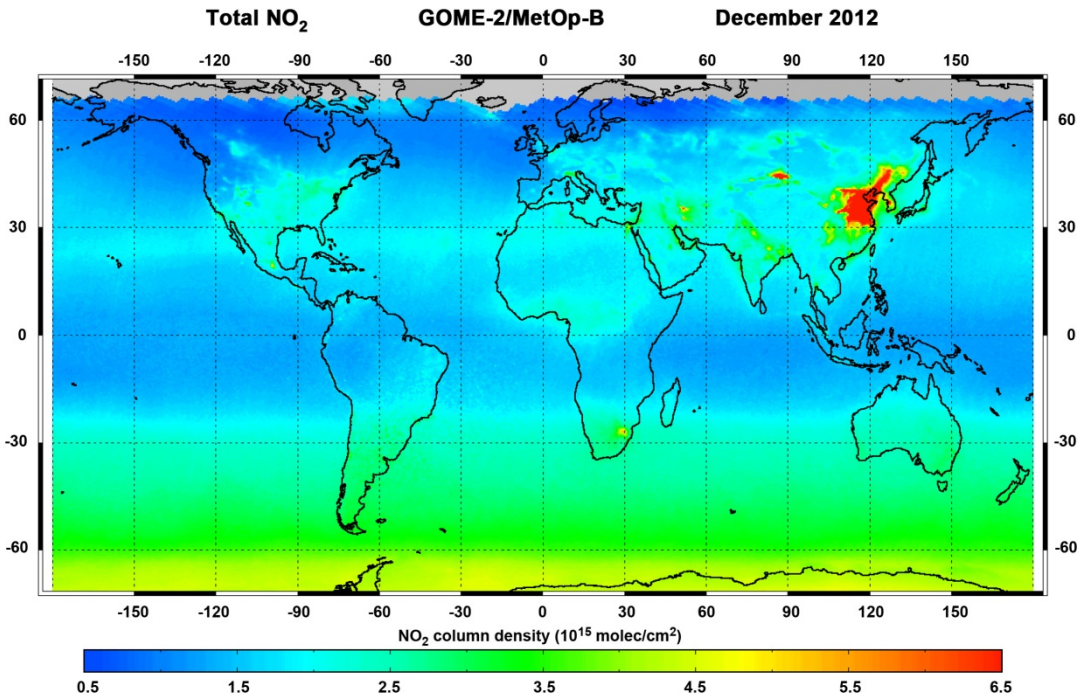

Fig. 3-1: Average total NO_2 columns for December 2012 as measured by GOME-2 on Metop-B.

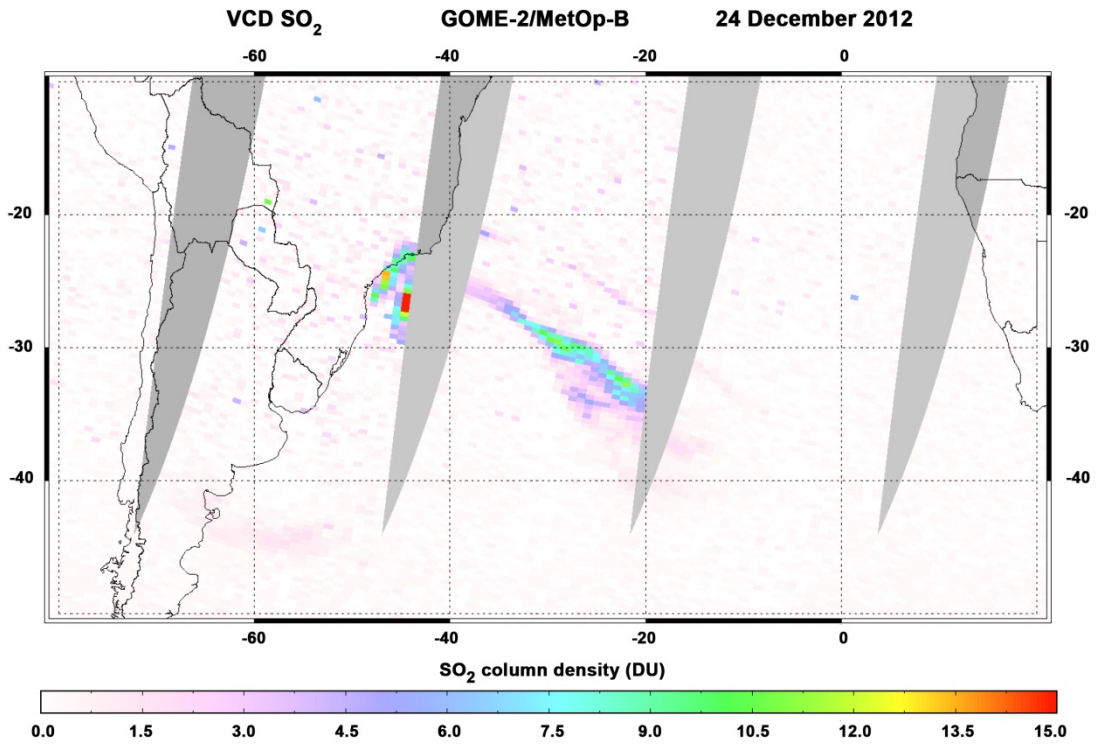

Fig. 3-2: Volcanic SO_2 plume from the eruption of Copahue volcano on the Chile/Argentina border as detected by GOME-2 on MetOp-B on 24 December 2012.

References

Valks P.J.M., Koelemeijer R.B.A., van Weele M., van Velthoven P., Fortuin J.P.F., and Kelder H.: Variability in tropical tropospheric ozone: Analysis with Global Ozone Monitoring Experiment observations and a global model. J. Geophys. Res., 108, 4328, 2003

Valks P., Pinardi G., Richter A., Lambert J.-C., Hao N., Loyola D., Van Roozendael M., and Emmadi S.: Operational total and tropospheric NO_2 column retrieval for GOME-2. Atmos. Meas. Tech., 4, 1491-1514, doi:10.5194/amt-4-1491-2011, 2011

Valks P., Loyola D., Hao N., Rix M., and Slijkhuis S.: Algorithm Theoretical Basis Document for GOME-2 Total Column Products of Ozone, Minor Trace Gases and Cloud Properties (GDP 4.5 for O3M-SAF OTO and NTO). DLR/GOME-2/ATBD/01, Iss./Rev.: 2/G, 2012

3.2 Validation of GOME-2 Water Vapour Product with Independent Satellite Observations

M. Grossi, S. Slijkhuis, D. Loyola, P. Valks, B. Aberle, S. Beirle (MPIC), K. Mies (MPIC), T. Wagner (MPIC), H. Gleisner (DMI), K.B. Lauritsen (DMI)

It is well known that water vapour is one of the most important atmospheric constituents and has a strong impact on the Earth's radiative balance. Thus, the knowledge of the effective distribution of Total Column Water Vapour (TCWV) is fundamental for weather monitoring as well as for the evaluation of climate models. Unfortunately, difficulties in observing water vapour in the troposphere have long hampered the observational and modeling studies, and significant limitations remain in coverage and reliability of observational humidity datasets. It is very important to assess the accuracy and improve the post processing of satellite data in order to have a consistent picture of the coherence of the results produced employing different technologies (e.g., ground-based measurements, microwave sensors, GPS).

GOME-2 H_2O Product

The operational GOME-2 H_2O data used in the validation of the water vapour data obtained from measurements of the GOME-2 instruments against independent satellite observations have been developed in the framework of the O3M-SAF and generated by MF-ATP using the GOME Data Processor (GDP) version 4.5 (*Valks et al. 2012*). The algorithm used for the retrieval of H_2O Vertical Column Density (VCD) is based on a classical Differential Optical Absorption Spectroscopy and employs a combined H_2O/O_2 retrieval in order to compute the TCWV (*Wagner et al. 2003*). This method relies on as little as possible external information on the state of the atmosphere and leads to rather stable and robust results, although being representative for cloud-free situations only, and shows the potential for climatological studies.

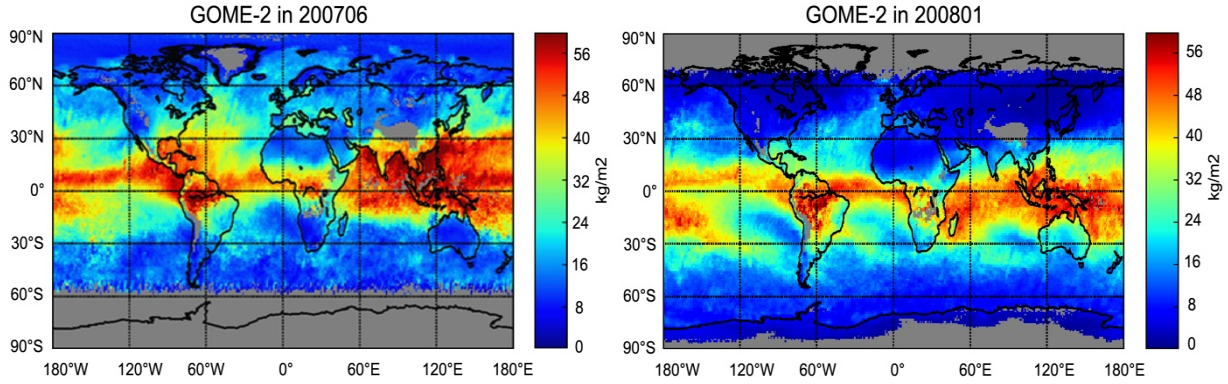

Fig. 3-3: Monthly mean maps of TCWV from GOME-2 for June 2007 (left) and January 2008 (right).

Fig. 3-3 shows the mean distribution of GOME-2 TCWV data for the months June 2007 and January 2008. In contrast to other satellite datasets, the GOME-2 product has the advantage that it covers the entire Earth, including both sea and continents, leading to a more consistent picture of the global distribution of the atmospheric humidity. The retrieval is performed in the visible spectral range and it is very sensitive to water vapour in the lower troposphere, which contributes the major fraction of the total atmospheric column.

From Fig. 3-3 we can observe that for both months there is high humidity in the tropics and low humidity at higher latitudes. Also the movement of the inner tropical convergence zone with seasons is clearly visible from the shift of the high water vapour column in the tropics between June 2007 and January 2008. In both hemispheres, the total column precipitable water vapour distribution follows the seasonal cycle of the near surface temperature and so the tropical total column precipitable water has a maximum during the northern hemisphere (NH) summer, and a minimum in winter.

GOME-2 H_2O Product Validation

We have compared the GOME-2 water vapour column product with 4 independent datasets. The first dataset is based on passive microwave observations from SSM/I orbits processed with the latest version of the HOAPS algorithm (HOAPS-3.2 dataset: *Fenning et al. 2012*). It is available over ocean only, however includes the TCWV also for cloudy scenes, both day and night overpasses and spans a very large time range (SSM/I has been in orbit since 1987).

The second dataset consists of combined SSM/I + MERIS TCWV Level 3 data (*Schroeder et al. 2010*). This dataset is based on radiance measurements in the microwave range taken by SSM/I over ocean and TCWV retrievals from measurements of the visible and near infrared by MERIS (over land and costal regions). MERIS provides water vapour column amounts for cloud free scenes for day time overpasses over land with a very good spatial resolution. However, like for GOME-2, the quality of the retrievals is affected by the presence of clouds.

Finally, we have compared GOME-2 data with Global Positioning System Radio Occultation (GPS RO) soundings from COSMIC (*Rocken et al. 2000*) and CHAMP (*Wickert et al. 2001*). We used the COSMIC RO data collected during the period from January 2007 to December 2008 from the FM4 micro-satellite. Despite the relatively small amount of data available, GPS RO measurements are valuable because their information can complement that provided by satellite radiance measurements. GPS RO measurements have good vertical resolution and very high temporal resolution. They are available for all weather conditions over both land and sea.

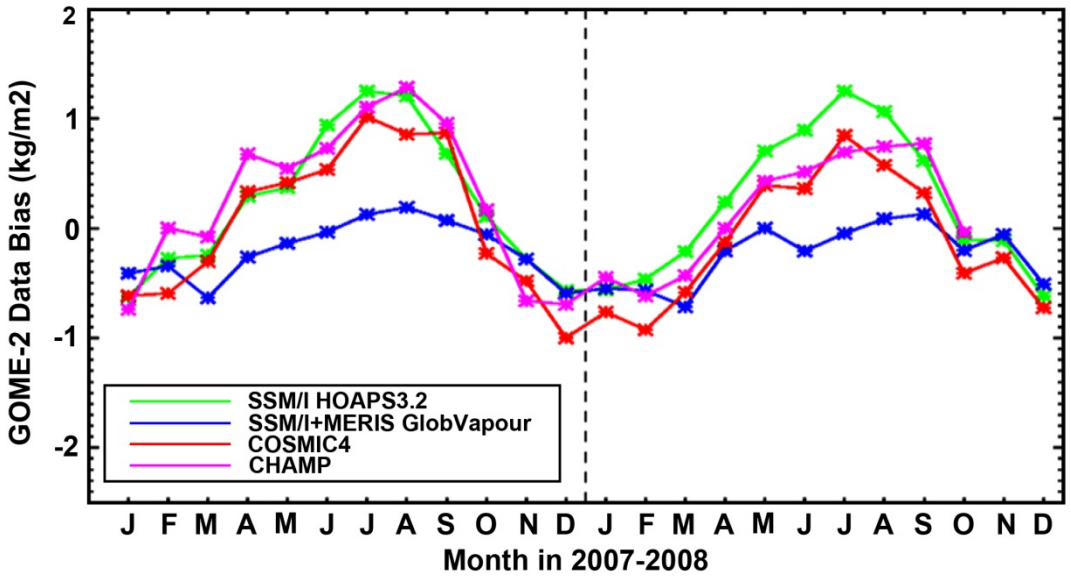

Fig. 3-4: Monthly mean TCWV bias between GOME-2 and four independent satellite datasets for the period January 2007 – December 2008.

We performed comparisons between GOME-2 and the four different datasets described above for the time period January 2007 – December 2008. Fig. 3-4 shows the time series of the globally averaged bias derived from the monthly mean TCWV distribution. The agreement between GOME-2 TCWV data and the other independent satellite measurements is very good for all comparisons: the mean biases for the full time series are close to 0, while the Root Mean Square Error (RMSE) varies between 3.5 and 7 kg/m^2 (see Table 3-1). In this contest, the validation and intercomparison has been performed in such a way that positive and negative bias imply respectively larger (and lower) GOME-2 data.

Data	Bias (kg/m^2)	RMSE (kg/m^2)
GOME-2 - SSM/I	0.23 +/- 0.64	3.5 +/- 0.45
GOME-2 - SSM/I+MERIS	-0.22 +/-0.27	4.0 +/- 0.46
GOME-2 - COSMIC4	-0.02 +/-0.63	7.0 +/- 0.24
GOME-2 - CHAMP	0.22 +/-0.63	6.9 +/- 0.31

Table 3-1: Statistics of the time period January 2007 – December 2008. Bias and RMSE refer to the average difference GOME2-DATA.

Further analysis of the GOME-2 and SSM/I HOAPS intercomparison (green line and points in Fig. 3-4) showed a positive bias in NH summer and a negative bias in NH winter, with the averaged TCWV for SSM/I HOAPS being higher than GOME-2 (0.23 kg/m^2, see Table 3-1). The monthly averaged bias ranges from -0.62 kg/m^2 in January 2007 to 1.25 in July 2007. We could infer a seasonal cycle in the geographic distribution of the bias between cloud affected measurements (GOME-2) and all sky (HOAPS) data sets, which is probably related, among other reasons, to the seasonability of cloud properties in some locations, as well as the variability of geographic distribution of major cloud structure at the ITCZ. We observed a similar seasonal variation in the bias between GOME-2 and GPS RO measurements. However, in this case some of the differences in TCWV are a result of the limited number of CHAMP and COSMIC measurements. Also the RMSE is larger for both the GPS RO observation due to the low number of collocations with GOME-2. Finally, for the SSM/I + MERIS dataset, we could see that the seasonal behaviour is not as evident as for the other comparisons, as a result of the different biases over land (MERIS) and sea (SSM/I). In general the MERIS measurements present a wet bias with respect to all other datasets, which might be partly caused by spectroscopic uncertainties, such as the description of the water vapour continuum. Interpreting these results, we should also have in mind the limitations of the GOME-2 retrieval. Although, as discussed before, a specific advantage of the visible spectral region is that it is sensitive to the water vapour concentration close to the surface and that it has the same sensitivity over land and ocean and can thus yield a consistent global picture, the accuracy of an individual observation is, in general, reduced for cloudy sky observations. In addition, since GOME-2 observations are made at 9:30 local time, especially in regions with a pronounced diurnal cycle, they might not be representative for the daily, and therefore monthly, average.

Conclusion

In summary, the agreement between GOME-2 and the 4 independent datasets analyzed in our study is very good. We found a mean bias within +/- 1 kg/m^2 for the time interval January 2007 – December 2008. The annual variability of the bias over land (and coastal area) is low, but over sea a clear seasonal cycle with highest values during Northern Hemisphere summer is observed for both SSM/I and GPS RO measurements. We observed negative values for the bias in the Northern Hemisphere winter. The GOME-2 data are typically drier than the COSMIC and CHAMP measurements in the northern hemisphere winter, both considering the monthly and seasonal mean water vapour total columns and higher in NH summer season, with minor differences located prevalently in the northern sub-tropical area. Based on the results of the validation with independent satellites data, we can conclude that there is a good agreement with GOME-2 H_2O measurements for all seasons and latitude.

References

Fennig K., Andersson A., Bakan S., Klepp C., Schroeder M.: Hamburg Ocean Atmosphere Parameters and Fluxes from Satellite Data - HOAPS 3.2 - Monthly Means / 6-Hourly Composites, Satellite Application Facility on Climate Monitoring, doi:10.5676/EUM_SAF_CM/HOAPS/V001, 2012

Rocken C., Kuo Y.-H., Schreiner W., Hunt D., Sokolovskiy S., and McCormick C.: COSMIC system description, Terr. Atmos. Oceanic Sci., 11(1), 21-52, 2000

Schroeder M., DUE GLOBVAPOUR Technical Specification Document (TSD), issue 1, revision 0, 16 April 2010

Valks P., Loyola D., Hao N., Rix M. and Slijkhuis S.: Algorithm Theoretical Basis Document for GOME-2 Total Column Products of Ozone, Minor Trace Gases and Cloud Properties (GDP 4.5 for O3M-SAF OTO and NTO), DLR/GOME-2/ATBD/01, Iss./Rev.: 2/GG, http://atmos.caf.dlr.de/gome2/docs/DLR_GOME-2_ATBD.pdf, 2012

Wagner T., Heland J., Zoger M., and Platt U.: A fast H_2O total column density product from GOME – Validation with in-situ aircraft measurements, Atmos. Chem. Phys., 3, 651–663, 2003

Wickert J. et al.: Atmosphere sounding by GPS radio occultation: First results from CHAMP, Geophys. Res. Lett., 28, 3263–3266, 2001

3.3 Interpolation of Atmospheric Composition Satellite Data for the Generation of ECVs

J. Waitz, D. Loyola

The production of consistent and stable long-term satellite-based essential climate variables (ECVs) is substantial for monitoring climate change. The accuracy of such ECVs depends on many factors. In addition to intrinsic errors of the retrieval algorithms, satellite spatial and temporal samplings as well as gridding are important contributors affecting the quality and representativeness of the ECV.

In particular, averaging a set of individual satellite measurements, like taking the monthly mean, can introduce systematic uncertainties. In a first step we used model data for ozone and water vapour to characterize the sampling error of ECVs generated using the satellites GOME/ERS-2, SCIAMACHY/ENVISAT, GOME-2/MetOp-A and SBUV2/NOAA-11. For analyzing the sampling errors we computed a 'simulated' satellite measurement from the model data by mapping them into the footprints of a real satellite as shown in Fig. 3-5.

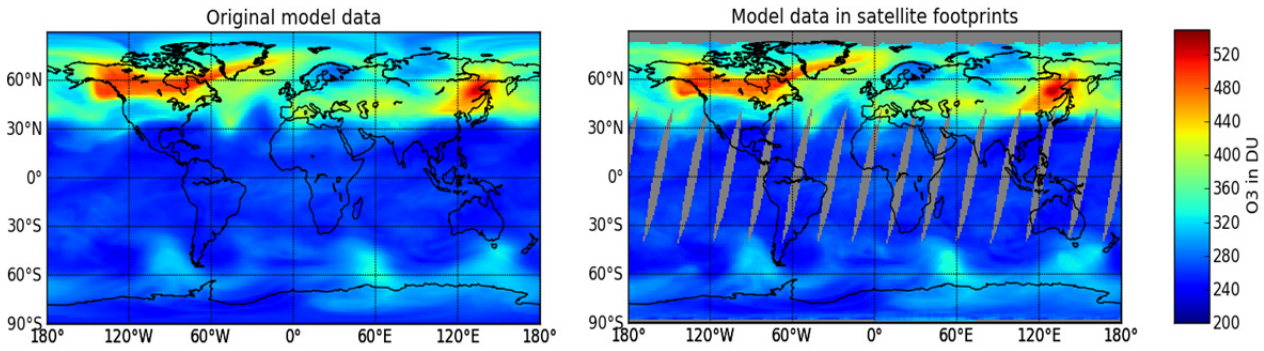

Fig. 3-5: Ozone column on the 1 March 2011. The original model data (left) and after mapping them into the satellite (GOME-2/MetOp-A) footprints (right).

We performed an area-weighted spatial interpolation of the model data to the polygons representing the satellite ground pixels and an interpolation in time to the satellite overpass period. The model data were provided every 6 hours in a regular grid with a step size of 1/8°. Using this procedure we simulated satellite measurements for a complete year. Then we computed the corresponding monthly mean ECV to compare them to the original model data.

The main goal of this work is to fill the gaps in satellite data sets for generating complete time-series minimizing the sampling errors. Having the model data mapped in the satellite format enabled us to investigate different interpolation methods with a data set for which we actually knew the missing values. This was identical to a real satellite, however with the advantage that original model data were available for comparison. A possible interpolation method is the *Kriging Approximation*. This procedure is based on minimizing the mean error of the weighting sum of the sampling values. It involves the determination of a semi-variogram model with its parameters from the known set of data points and the calculation of the weighting coefficients. In a first approach it turned out that the determination of the semi-variogram consumed considerable computation time. Therefore investigations continue to prove whether variations of the *Kriging Approximation* or other interpolation methods are more suitable in terms of computational cost, robustness and accuracy.

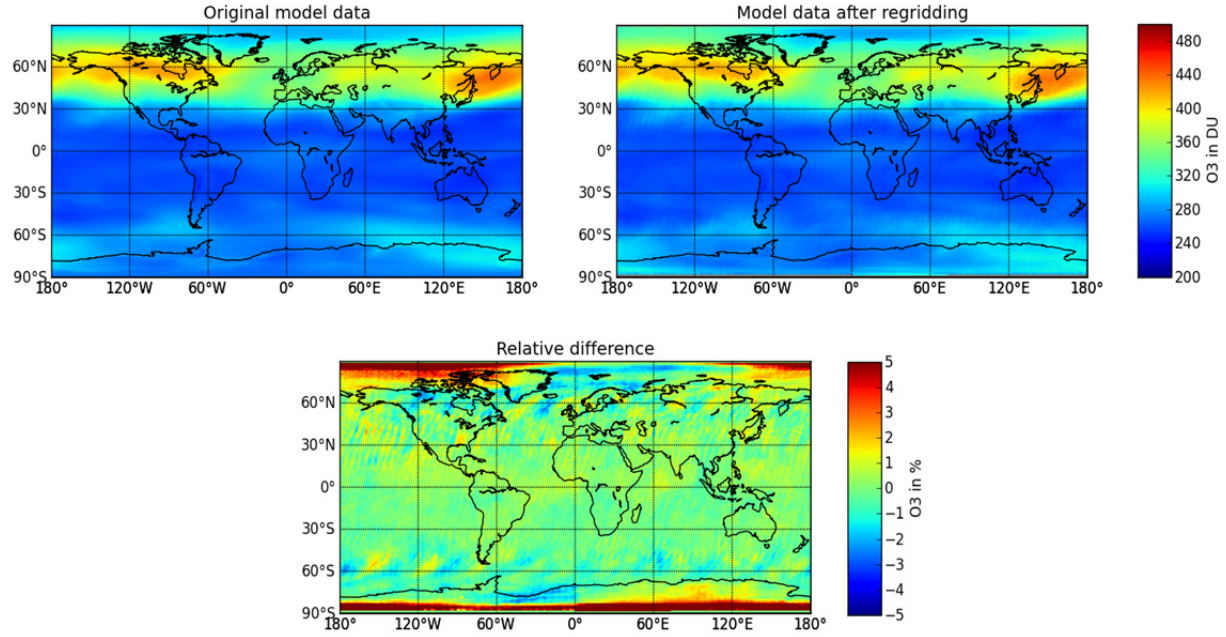

Fig. 3-6: Monthly mean ozone column for March 2011 of the original model data (upper left) and after mapping them into the satellite (GOME-2/MetOp-A) footprints and back in the regular grid (upper right). The bottom panel shows the relative difference between both.

In preparation for the actual interpolation testing we mapped data of the 'model satellite' back into a regular grid. Again, as in the first mapping from the regular grid into the satellite footprints, sampling errors occur in this step. Fig. 3-6 shows the comparison of the monthly mean ozone of March 2011 between the original model data and the data after mapping it into the 'footprints' of GOME-2 and back into the regular grid. The relative difference lies in general below 2%, except for the polar regions where it reaches up to 27%. This is due to the fact that the original pixels at the poles are given in a longitude/latitude grid. When mapping them onto the much larger satellite pixels (length specified in meters), they overlap causing the observed discrepancies.

3.4 Retrieval of OH by Far Infrared Limb Sounding: A Sensitivity Study

J. Xu, F. Schreier, P. Vogt (MF-EXV), A. Doicu, T. Trautmann

One of the main chemical species controlling the oxidizing capability of the global atmosphere is the hydroxyl radical OH. Measuring OH in the stratosphere can be achieved with the TELIS spectrometer (TErahertz and submillimeter Limb Sounder) using the 1.8 THz channel. In order to understand how the performance of the OH retrieval is affected by an imperfect instrumental knowledge, we have carried out a corresponding error analysis. We retrieved OH from a single limb scan that largely resembles typical TELIS observations by the 1.8 THz channel. For this dedicated OH microwindow, the local oscillator frequency was set to 1830.10 GHz and the intermediate frequency domain to 4–6 GHz, as employed in the 2009 flight. OH and O_3 were considered as the target molecules of multi-profile inverse problem.

Calibration Error

For TELIS, nonlinearities in the signal chain influence the radiometric accuracy. Therefore, the radiometric calibration of TELIS was simulated properly in order to investigate the nonlinearity effect on the retrieval. As the nonlinearity is caused by saturation effects in the amplifier chain, it leads to a compression of the measured output compared to the linear case. In our study, the modeled calibrated spectrum with the compression of 30% as the worst-case scenario was used for retrieval.

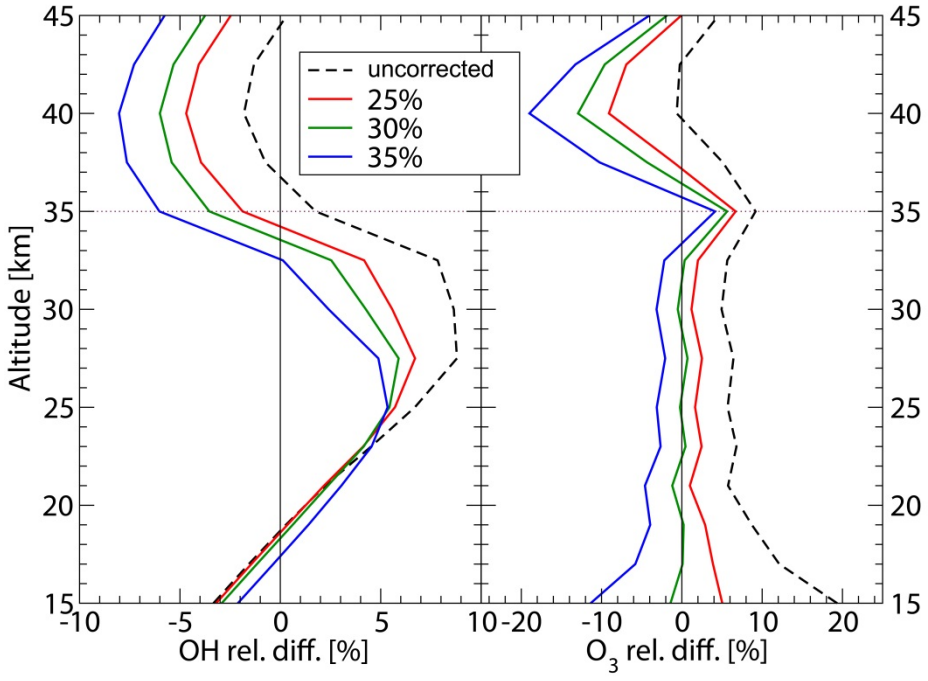

Fig. 3-7: Relative differences of OH and O_3 with respect to the true profile. The retrievals are done for the noisy synthetic measurements which are generated by the calibrated spectra with 30% compression in the hot load measurements. 5% uncertainty is taken into account in the pseudo-correction scheme. The dotted maroon horizontal line refers to the observing altitude of TELIS.

A pseudo-correction scheme was implemented, which superimposed the nonlinearity onto the model spectra at each iteration step. Moreover, the retrievals were repeated with the compression set to 25% and 35%, respectively. The relative differences with respect to the true profile (Fig. 3-7) implied that the nonlinearity effect was more severe on O_3, which caused a largest error at 15 km. The OH retrieval was not affected below 21 km because there is no strong OH line at lower altitudes. As expected, the nonlinearity could affect the retrieval of OH at higher altitudes where the spectral feature is stronger. The errors with correction of 25% and 35% seemed to be symmetric with respect to the case of 30% (above 25 km for OH).

Instrumental Knowledge

Excluding the nonlinearity error, important instrumental error sources such as sideband ratio and pointing error were studied by propagated error by using the linear mapping method in the framework of a linearized forward model about the true state.

For an ideal double sideband receiver the sideband ratio is equal to one. However, in practice this ratio is estimated to lie in the range of 0.95 to 1.05 for the 1.8 THz channel. In the left panel of Fig. 3-8 the propagated errors introduced by a relative bias are shown. The large sideband ratio bias can result in significant errors in the retrieval of OH.

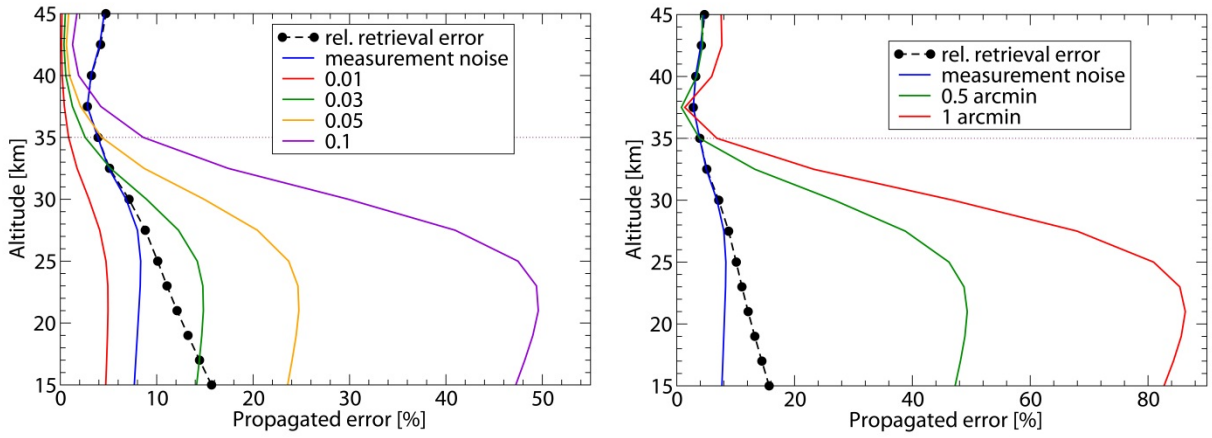

Fig. 3-8: Left: propagated error of sideband ratio onto the OH retrieval with the sideband ratio bias ranging from -0.1 to 0.1. Right: propagated error of pointing with the error on the systematic pointing bias.

A pointing error could be another severe error source for the OH retrieval. Although TELIS receives its pointing information from a highly stable attitude and heading reference system equipped on MIPAS-B, the systematic pointing bias is 3.4', corresponding to a 500 m deviation for a tangent altitude of 15 km. By assuming uncertainties of 0.5' and 1' in the systematic pointing bias, the propagated errors are shown in the right panel of Fig. 3-8. As the pointing error yields a shift of all molecule profiles and O_3 is the most important contributor to the signal in this case, an unresolved shift of the O_3 profile is the reason for the large deviation in the OH retrieved profile (Fig. 3-9, left panel). This large error could be substantially reduced by performing the joint retrieval of OH and O_3, as can be inferred from the right panel of Fig. 3-9.

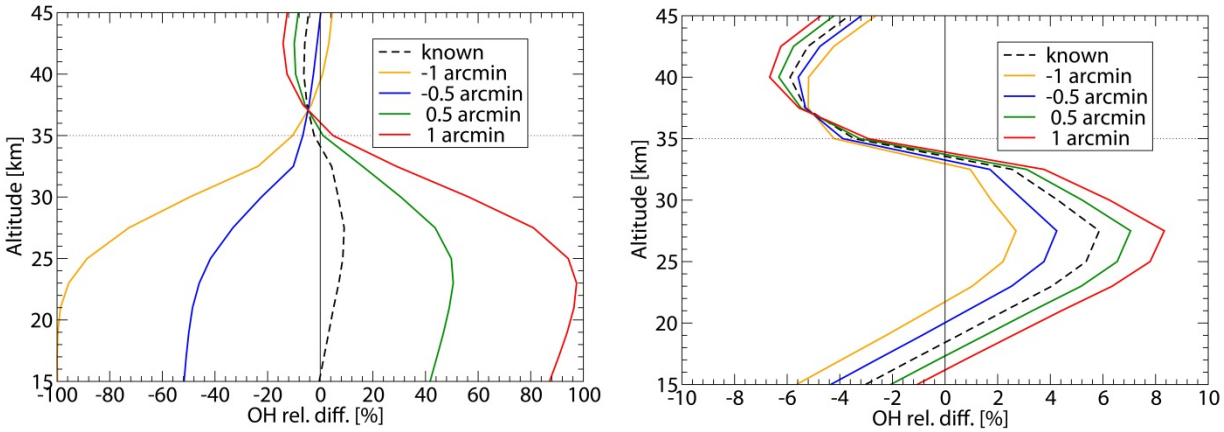

Fig. 3-9: Relative differences in the OH profile for single-target retrieval (left panel) and joint retrieval of OH and O_3 (right panel) with uncertainties of 0.5' and 1' in the systematic pointing bias. For reference the retrieval result for the perfectly known pointing information is given in dashed black line.

3.5 AC2020: Radiative Transfer Models for Atmospheric Correction

T. Trautmann, D. Efremenko, A. Doicu

The future, e.g. the European Sentinels (S2, S3) or the national EnMAP, as well as the current (RAPID EYE) optical missions provide observational data with highly improved temporal, spatial and spectral resolution. Using such instruments will offer the opportunity for observing both land surfaces and water bodies with unprecedented details. An important prerequisite for the synergetic, scientific and commercial use of these multi-, super- and hyperspectral sensor systems is the provision of an operational software system which allows for a reliable atmospheric correction procedure of the observed radiances with inherent qualitative and quantitative comparability for the observed scenes. A central component for the extraction of, e.g., land use and vegetation parameters or of geophysical parameters (water constituents) for the columnar water body from hyperspectrally sensed data is the *atmospheric correction (AC)*.

Atmospheric correction is defined as establishing the relationship between the radiance received at the sensor, i.e. above the atmosphere, and the radiance which had directly left the surface. Since the presence of the atmosphere influences the radiation travelling from the surface to the sensor, AC has to be taken into account in visible, near-infrared or infrared remote sensing.

Usually the radiative transfer theory is employed to estimate the effect of the intervening atmosphere on the observed spectral radiance at sensor level, either for an air-borne or space-borne platform. As part of the atmospheric correction procedure, it generally allows to account for all physically relevant processes under the provision that some a priori knowledge about the observed scene and the state of the atmosphere at the time of the observation exists.

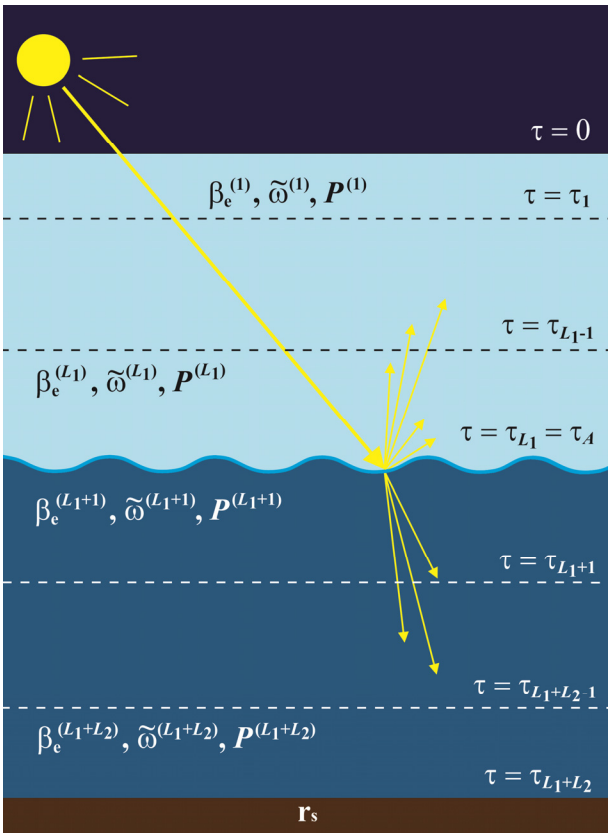

Fig. 3-10: A Sun illuminated scene with an atmospheric medium (L_1 layers) above the water body (L_2 layers). Optical depth, extinction coefficient, single-scattering albedo and scattering phase matrix are denoted by $\tau, \beta_e, \tilde{\omega}$ and $\boldsymbol{P}$. The reflection function of the sea floor is given by $\mathbf{r}_s$.

Based on the experience gained with the ATCOR (*Atmospheric/Topographic Correction for Satellite Imagery*) software package at the German Remote Sensing Data Center (DFD) in the past years, our

intention is to develop a new generic software environment called 'AC2020' (atmospheric correction 2020) which extends the ATCOR capabilities with respect to:

- usability for both land surfaces and water bodies
- independence from any proprietary atmospheric radiative transfer model
- independence from any proprietary image processing software
- modern platform independent IT architecture using, e.g., the freely available Python programming language
- possibility to integrate the newest and most enhanced versions of atmospheric radiative transfer models
- modular structure for including flexible atmospheric parameterizations
- consideration of Sun-sensor-target geometry including BRDF effects
- integration into the EOC processing chain CATENA.

The usage of open source tools (for programming languages, data visualization, large data batch processing, etc.) will dramatically ease the portability and maintainability of the finally developed software system.

In the coming years the work of MF-ATP will focus on the following items:

- further development and adaptation of a one-dimensional atmospheric radiative transfer model which
  - provides the full functionalities of the MODTRAN packet as used in the current ATCOR
  - generalizes the spectrally resolved radiative transfer for simulating the coupled systems atmosphere/land surface as well as atmosphere/water surface
- state-of-art treatment of polarized radiation
- taking the bi-directionality of the land surface/water body leaving spectral radiation into account
- accurate and fast treatment of the absorption due to atmospheric trace gases for arbitrarily fine spectral intervals
- consideration of concurrent atmospheric profiles (temperature, water vapour content, ozone amount, background aerosol) for the observed scenes
- improved correction of atmospheric haze and cirrus clouds
- treatment of clouds for complex shadow scenes and over inhomogeneous surface scenes.

In recent years MF-ATP has developed several state-of-art models for unpolarized and polarized one- and multidimensional atmospheric radiative transfer, e.g., *Doicu and Trautmann (2009a, 2009b)*, *Gimeno García et al. (2012)*, *Efremenko et al. (2013)*, and *Doicu et al. (2013)*. These model developments shall constitute the backbone of AC2020's radiative transfer core.

References

Doicu A., Efremenko D., and Trautmann T.: A multi-dimensional vector spherical harmonics discrete ordinate method for atmospheric radiative transfer. Journal of Quantitative Spectroscopy and Radiative Transfer, DOI 10.1016/j.jqsrt.2012.12.009, 2013

Doicu A., and Trautmann T.: Discrete ordinate method with matrix exponential for a pseudo-spherical atmosphere: Vector case. Journal of Quantitative Spectroscopy and Radiative Transfer, 110, 159-172, DOI: 10.1016/j.jqsrt.2008.09.013, 2009a

Doicu A., and Trautmann T.: Adjoint problem of radiative transfer for a pseudo-spherical atmosphere and general viewing geometries. Journal of Quantitative Spectroscopy and Radiative Transfer, 110 (8), 464-476, DOI: 10.1016/j.jqsrt.2009.01.027, 2009b

Efremenko D., Doicu A., Loyola D., and Trautmann T.: Acceleration techniques for the discrete ordinate method. Journal of Quantitative Spectroscopy and Radiative Transfer, 114, 73-81, DOI: 10.1016/j.jqsrt.2012.08.014, 2013

Gimeno García S., Trautmann T., and Venema V.: Reduction of radiation biases by incorporating the missing cloud variability via downscaling techniques: A study using the 3-D MoCaRT model. Atmospheric Measurement Techniques, 5, 2261-2276, 2012

3.6 Intercomparison of Three Microwave/Infrared High Resolution Line-by-Line Radiative Transfer Codes

F. Schreier , S. Gimeno García, M. Milz, A. Kottayil (both Lulea University of Technology, Division of Space Technology, Kiruna, Sweden)

Line-by-line (LbL) modeling of atmospheric radiative transfer is essential for the analysis of a growing number of high resolution infrared (IR) and microwave remote sensing instruments. Because the quality of the retrieval products critically depends on the accuracy of the radiative transfer codes used as forward model in the inversion process, verification and validation of these codes is crucial, and accordingly several code intercomparisons have been performed.

Here an intercomparison of three LbL codes developed independently for atmospheric sounding is presented: ARTS, GARLIC (MIRART) and KOPRA. Note that ARTS – MIRART and KOPRA – MIRART intercomparisons (including some other models) have already been performed in the context of the *Third International Radiative Transfer Modeling Workshop* and the AMIL2DA project, respectively (*Melsheimer et al. 2005*; *von Clarmann et al. 2002*).

- ARTS (Atmospheric Radiative Transfer Simulator) is a public domain project initiated and developed jointly by the University of Bremen and Chalmers University, Gothenburg (*Bühler et al. 2005*; *Eriksson et al. 2011*, see also http://www.sat.ltu.se/arts/). It has originally focused on microwave applications with uplooking (MIAWARA, AMSOS), downlooking (AMSU-B, MHS) and limb viewing instruments (ODIN, SMILES).
- GARLIC (Generic Atmospheric Radiation Line-by-line Infrared Code) is the modern Fortran90 re-implementation of MIRART, originally designed for far and mid IR applications (*Schreier and Schimpf 2001*) with arbitrary observation geometries, instrumental field of view and spectral response functions. Among others it has been used to simulate and analyze limb observations with MIPAS and TELIS (TeraHertz Limb Sounder), and thermal and near IR nadir spectra of AIRS, IASI, and SCIAMACHY. Recently it has also been applied to (exo-)planet atmospheric studies.
- KOPRA (Karlsruhe Optimized and Precise Radiative transfer Algorithm) is a line-by-line, layer-by-layer model for forward calculation of infrared atmospheric transmittance and radiance spectra for various geometries and was specifically developed for the analysis of mid infrared limb emission sounder data (*Stiller et al. 2002*). It is used for retrievals of limb and uplooking instruments observing thermal emission and solar absorption spectra (MIPAS aboard ENVISAT, balloon, or aircraft, GLORIA or ground based FTIR).

In this intercomparison we considered a thermal infrared nadir sounding application and modeled the upwelling radiation seen by a space-borne, vertically downlooking observer. In particular we used a HIRS (High resolution Infrared Radiation Sounder) setup and compute radiances for the 19 HIRS channels and a set of 42 atmospheric profiles, the *Garand et al. (2001*) dataset, comprising pressure, temperature, water vapour, carbon dioxide, ozone etc.,) representative of most meteorological situations. Absorption of the main molecular absorbers in the infrared were considered (H_2O, CO_2, O_3, CH_4, N_2O, and CO) with line spectroscopic data taken from the HITRAN database and additional continuum corrections.

For all 42 Garand atmospheres, the radiance spectra computed by the three codes (i.e. the monochromatic spectra convolved with the HIRS channel functions and converted to equivalent brightness temperatures) were visually identical. A detailed analysis of brightness temperature differences indicated a good agreement between ARTS, GARLIC, and KOPRA for most channels with differences in the sub-Kelvin range, in the same magnitude as reported for the LbL models participating in the *Garand et al. (2001)* study. However, larger deviations of up to a few Kelvin were observed for a few channels (Fig. 3-11).

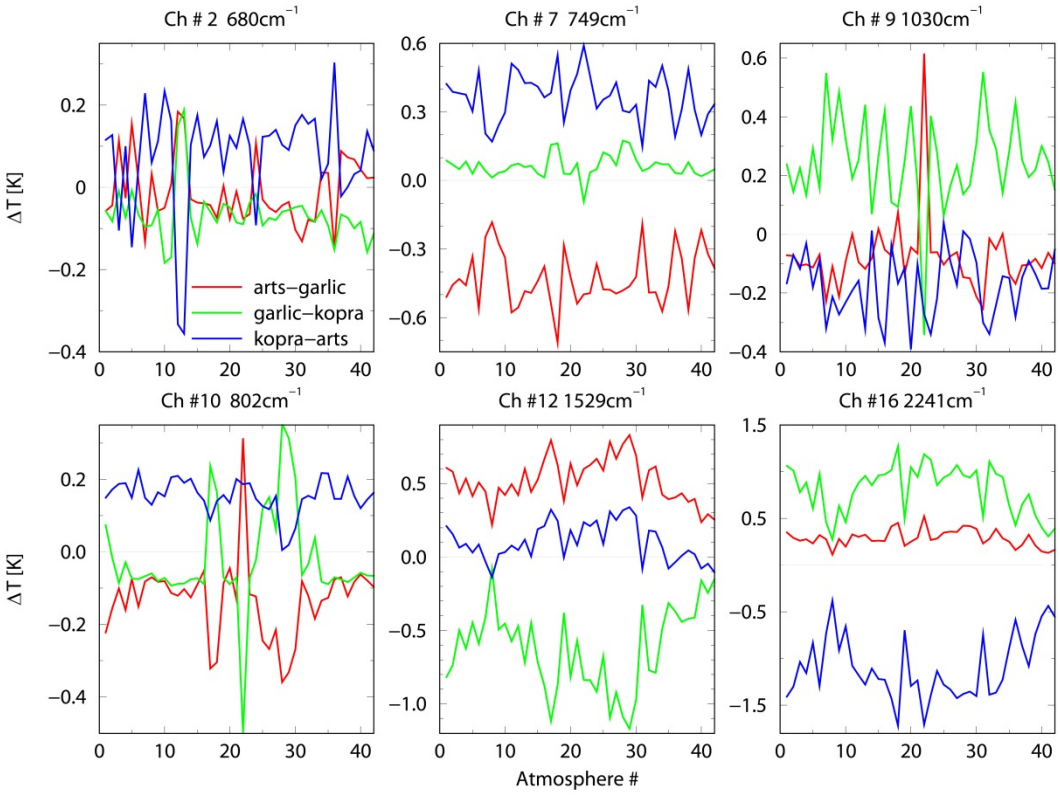

Fig. 3-11: Difference brightness temperatures as a function of profile number for 6 selected channels.

Remaining discrepancies in some channels are currently under investigations, potential reasons discussed comprise (among others):

- continua (e.g. H_2O, CO_2; notably different versions of the MTCKD continuum)
- different line strength conversion schemes
- various LbL optimization schemes (e.g. wing truncation, weak line rejection)
- evaluation of path integrals.

A detailed analysis of these issues will be presented in a forthcoming paper.

References

Bühler S.A., Eriksson P., Kuhn T., von Engeln A., and Verdes C.: ARTS, the atmospheric radiative transfer simulator. J. Quant. Spectrosc. & Radiat. Transfer, 91:65–93, 2005

von Clarmann T., et al.: Modeling of atmospheric mid–infrared radiative transfer: The AMIL2DA algorithm intercomparison experiment. J. Quant. Spectrosc. & Radiat. Transfer, 78:381–407, 2002

Eriksson P., Bühler S.A., Davis C., Emde C., and Lemke O.: ARTS, the atmospheric radiative transfer simulator, version 2. J. Quant. Spectrosc. & Radiat. Transfer, 112(10):1551–1558, 2011.

Garand L., et al.: Radiance and Jacobian intercomparison of radiative transfer models applied to HIRS and AMSU channels. J. Geophys. Res., 106(D20):24017–24031, 2001

Melsheimer C., et al.: Intercomparison of general purpose clear sky atmospheric radiative transfer models for the millimeter/submillimeter spectral range. Radio Science, 40:RS1007, 2005

Schreier F. and Schimpf B.: A new efficient line–by–line code for high resolution atmospheric radiation computations incl. derivatives. In W.L. Smith and Y. Timofeyev, editors, IRS 2000: Current Problems in Atmospheric Radiation, pages 381–384. A. Deepak Publishing, 2001

Stiller G.P., von Clarmann T., Funke B., Glatthor N., Hase F., Höpfner M., and Linden A.: Sensitivity of trace gas abundances retrievals from infrared limb emission spectra to simplifying approximations in radiative transfer modelling. J. Quant. Spectrosc. & Radiat. Transfer, 72:249–280, 2002

3.7 The 2D/3D Vector Radiative Transfer

A. Doicu, D. Efremenko, T. Trautmann

In some applications of remote sensing, the 2D and 3D effects have to be taken into account. At the same time, the radiative transfer codes are supposed to be robust. Moreover, given the polarization measurements, one can improve the quality of data processing and solve a wider class of inverse problems. Thus, a radiative transfer code which is multidimensional, yet fast, is of high importance for remote sensing applications. The Spherical Harmonics Discrete Ordinate Method (SHDOM, *Evans 1998*) is a very powerful multi-dimensional scalar model for atmospheric science. We extended the SHDOM formalism on the vector case.

The Spherical Harmonics Discrete Ordinate Method

The SHDOM has the following features, which increase the efficiency of the 3D model:

- The method combines the spherical harmonic and the discrete ordinate representation of the radiance field. The streaming of the radiation is accurately modeled in the discrete ordinate space, while the computation of the scattering integral is efficiently performed in the spherical harmonic space. Moreover, storing the source function as a spherical harmonic series at each grid point requires less computer memory as compared with a purely discrete ordinate method.
- The exiting corner-point radiance is computed by using the short characteristic method, in which the extinction and the extinction/source function product are assumed to vary linearly along the characteristic.
- The so-called *adaptive grid technique* improves the solution accuracy by increasing the spatial resolution in regions where the source function is changing more rapidly.

The Construction of the Generalized Spherical Harmonics

The radiative transfer equation contains a double integral over azimuthal and polar angles which makes further discretization inefficient. In the scalar case, one integral is removed due to the symmetry of the phase function. The 1D vector radiative transfer equation is solved by converting it from the Stokes basis to the circular basis, removing one integral and then converting back to the Stokes basis. In order to save the methodology of the SHDOM code for the vector case, the design of the 3D polarized model is based on the construction of complex and real generalized spherical harmonics in the energetic representation of the Stokes vector.

We introduced the complex generalized spherical harmonics and proved the orthogonality property for them (*Doicu 2012*). Expanding the phase matrix, the Stokes vector and the source function by spherical harmonics, one can get the relation between them in the spherical harmonics space:

$$\mathbf{J}_{nm} = \frac{\omega}{2}\mathbf{G}_n\mathbf{I}_{nm} + \frac{\omega}{2}\mathbf{G}_n\mathbf{Y}_{nm}^{\mathrm{H}}(-\mu_0,\varphi_0)\mathbf{F}_0 e^{-\tau_{ext}^{sun}}$$

where $\mathbf{J}_{nm}$, $\mathbf{I}_{nm}$, $\mathbf{G}_n$ are the expansion coefficients of the source function, the Stokes vector and the phase matrix over the generalized spherical harmonics respectively, $\mathbf{F}_0$ is the initial state vector, ω is the single scattering albedo.

The Vector Spherical Harmonics Discrete Ordinate Method (VSHDOM)

The Vector Spherical Harmonics Discrete Ordinate Method (VSHDOM) can use the complex or the real generalized spherical harmonics. The radiative transfer equation is solved iteratively by using the generalized spherical harmonic and the discrete ordinate representations of the Stokes and the source vectors. Each iteration consists of four steps:

- the transformation of the source vector from generalized spherical harmonics to discrete ordinates,
- the integration of the source vector along discrete ordinate directions to compute the Stokes vector,
- the transformation of the Stokes vector from discrete ordinates to generalized spherical harmonics,

- the calculation of the source vector from the Stokes vector in the generalized spherical harmonics space.

Restricting our analysis to macroscopically isotropic and mirror-symmetric media we were able to maintain two powerful features of the scalar model: the combination of the generalized spherical harmonic and the discrete ordinate representations of the radiance field, and the use of a linear short characteristic method for computing the corner-point values of the Stokes vector.

In the framework of the generalized spherical harmonics formalism, some special attributes of SHDOM, as for example, the delta-M (*Wiscombe 1977*) scaling method equipped with the TMS (*Nakajima 1988*) correction, the cell splitting criterion for the adaptive grid technique, and the initialization of the Stokes vector, have been extended in a natural way to the vector case. Our numerical simulations have shown that the implementations with complex and real generalized spherical harmonics yield the same solution accuracy, but the real model is by a factor of 1.4 faster. VSHDOM also includes an independent column approximation based on the one-dimensional discrete ordinate method with matrix exponential. This approach is more time consuming than the iterative approach, but it requires less computer memory.

The adaptive grid technique improves the solution accuracy. In fact, this improvement is significant for the I component, and rather moderate for the Q component. The reason is that for a cloudy atmosphere and in the UV spectral region, the Q component is much smaller than the I component. If the linearly polarized component of the Stokes vector must be computed with high accuracy, then the splitting criterion as well as the solution criterion should be formulated in terms of the Q component rather than in terms of the entire Stokes vector.

References

Evans K.F.: The spherical harmonic discrete ordinate method for three-dimensional atmospheric radiative transfer, J. Atmos. Sci. 55, 429-446, 1998

Doicu A., Efremenko D., Trautmann T.: A multi-dimensional vector spherical harmonics discrete ordinate method for atmospheric radiative transfer, *JQSRT submitted*, 2012

Nakajima T., Tanaka M.: Algorithms for radiative intensity calculations in moderately thick atmospheres using a truncation approximation, J. Quant. Spectrosc. Radiat. Transfer. 40, 51–69, 1988

Wiscombe W.J.: The delta-M method: rapid yet accurate radiative flux calculations for strongly asymmetric phase functions, J. Atmos. Sci. 34, 1408–22, 1977

3.8 Acceleration Techniques of the Radiative Transfer Codes

D. Efremenko, A. Doicu, D. Loyola, T. Trautmann

Nowadays the amount of satellite remote sensing data is increasing due to the state-of-the-art instruments with high spatial and spectral resolution, e.g. like GOME-2. A massive amount of data is expected from the new generation of European atmospheric composition sensors: Sentinel 5 Precursor, Sentinel 4 and Sentinel 5. The atmospheric Sentinel instruments will generate two orders of magnitude more data than GOME-2 today. In this regard, the fast processing and interpretation of such data is a key component for new applications like air quality monitoring and chemical weather prediction. The bottle-neck of the remote sensing algorithms is the solvers for the radiative transfer equation (RTE). Mostly, the numerically exact solution is derived in the discrete ordinate method (DOM) formalism (*Chandrasekhar 1950*). We have been working on the acceleration of the discrete ordinate method in the framework of software tool DOME developed in DLR.

The Small-angle Modification

The first novelty which has been added in a retrieval tool is the small-angle modification of DOM. To solve numerically the RTE, one has to replace the integrals by the Gaussian quadrature. This is impossible to do due to the delta-function in the boundary conditions. Moreover, the phase functions of large particles such as cloud droplets are strongly anisotropic due to the strong peak in the forward

scattering direction. A large number of Legendre terms are required for accurate diffuse radiance calculations. Different approaches were designed to accelerate the solution of the radiative transfer equation without significant loss of accuracy. In the delta-M method (*Wiscombe 1977*), the exact phase function is approximated by a linear combination of a delta-function and a truncated phase function. In this way, the original transfer equation with a strong asymmetry parameter is reduced to a more tractable problem with less anisotropic phase function. An alternative method consists in the elimination of the anisotropic part of the total radiance for further discretization. This idea has evolved from the Eddington–Milne approach, in which the anisotropic part is due to the non-scattered radiation, in the small-angle modification of the radiative transfer equation (*Budak 2012, Efremenko 2013a*), in which the anisotropic part is described by the Goudsmit–Saunderson solution (*Goudsmit 1940*). Thus, the desired solution is represented as the sum of two parts: the anisotropic one I_a that contains all the solution singularities, and the regular one I_r, the smooth function of angular variables:

$$I = I_a + I_r$$

We extended the small-angle modification on the pseudospherical case by introducing the correction term – the difference between single scattering solution in the plane-parallel and spherical geometries. Numerical simulations reveal the supremacy of the small-angle modification over the delta-M approach. But there is no absolute winner in the comparison between the small-angle modification and conventional correction methods such as the TMS-correction (*Nakajima 1988*).

The Left Eigenvector Matrix (LEM) Approach

Solving the RTE by the discrete ordinate method, one has to compute a matrix exponential with a layer matrix as a power of exponential. Usually, it is evaluated by the spectral decomposition. The key idea is that for any matrix, which has a complete set of linearly independent eigenvectors, the inverse of the right eigenvector matrix is the transpose of the left eigenvalue matrix. The steps of the left eigenvector matrix approach (*Efremenko 2013b*) can be summarized as follows:

- **Step 1**: We apply a similarity transformation (*Waterman 1981*) to the layer matrix to obtain a scaled layer matrix. The transformation matrix is a diagonal matrix, and the block-matrix components of the scaled layer matrix are symmetric. This transformation does not change the eigenvalues.
- **Step 2**: We compute the left and the right eigenvectors of the scaled layer matrix. The key point in this calculation is the special structure of the transpose of the scaled layer matrix. More precisely, the block-matrix components of the transpose scaled matrix are the block-matrix components of the scaled matrix, and both the right and the left eigenvector matrices can be expressed in terms of the same block-eigenvectors, with appropriate normalization constants.
- **Step 3**: We apply a back transformation to relate the right eigenvector matrix of the original layer matrix, and its inverse, to the right and the left eigenvector matrices of the scaled layer matrix. These transformations involve matrix products with diagonal matrices, and are not time consuming. The left eigenvalue approach can be simply extended to the vector case.

To analyze the efficiency of the LEM approach, we performed the simulations for a 40 layer atmosphere with fixed number of azimuthal harmonics. We use GNU profiler `gprof` to determine the most time-consuming subroutines. These are the matrix multiplication and the eigenvalue problem. Both these functions have near cubic dependence of the computational time over the number of discrete ordinates. The total computational time follows the same dependence. The computational time as a function of the number of discrete ordinates is shown in Fig. 3-12 (left). The average speedup is about 15 %. Probably the acceleration will be more evident in the vector RTE codes as the layer matrix dimension in the vector case is 4 times larger.

Telescoping Techniques

The telescoping technique relies on the fact that the azimuthal expansion coefficients of the phase functions vanish for all azimuthal harmonic number $m > 2$, and all Rayleigh layers. Hence, the layer matrix is diagonal and the source vector vanishes. The technique can be applied for the whole-atmosphere approach and the matrix operator method. We made two tests with and without telescoping option and measured the time as function of the number of azimuthal modes with fixed

number of discrete ordinates. For the first three modes obviously the telescoping technique does not yield any acceleration, but it reduces the computational time of higher azimuthal modes drastically. Since usually the Cauchy convergence criterion is satisfied for a number of azimuthal harmonics between 4 and 8, we conclude that the telescoping technique provides the acceleration between 20 and 40 % for our computations (Fig. 3-12 right).

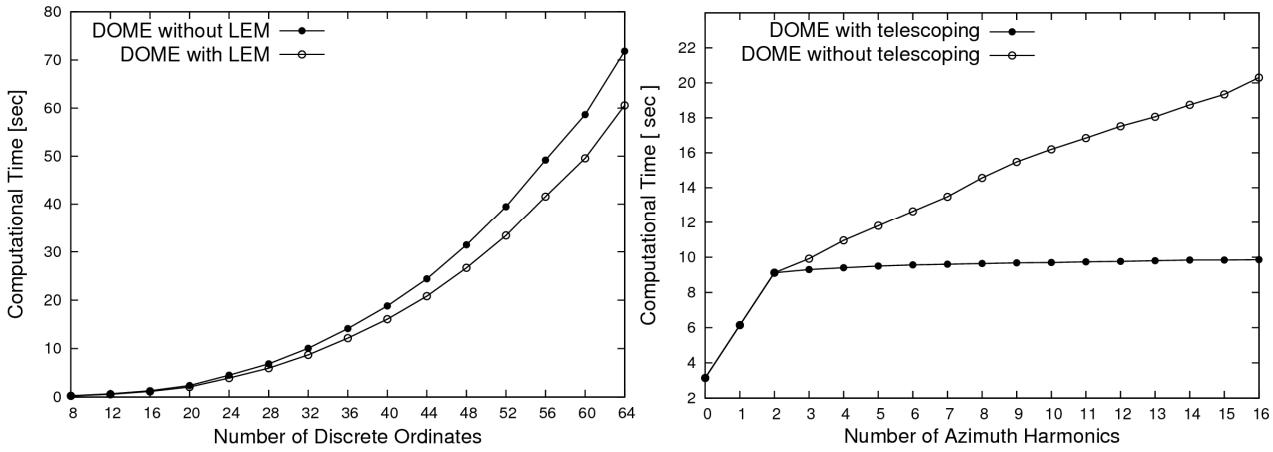

Fig. 3-12 left: The computational time of DOME code with and without the left eigenvector matrix approach as a function of the number of discrete ordinates. Right: The computational time of DOME code with and without the telescoping as a function of the number of azimuthal harmonics.

References

Budak V.P., Efremenko D.S., Shagalov O.V.: Efficiency of algorithm for solution of vector radiative transfer equation in turbid medium slab, J.Phys.Conf. Series. 369, 012021(1-10), 2012

Chandrasekhar S.: Radiative transfer. London: Oxford University Press; 1950

Efremenko D., Doicu A., Loyola D., Trautmann T.: Small-angle modification of the radiative transfer equation for a pseudo-spherical atmosphere, J.Quant. Specrosc. Radiat. Transfer. 144, 82-90, 2013a

Efremenko D., Doicu A., Loyola D., Trautmann T.: Acceleration techniques for the discrete ordinate method, J. Quant. Spectrosc. Radiat. Transfer. 144, 73-81, 2013b

Goudsmit S Saunderson J.L.: Multiple scattering of electrons, Phys. Rev. 57, 24–9, 1940

Nakajima T., Tanaka M.: Algorithms for radiative intensity calculations in moderately thick atmospheres using a truncation approximation, J. Quant. Spectrosc. Radiat. Transfer. 40, 51–69, 1988

Waterman P.C.: Matrix-exponential description of radiative transfer. J. Opt. Soc. Am. 71, 410–422, 1981

Wiscombe W.J.: The delta-M method: rapid yet accurate radiative flux calculations for strongly asymmetric phase functions, J. Atmos. Sci. 34, 1408–22, 1977

3.9 ADM-Aeolus: Extinction and Backscattering Profiles for Realistic Aerosols

K. Schmidt, T. Trautmann

One goal of the ADM-Aeolus III project consists in the further development, optimization, and adjustment of the ESA end-to-end simulator (E2S) and the level 1b reference processor (L1BP) with respect to the treatment of the lidar signal scattering on aerosols and particles, in particular, within cirrus and polar stratospheric clouds by means of sensitivity tests and simulations. On the basis of these investigations, recommendations for the algorithm and software optimization of the operational ESA-L1BP are derived.

The scattering enters the ESA-E2S, which simulates the space-borne lidar measurements, in terms of extinction and backscattering altitude profiles of the different particles. In order to estimate, in particular, the effect of nonspherical particles in comparison to spherical ones, spheroidal shapes are considered. Oblate and prolate spheroids represent the simplest deviation from spheres. More realistic and complex particle shapes can be taken into account if significant effects caused by the spheroids are observed. In doing so, the scattering database for spheroidal particles (*Schmidt et al. 2009*) is used. An ensemble of spherical and spheroidal particles, respectively, with a given refractive index and averaged over a size distribution is assumed in each altitude layer. Randomly oriented oblate and prolate spheroids with equally distributed aspect ratios, present in the database, are considered. The corresponding refractive indices, size distributions, and number density altitude profiles are taken from the literature. In a first step, dry mineral aerosols have been considered since their shapes are known to be dominated by nonspherical ones. Fig. 3-13 shows an example of the altitude profiles of mineral dust in the accumulation mode. The refractive index of (1.5,0.005) and the parameters of the monomodal log-norm size distribution have been taken from *Gasteiger et al. (2011)* when modeling mineral dust aerosols within the SAMUM project. The number densities in each altitude layer have been derived from the given ESA-E2S standard aerosol profile.

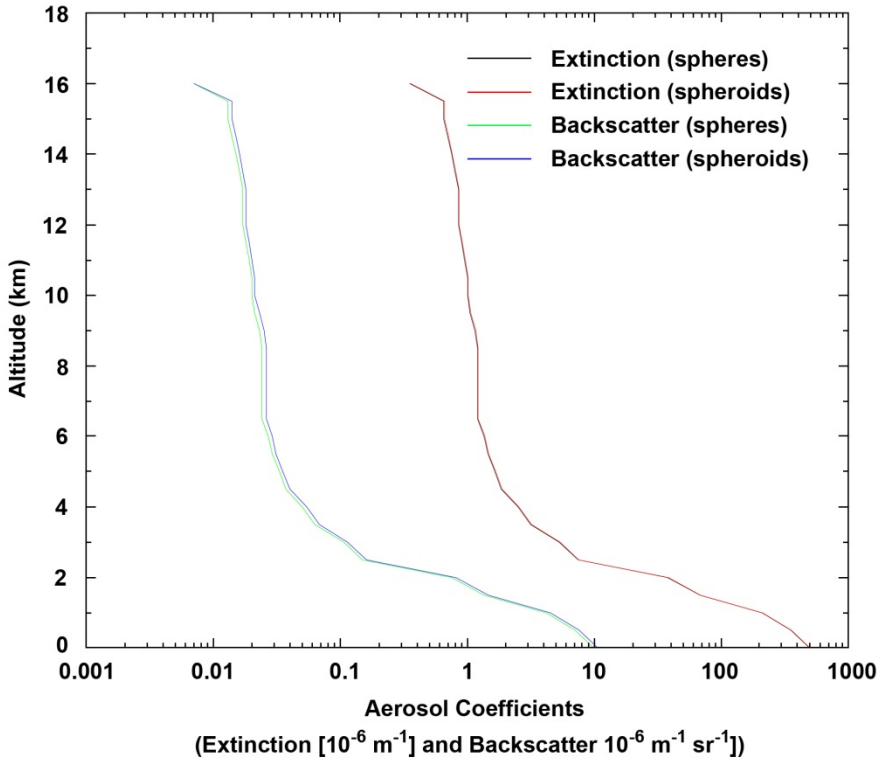

Fig. 3-13: Extinction and backscattering altitude profiles of mineral dust aerosols (for details see text).

Almost no differences between the profiles of spheres and spheroid mixtures are obvious in Fig. 3-13. The ESA-E2S simulation data enter the L1BP to derive line-of-sight wind velocities. As expected from Fig.

3-13, first L1BP tests show practically no particle shape sensitivity. The situation can change, however, when deriving aerosol and cloud properties by means of L2AP (level 2a processor).

References

Gasteiger J., Wiegner M., Groß S., Freudenthaler V., Toledano C., Tesche M., and Kandler K.: Modelling lidar-relevant optical properties of complex mineral dust aerosols, Tellus, 63B, 725-741, 2011

Schmidt K., Wauer J., Rother T., and Trautmann T.: Scattering database for spheroidal particles, Applied Optics, 48, 2154-2164, 2009

3.10 MoCaRT – Monte Carlo Radiative Transfer Model

S. Gimeno García, T. Trautmann, F. Schreier

The Monte Carlo Radiative Transfer model (MoCaRT) is a flexible model designed to address different goals in atmospheric radiative transfer applications with special focus in the three-dimensional radiation effects (*Gimeno García et al. 2012*).

MoCaRT has three main components implemented:

- **Optical**: The optical block accounts for the calculation of optical properties from given atmospheric conditions of pressure, temperature, molecular abundances and, if present, cloud and aerosol composition and microphysical properties.
- **Radiative**: The radiative block accounts for the radiative transfer through the optically active medium defined in the optical part.
- **Instrumental**: The instrumental block considers the spectral response function of an arbitrary instrument. The instrumental noise is simulated by the noise implicit to the Monte Carlo method.

In order to reach a fast and accurate convergence, several variance reduction and acceleration techniques have been implemented in MoCaRT. Here, we will only describe briefly the diverse implemented techniques. Usually, photon tracing, i.e., the randomly generation of photon trajectories, is the part of the code that consumes most of the computing time in Monte Carlo RT codes and MoCaRT is not an exception. One-dimensional photon tracing algorithms are faster than their three-dimensional counterparts, since they do not have to account for photon horizontal location. Making use of this fact, it is possible to speed up the photon tracing process by considering a 3-D inhomogeneous atmosphere as if it were one-dimensional. This goal is achieved by considering the maximum extinction coefficient values within vertical layers $k_{ext}^{max}(z)$, and introducing a virtual interaction event that left photons unaltered. Assigning the probability weight of $k_{ext}(x,y,z)/k_{ext}^{max}(z)$ to the 'maximum extinction' event and $1-k_{ext}(x,y,z)/k_{ext}^{max}(z)$ to the virtual scattering event, the photon tracing is unbiased. The method was described first by *Marchuk et al. (1980)*. They considered the maximum values of the whole medium and called it *maximum cross-section method*. Since we apply the method for a layered medium, it can be called the *stratified maximum cross-section method*. This method works well when the maxima are not much larger than the extinction coefficients within layers. Special care has to be taken in case of different phase functions in the medium. This method is used for flux density calculations. In case of radiances, slower but more robust 3D (or 2D) tracing algorithms are used.

Several variance reduction methods are related to the manner that the photon-matter interactions are described in the model. The most intuitive method is to describe the history of single photons and their interaction with the medium as they behave in nature: they have constant energy, change direction after scattering events and disappear whenever an absorption event takes place. We refer to this method as *crude* Monte Carlo. Another method is the so-called *weighted scattering*. In this case, the energy of the photons is reduced after each interaction according to the local single scattering albedo, and absorption never occurs. This method can be seen as the representation of a bundle of photons moving in the same direction through the atmosphere, where the energy reduction can be interpreted as the loss of a certain number photons due to absorption. A third method considers the interaction of photons with a pure-scattering atmosphere. In this case, the photons' energy is continuously attenuated

while moving through the atmosphere, from one scattering event to the next, according to the Beer's law. Note that during the energy attenuation process only the absorption optical thickness is considered. We will refer to this method as *continuous absorption*. All these methods are implemented in MoCaRT and the appropriateness of one or the other depends on the medium properties and the application.

The estimation of the radiation fields of interest can be performed in-situ at place of a virtual detector or summing up contributions of the photons when flying through the atmosphere. In the first case, photon 'scoring', i.e. contribution to radiance or flux, is only considered if photons physically reach the detector. This method is appropriated for the computation of fluxes but not for radiances. In the latter case, the local estimate method (*Marchuk et al. 1980*) is more suitable. In this method, the contribution is calculated at each interaction point by scoring according to the probabilities of the photons to reach the detector thus allowing a faster convergence. Making use of the reciprocity theorem, the radiative transfer can be simulated by solving the adjoint equation (backward Monte Carlo method). In this case, 'inverse' photons are traced from the detector and the local contributions are summed up according to the probabilities of the inverse photons to reach the source. This method is especially convenient for parallel beam illumination, as in case of solar irradiation.

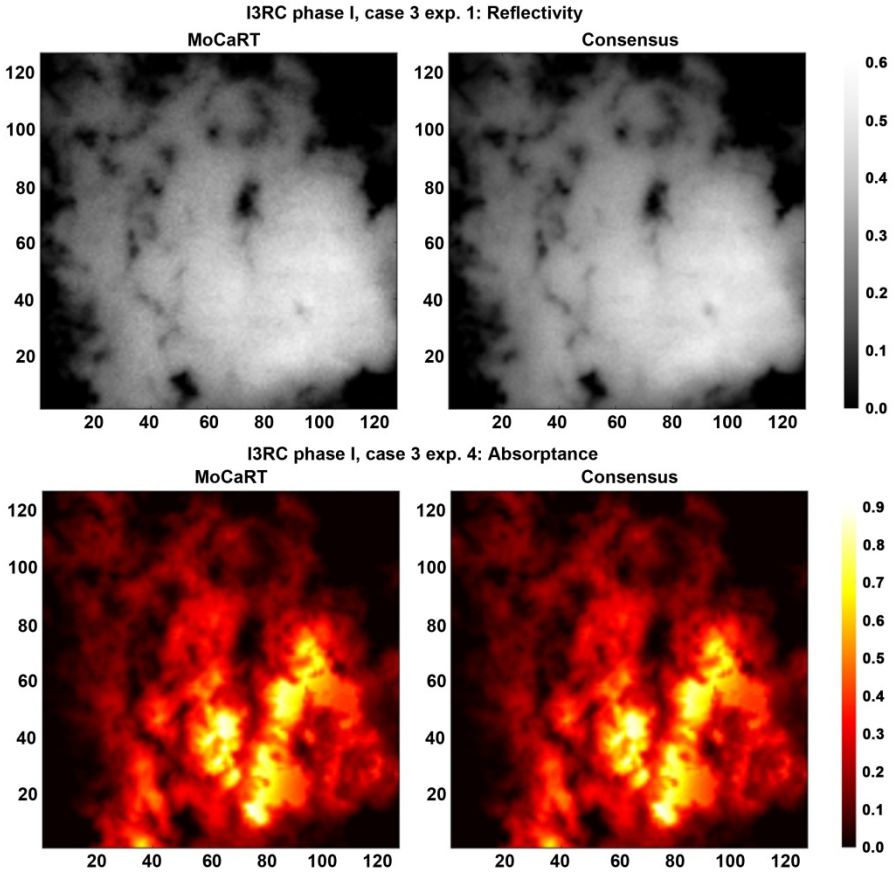

Fig. 3-14: I3RC project phase I. Case 3 represents a Landsat cloud. MoCaRT results are compared to the consensus results of the participants in I3RC project. The left column shows the MoCaRT and the right column, the consensus results. The top row illustrates the reflectivity fields and the bottom one absorptance. Differences are well within the Monte Carlo noise.

The scattering phase function can take very different shapes. Molecular scattering produces smooth phase functions, whereas the scattering by large particles is described by sharp forward-peaked phase functions. In the latter case, the convergence to the solution is slowed down and a higher number of realizations (photons) is needed. In order to accelerate convergence, the regionalization method of the local estimate technique presented in *Barker et al. (2003)* is implemented. The truncated radiance contributions – up to a given 'tunable' threshold – are summed up as usual, and the contributions that exceed this threshold are stored in a scene 'radiance surplus bucket'. After the computation, the bucket

is decanted over the scene such that regions with higher truncated radiances linearly become more portion of the radiance bucket. This method delivers smoother radiation fields using less number of photons. The scene mean value is unbiased, but local biases may occur depending on the contribution threshold. The only difference to the Barker et al. regionalization method is that our radiance contributions include the single scattering albedo at the locations of each scattering event (*weighted scattering method*).

Fig. 3-14 presents a comparison of MoCaRT with the consensus results of the Intercomparison of Three-Dimensional Radiation Codes (I3RC) project (*Cahalan et al. 2005*). Although the extinction field is highly variable and the solar illumination is not perpendicular, MoCaRT results compare very well with the consensus results. The mean, maximal and minimal values agree better than 0.1%, which is clearly better than the required accuracy in the I3RC project.

References:

Barker H., Goldstein R., and Stevens D.: Monte carlo simulation of solar reflectances for cloudy atmospheres, Journal Atmos. Sci., 60, 1881–1894, 2003

Cahalan R. F. et al.: The i3rc – bringing together the most advanced radiative transfer tools for cloudy atmospheres, B. Am. Meteorol. Soc., 86, 1275–1293, doi:10.1175/BAMS-86-9-1275, 2005

Gimeno García S., Trautmann T., and Venema V.: Reduction of radiation biases by incorporating the missing cloud variability via downscaling techniques: a study using the 3-D MoCaRT model. Atmospheric Measurement Techniques, 5, 2261-2276, 2012

Marchuk G., Mikhailov G., and Nazaraliev M.: The Monte Carlo methods in atmospheric optics, Springer Series in Optical Sciences, 1980

3.11 New Edition of the Electromagnetic Wave Scattering Book

T. Rother, M. Kahnert (SMHI)

Because of the success of the first edition of the book *Electromagnetic Wave Scattering on Nonspherical Particles: Basic Methodology and Simulations*, published by Springer in 2009 (see annual report 2008), we have been requested to prepare a second edition. After discussions with the Executive Editor in Physics of Springer we decided to prepare an extended edition with an additional chapter and several additional sections which support both the methodological and practical aspects of the book.

The following aspects have been additionally included:

- A new chapter *Scattering on Particles with Discrete Symmetries*, comprised of
  - Introduction
  - Explicit Commutation Relations of the T-matrix
  - Symmetry Groups
  - Irreducible Representations.

In many applications one can achieve great simplifications by invoking symmetry assumptions about the particles' geometry. The simplifications result in a substantial expedition of numerical computations, and in an increase of the stability of the numerical algorithms. The Green function formalism developed in the first edition provides a powerful starting point for discussing symmetries in boundary value problems. This topic was therefore included in the new edition.

- A new application-oriented section on *Morphology Dependent Resonances*

Morphology dependent resonances are highly sensitive to the morphology (i.e., geometry and refractive index) of the scattering particle, and, therefore, of special importance in several different measurement methods like fluorescence and Raman spectroscopy. With this section we intended moreover to demonstrate the capability of the software package 'mieschka', which is also part of the book, to reveal this effect adequately.

- A new application-oriented section on *High-Order Chebyshev Particles*

This section demonstrates the achievable advantages when combining group theoretical approaches with an iterative T-matrix solver was taken from a recent publication (see annual report 2011). The focus in this section is on 3D-Chebyshev particles at higher size parameters.

- A new section *Description of Program Tsym*

The program 'Tsym' is a new, freely available, open-source T-matrix program. It was especially developed to analyze the scattering behaviour of non-axisymmetric but homogeneous particles. It is based on the group theoretical methods and the iterative T-matrix approach discussed in detail in the methodological part of the new edition.

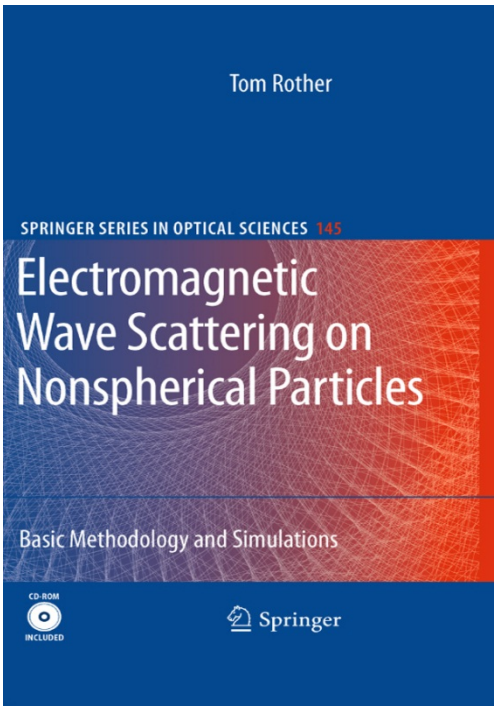

Fig. 3-15: Tom Rother: Electromagnetic Wave Scattering on Nonspherical Particles: Basic Methodology and Simulations, Springer Series in Optical Sciences, ISBN 978-3-642-00703-3, e-ISBN 978-3-642-00704-0, Springer 2009

Cover text: 'This book gives a detailed overview of the theory of electromagnetic wave scattering on single, homogeneous, but nonspherical particles. A related Green's function formalism is systematically developed which provides a powerful mathematical basis not only for the development of numerical approaches but also to discuss those general aspects like symmetry, unitarity, and the validity of Raleigh's hypothesis. Example simulations are performed in order to demonstrate the usefulness of the developed formalism as well as to introduce the simulation software which is provided on a CD-ROM with the book.'

The corresponding manuscript was finished in 2012 and submitted to Springer such that a publication date in 2013 can be expected.

4. Atmospheric Remote Sensing – Applications

4.1 Dragon 3 Project Overview: Assessment of the Impact of East Asian Monsoon on Air Quality in China

N. Hao, P. Valks, T. Trautmann

The *Dragon* programme is a cooperation between ESA and the Ministry of Science and Technology (MOST) of the P.R. China. *Dragon 3* has formally commenced at the 2012 Beijing Symposium and will last four years. It focuses on exploitation of ESA, third party mission products (TPM) and Chinese EO data for geo-science and applications development in land, ocean and atmospheric applications. The programme brings together joint Sino-European teams to investigate 50 thematic projects.

Our proposal titled 'Assessment of the impact of East Asian Summer Monsoon on the air quality over China' had been accepted in the framework of the *Dragon 3* cooperation call. The proposal was prepared by MF-ATP, Institute for Climate and Global Change Research, Nanjing University (ICGCR-NJU), Department of Civil and Structural Engineering (CSE), The Hong Kong Polytechnic University (HKPU) and Laboratoire Atmosphères, Milieux, Observations Spatiales (LATMOS).

Background and Objective

Air pollution is one of the most pestering environmental problems in developing Asian countries like China. In this region, studies showed that the East Asian monsoon plays a significant role in characterizing the temporal variation and spatial patterns of air pollution, since monsoon is a major atmospheric system affecting air mass transport, convection, and precipitation. As illustrated in Fig. 4-1, the monsoon climate controls air pollution transport in East Asia, especially for 'long-life' species like ozone. Publicly available in-situ observations cannot provide sufficient spatial coverage for long periods and are often not fully consistent. Therefore, knowledge gaps still exist in the understanding of how the Asian monsoon impacts air quality in China under the background of global climate change. Satellite retrievals yielding consistent information with high spatial coverage for a long period can well document the change of air pollution with monsoon.

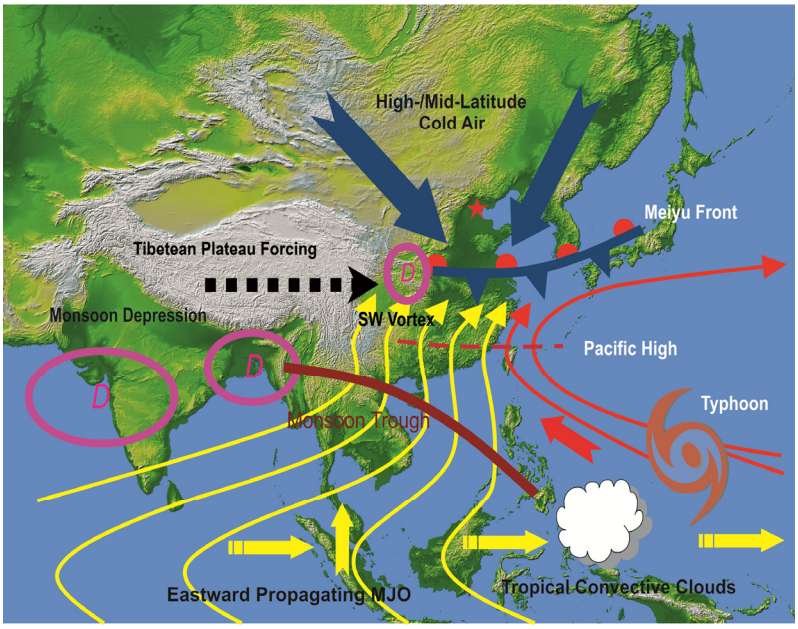

Fig. 4-1: East China is dominated by East-Asian monsoon climate

We attempt to combine satellite observations throughout the troposphere with ozone-sonde and aircraft measurements to provide a holistic view of the monsoon impact on tropospheric air pollutants over China. We apply multi-platform satellite observations to analyze tropospheric ozone, CO, precursors of ozone (NOx, HCHO and CH_4) and other related trace gases in this region. Thus we can show the potential of using the current generation of satellite instruments to monitor air quality

changes caused by the East Asian monsoon circulation. A global chemical transport model will be used to simulate the monsoon impact and to compare it with satellite measurements. The project will also contribute to explore the potential impact of air pollutants over China on a regional climate change (the strength and tempo-spatial extension of the monsoon).

An improved algorithm for tropospheric NO_2 and HCHO retrieval for GOME-type instruments will be used to provide quantitative estimates of the NO_2 pollution in China, considering cloud and aerosol effects. In addition, tropospheric ozone algorithms from IASI shall be further improved in particular to measure the lower atmospheric layers. Finally, validation of such algorithms by comparing satellite measurements over China with ground-based and aircraft measurements is envisaged.

Analysis Method

Our department will provide the operational GOME-2 ozone, tropospheric NO_2 and HCHO products (O3M-SAF products), as well as tropospheric ozone products from GOME-2. The tropospheric NO_2 column algorithms for GOME-2 and OMI can be found in *Boersma et al. (2007)* and *Valks et al. (2011)*. The tropospheric HCHO columns from SCIAMACHY and GOME-2 are retrieved with the DOAS method in the UV range around 335 nm. For the determination of the vertical columns, tropospheric air mass factors are used that are based on a priori HCHO profiles from the IMAGES global chemistry transport model (*De Smedt et al. 2012*). Various tropospheric ozone column products from GOME-type instruments, which are based on different retrieval algorithms such as residual method, the convective cloud differential and cloud-slicing methods, form the data base for our studies. The operational SCIAMACHY CO and CH_4 column products are retrieved with the new BIRRA (Beer InfraRed Retrieval Algorithm) code using near infrared nadir observations. For cloud free situations, nadir looking TIR instruments such as IASI can measure the atmospheric radiation down to the ground and, for some species, vertical information can be derived from the shape of the molecular absorption lines, provided ground emissivity, surface temperature and atmospheric temperature are known at the location of the measurement. For simulating the long-term (1994-2010) change of ozone and related precursors in China, the global chemical transport model MOZART (The Model for Ozone and Related Chemical Tracers, version 4) developed by NCAR (National Center for Atmospheric Research) is expected to provide the corresponding input.

Preliminary Results

IASI observations of tropospheric ozone over three Chinese megacities from 2008 to 2011 have been investigated. Fig. 4-2 (top) shows the monthly mean tropospheric ozone column over East China for January and August 2011. As shown in Fig. 4-2 (bottom), the different ozone seasonal patterns in Beijing, Shanghai and Guangzhou are consistent with ground-based measurement from other researchers. In Beijing the high ozone episodes are frequently observed during the summer, while in Guangzhou maximum ozone values can be observed in spring and autumn. It demonstrates the capability of satellite infrared nadir measurements to capture seasonal variations of tropospheric ozone in largely polluted regions.

The CH_2O/NO_2 column ratio is an indicator of surface ozone-NOx-VOC sensitivity because the bulk of both species over polluted regions are within the planetary boundary layer (PBL) and the columns are closely related to NOx and VOC emissions (*Martin et al. 2004*). *Duncan et al. (2010)* estimated that the limiting conditions should occur when the ratio is <1 (VOC-limited) or >2 (NOx-limited). Fig. 4-3 (left) displays the monthly mean CH_2O/NO_2 ratios for August 2007 over China. In most of China, the ratios >2 indicate NOx-limited conditions. Over Bohai, the Yangtze River Delta (YRD), and the Pearl River Delta (PRD) regions with high NOx emissions, the ratios exhibit values <2. Southern China except PRD region typically had the larger ratios than eastern China because of lower NOx emissions. As shown in Fig. 4-3 (right), the CH_2O/NO_2 ratios from March to November 2007 indicate VOC-limited and transition regime over three Chinese megacities. The implied ozone-precursor sensitivity from the CH_2O/NO_2 ratio reported here is broadly consistent with results from other studies using models and in situ data.

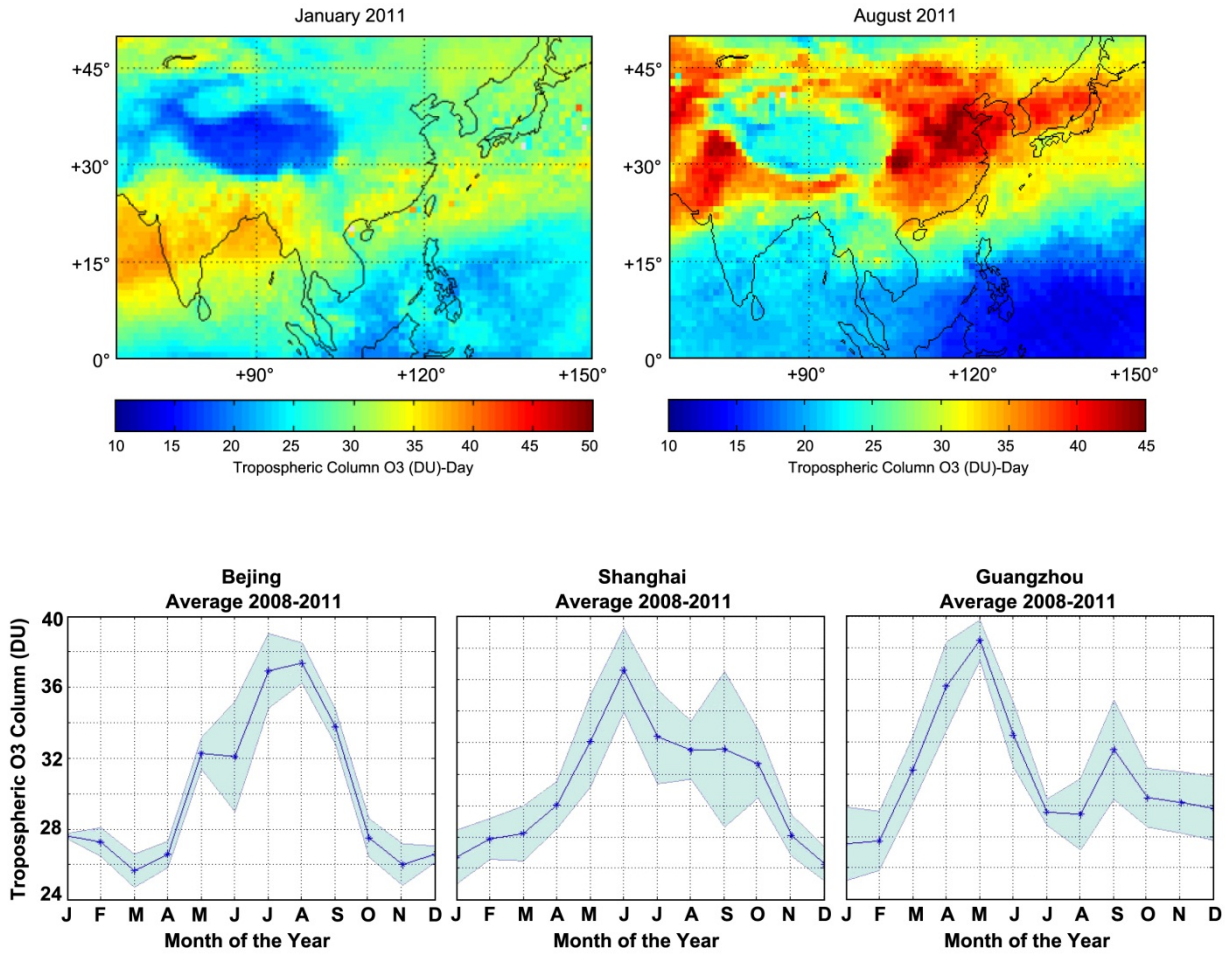

Fig. 4-2: Top: IASI tropospheric ozone column for the months of January and August 2011 over China. Bottom: Seasonal distribution of the IASI tropospheric ozone in the Chinese megacities – Beijing, Shanghai and Guangzhou.

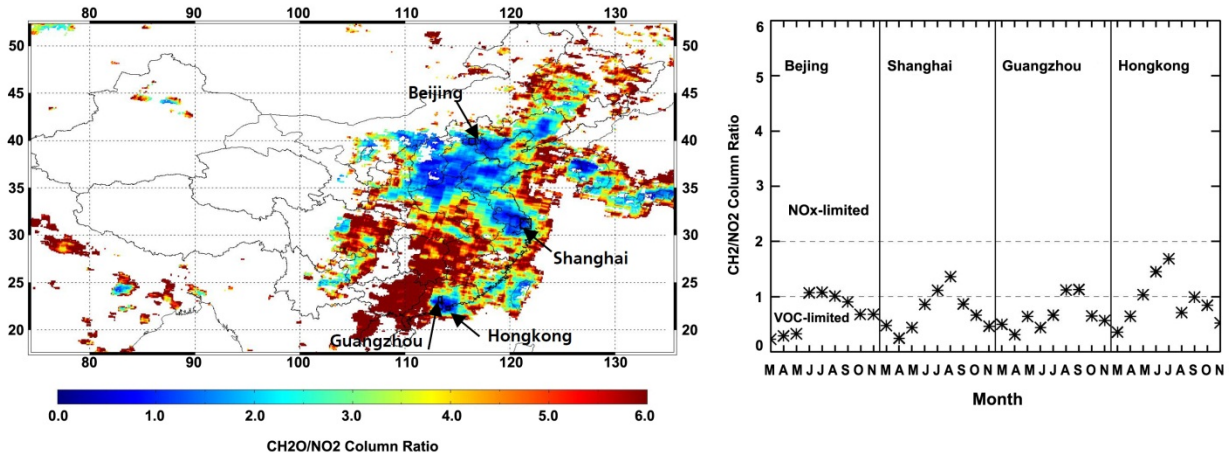

Fig. 4-3: Left: Monthly mean CH_2O/NO_2 column ratios from the GOME-2 instrument for China in August 2007. White areas indicate where CH_2O data are below the detection limit and NO_2 columns less than 1×10^{15} molec cm^{-2}. Right: Monthly mean CH_2O/NO_2 ratios retrieved from the GOME-2 instrument from March to November 2007 for Beijing, Shanghai, Guangzhou and Hongkong.

References

Boersma K.F., Eskes H.J., Veefkind J.P., Brinksma E.J. et.al.: Near-real time retrieval of tropospheric NO2 from OMI, Atm. Chem. Phys., 2013-2128, sref:1680-7324/acp/2007-7-2103, 2007

De Smedt I., Van Roozendael M., Stavrakou T., Müller J.-F., Lerot C., Theys N., Valks P., Hao N., and van der A R.: Improved retrieval of global tropospheric formaldehyde columns from GOME-2/MetOp-A addressing noise reduction and instrumental degradation issues, Atmos. Meas. Tech., 5, 2933-2949, doi:10.5194/amt-5-2933-2012, 2012

Duncan B.N., Yoshida Y., Olson J.R. et al.: Application of OMI observations to a space-based indicator of NOx and VOC controls on surface ozone formation. Atmos. Environ., 44, 18, 2213-2223 DOI: 10.1016/j.atmosenv.2010.03.010, 2010

Martin R. et al.: Space-based diagnosis of surface ozone sensitivity to anthropogenic emissions. Geophysical Research Letters 31, L06120. doi:10.1029/2004GL019416, 2004

Valks P., Pinardi G., Richter A., Lambert J.-C., Hao N., Loyola D. et al.: Operational total and tropospheric NO2 column retrieval for GOME-2. Atmos. Meas. Tech., 4, 1491-1514, 2011

4.2 The EVOSS Project

P. Hedelt, P. Valks

Volcanic eruptions can be major hazards to local population and aviation and are also important for climate change. Unfortunately only a limited number of volcanoes are currently monitored from ground. Space-based atmospheric sensors allow to regularly monitor volcanic SO_2 and ash emissions on a global scale.

The EVOSS project (European Volcano Observatory Space Sciences), started in 2010, aims at gathering data from multiple satellites as well as ground-based data in order to allow the near-realtime monitoring of potentially active volcanoes, especially in the case of volcanic hazards. The web-based front end of the EVOSS information system is the Virtual Volcano Observatory (VVO). The VVO provides information that is tailored to the geographical area of interest for each user. It furthermore enables the user to access and download products or to select products for further visualization in the virtual map. Furthermore it allows for a multi-temporal analysis of SO_2 and radiant flux measurements over volcanic areas as well as the visualization of sequences of either SO_2 column or radiant flux measurements. EVOSS gathers ground deformation data and topographic change mapping by SAR, thermal anomalies based on TERRA and AQUA MODIS data, volcanic emissions (SO_2 and ash) based on MSG/SEVIRI, MetOp-A/IASI, MetOp-A/GOME-2 and ENVISAT/SCIAMACHY data.

The EVOSS testing phase started on 30 September, 2011 with the monitoring of 18 volcanoes located in Europe and Africa (including e.g. Etna, Eyjafjallajoküll, Nabro) both in real- and delayed-time mode. Since 2012 the EVOSS system is fully operational in realtime. The end of the project is currently projected for February 2013.

MF-ATP provides near-realtime SO_2 data from MetOp-A/GOME-2 to the EVOSS system. The operational SO_2 retrieval is performed in the framework of EUMETSAT's Ozone and Atmospheric Chemistry Monitoring SAF (O3M-SAF). Total SO_2 columns are corrected for the dependence on total ozone, the solar zenith angle and the temperature dependence of SO_2 cross-sections. Since the volcanic plume height is rarely available during a volcanic event, the total SO_2 column is retrieved for three different plume heights (2.5, 6 and 15 km) which represent typical volcanic events: passive outgassing of low volcanoes (2.5 km), moderate volcanic eruptions or passive degassing of high volcanoes (6 km) and explosive eruptions (15 km).

During the EVOSS test phase several volcanic events have been monitored by MetOp-A/GOME-2, including the eruption of Nabro (Eritrea) on 15 June 2011 and Merapi (Indonesia) on 5 November 2010. On 5 May 2010 the eruption of the Iceland volcano Eyjafjallajoküll transported large amounts of ash and SO_2 into the atmosphere. Carried by winds high up in the atmosphere, the volcanic ash cloud first led to the closure of airports throughout the UK and Scandinavia, and later in the rest of northern and

western Europe because of its unknown risk for aviation safety. Our research activities, focusing on the determination of the correct plume height, show a good agreement between retrieved plume heights based on GOME-2 data and in-situ data, visual observations, radar data and modeling results (see *Rix et al. 2012*).

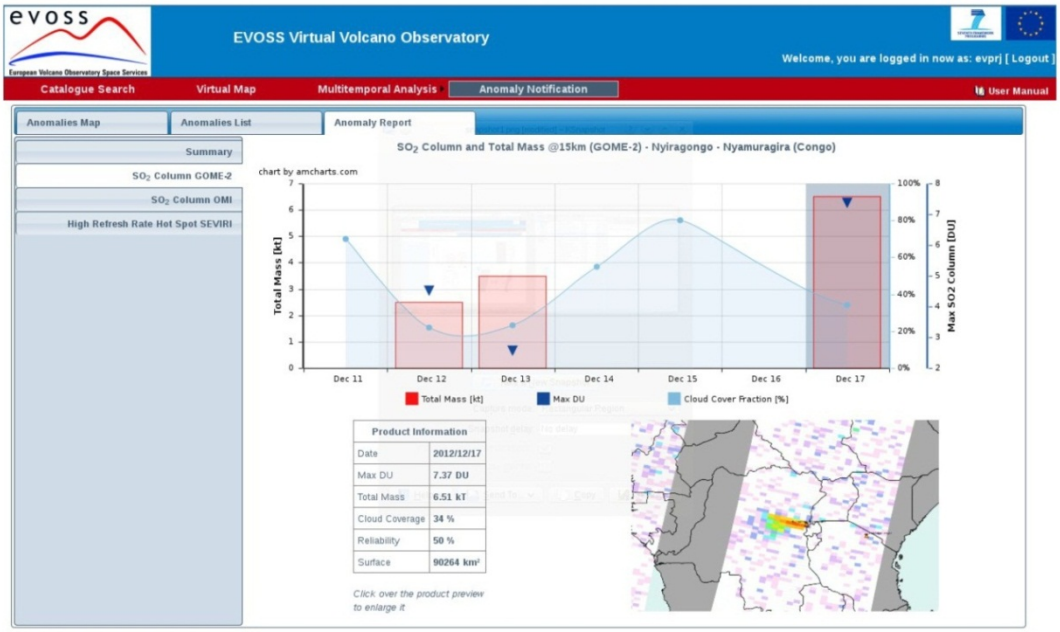

Fig. 4-4: Screenshot of one of the pages of the EVOSS website.

References

Rix et al.: Volcanic SO2, BrO and plume height estimations using GOME-2 satellite measurements during the eruption of Eyjafjallajökull in May 2010, Journal of Geophysical Research, 117, 2012

4.3 Exoplanet Atmospheres: Radiative Transfer and Remote Sensing

M. Vasquez, F. Schreier, S. Gimeno García, D. Kitzmann (TUB-ZAA), B. Patzer (TUB-ZAA), H. Rauer (DLR-PF and TUB-ZAA), and T. Trautmann

More than 850 exoplanets have been discovered in the past 20 years, a few thousands exoplanet candidates have been announced and extrapolation suggests that actually there should be millions of exoplanets in our galaxy. Among the confirmed exoplanets a few dozens have a mass lower than 10 Earth masses, some of them orbiting in the habitable zone of their central star. Accordingly, the spectroscopic characterization of these Earth-like planets' atmosphere, nb. the estimation of temperature and composition, is attracting increasing attention. In particular the feasibility to detect biosignatures, i.e. spectral features due to molecules related to biology, of terrestrial exoplanets has been discussed in several papers.

Along with molecules, planetary atmospheres may have condensates forming clouds that impact atmospheric chemistry, dynamics, and radiation. Hence for remote sensing of exoplanet atmospheres it is important to study the impact of clouds on planetary spectra. In two recent papers infrared radiative transfer in atmospheres of Earth-like planets around F, G, K, and M stars for clear-sky as well as cloudy atmospheres has been investigated using the GARLIC line-by-line code coupled to DISORT enabling a rigorous modeling of radiative transfer in scattering atmospheres with high spectral resolution (*Vasquez 2013a*, *2013b*, see also Annual Reports 2010 and 2011).

In order to learn about the feasibility of identifying molecular signatures in cloud-covered planets, the detailed analysis of the radiation source regions can provide information, i.e. radiation mainly coming

from the upper atmosphere is less likely to be hidden by clouds. In this regard the study of weighting functions is particularly useful. Weighting functions, originally introduced in the context of temperature sounding for meteorology and planetary science, are a quantitative measure that describe how different altitude regimes contribute to the upwelling radiation.

Fig. 4-5 illustrates weighting functions for clear-sky F-star and M-star planets (top-left and right), and F-star planet covered by low (H_2O) and high (ice) clouds. The location of the cloud layer (2 km or 10 km) is clearly visible in the lower two graphs. In the 4.3 and 15 µm region characterized by strong carbon dioxide absorption radiation is mostly originating in the upper atmosphere above the cloud layers and hence the impact of clouds is small especially in the band centers. In the very center of the ozone band around 9.6 µm absorption is weak, and radiation is mainly coming from the low troposphere of the cloud-free atmosphere, whereas the cloud deck is the main source of radiation in both cloud cases. However, for wavelengths with high O_3 absorption, the altitude region of the O_3 concentration peak contributes strongly to the upwelling radiation in all cases.

Knowledge of the planets' temperature structure is crucial for the correct interpretation of molecular signatures in order to avoid false-positive or negative conclusions. Weighting functions visualize a one-to-one wavenumber (or wavelength) to altitude mapping: Radiation in the CO_2 band center reveals information from upper atmospheric layers, and radiation in the wings from the lower atmosphere. Fortunately the altitude-wavenumber correspondence is only slightly modified by the star type and cloud coverage (at least for the stratosphere), so experience gained in atmospheric temperature sounding – well established from studies of Earth and planets in our own solar system – should be a good starting point for exoplanet temperature remote sensing.

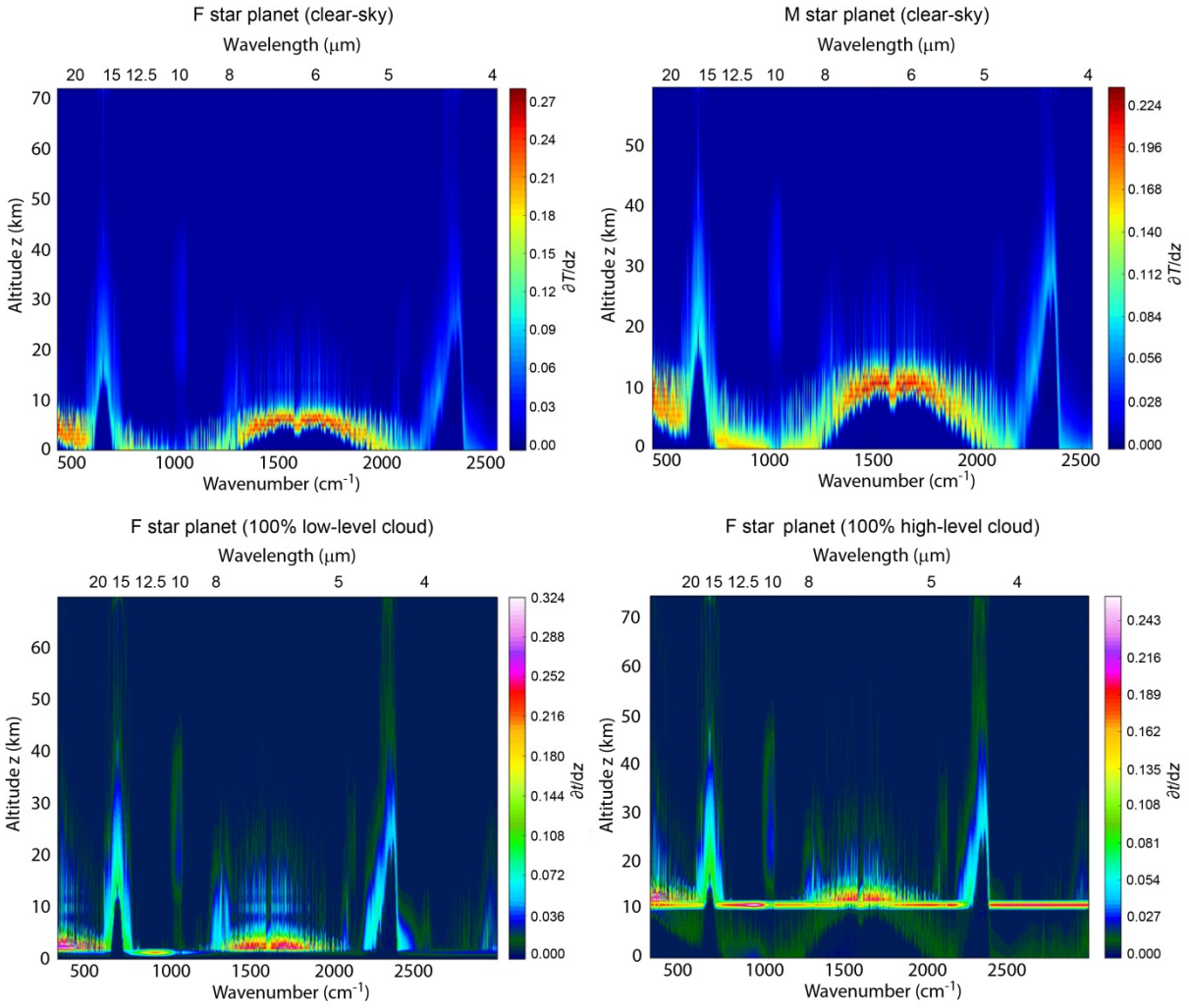

Fig. 4-5: Weighting functions for clear-sky F-star and M-star planets (top: left and right), and a F-star planet covered by low (H_2O) and high (ice) clouds (bottom: left and right). For details see text.

References

Vasquez M., Schreier F., Gimeno García S., Kitzmann D., Patzer B., Rauer H., and Trautmann T.: Infrared radiative transfer in atmospheres of Earth-like planets around F, G, K, and M stars I. Clear-sky thermal emission spectra and weighting functions. Astronomy & Astrophysics, 549, A26, 2013

Vasquez M., Schreier F., Gimeno García S., Kitzmann D., Patzer B., Rauer H., and Trautmann T.: Infrared radiative transfer in atmospheres of Earth-like planets around F, G, K, and M stars II. Thermal emission spectra influenced by clouds. Astronomy & Astrophysics, submitted, 2013

4.4 Spectral Features of Earth-like Planets and Their Detectability

P. Hedelt, P. von Paris (DLR-PF, LAB), M. Godolt (TUB), S. Gebauer (TUB), J.L. Grenfell (TUB), H. Rauer (TUB, DLR-PF), F. Schreier, F. Selsis (LAB), T. Trautmann

The possibility of finding potentially habitable or even inhabited terrestrial planets is one of the exciting motivations for the search of extrasolar planets. So far, more than 50 planets with masses below 10 Earth masses are known among the more than 800 detected extrasolar planets. For short-period orbits with periods < 50 days, 11-17% of all stars host at least one low-mass planet. Estimates inferred from microlensing surveys imply that the mean number of planets per star is > 1 (*Cassan et al. 2012*). Already, some potentially habitable super-Earths in or very close to the habitable zone (HZ) of their central star have been discovered. Hence, the detection of potentially habitable terrestrial planets is within reach of present-day instrumentation. The next step would be to search such potentially habitable worlds for the indications of the presence of life, so called *biomarkers*. To be detectable remotely from Earth, such biomarkers are necessarily surface or atmospheric spectral signatures.

Earth is so far the only known example of a habitable and inhabited planet, which can be used to investigate the parameter space of habitable conditions. It is straightforward (at least conceptually) to build a spectrum from a given arbitrary atmospheric composition. The inverse problem, however, i.e. to infer the characteristics of a planet from a spectrum, is much more difficult due to its ill-posed nature. It is nevertheless of paramount importance to understand what type of planet lies behind a given observed spectrum. Spectroscopic or photometric techniques enable the detection and even the investigation of the atmosphere of a transiting exoplanet. However, a huge number of parameters affect the atmospheric and spectral appearance of a given Earth-like planet.

We have investigated for which conditions (in terms of orbital distance in the HZ and type of central star) molecular absorption bands can be detected with near-future telescope facilities. We calculated atmospheric profiles for a set of hypothetical planets, using the one-dimensional, cloud-free coupled climate and photochemical model of *Rauer et al. (2011)*. The profiles are calculated for an Earth-like planet located at three different orbital positions assuming it is orbiting three different main-sequence central stars. The central stars chosen are a F-type star, a G-type (solar-like) star and a K-type star. We have selected three orbital distances to the central star within the HZ, where the surface temperature is 273K (0°C), 288K (15°C) or 303K (30°C), corresponding to a definition of the HZ given by *Dole et al. (1964)* for complex life. Using the radiative-transfer model MIRART-SQuIRRL (*Schreier et al. 2001*) we then calculated high-resolution synthetic emission and transmission spectra using the atmospheric profiles.

Results

On increasing the orbital distance, we found that the total column amount of O_3, CH_4, N_2O and HNO_3 increases, whereas H_2O decreases. The increase is related to atmospheric chemistry, whereas the decrease in H_2O is related to the decreasing stellar insolation, which provides colder atmospheric temperatures and hence condensation of water. This atmospheric response is also visible in high-resolution transmission and emission spectra (see Fig. 4-6). S/N ratios using high-resolution spectroscopy are very low for Earth-like exoplanets. Higher S/N ratios can be obtained by using photometric filters by integrating over a fixed spectral bandpass. We have studied the spectral response using two near- and thermal-infrared photometric instruments that are planned for the JWST (James Webb Space Telescope). In order to determine if an absorption band is present in a given filter, reference filters have to be chosen that are positioned over atmospheric windows, hence do not cover molecular absorption bands.

Two filters were identified, that can be used as reference filters (at 3.7 µm and 11.3 µm). We found that the spectral response of H_2O and CH_4 is also visible using photometric filters. The atmospheric response of the other molecules is too weak as to detect this in the low-resolution filters.

We furthermore investigated the detectability of the absorption bands when using e.g. the ground-based E-ELT (European Extremely Large Telescope) and the space-borne JWST. For this, we calculated the background-limited S/N ratios in the filters, and found that the contrast between stellar and planetary emission during secondary eclipse observations is too small as to detect any absorption band. However, during primary eclipse, absorption bands of CO_2, H_2O, CH_4 and O_3 can be detected for some scenarios.

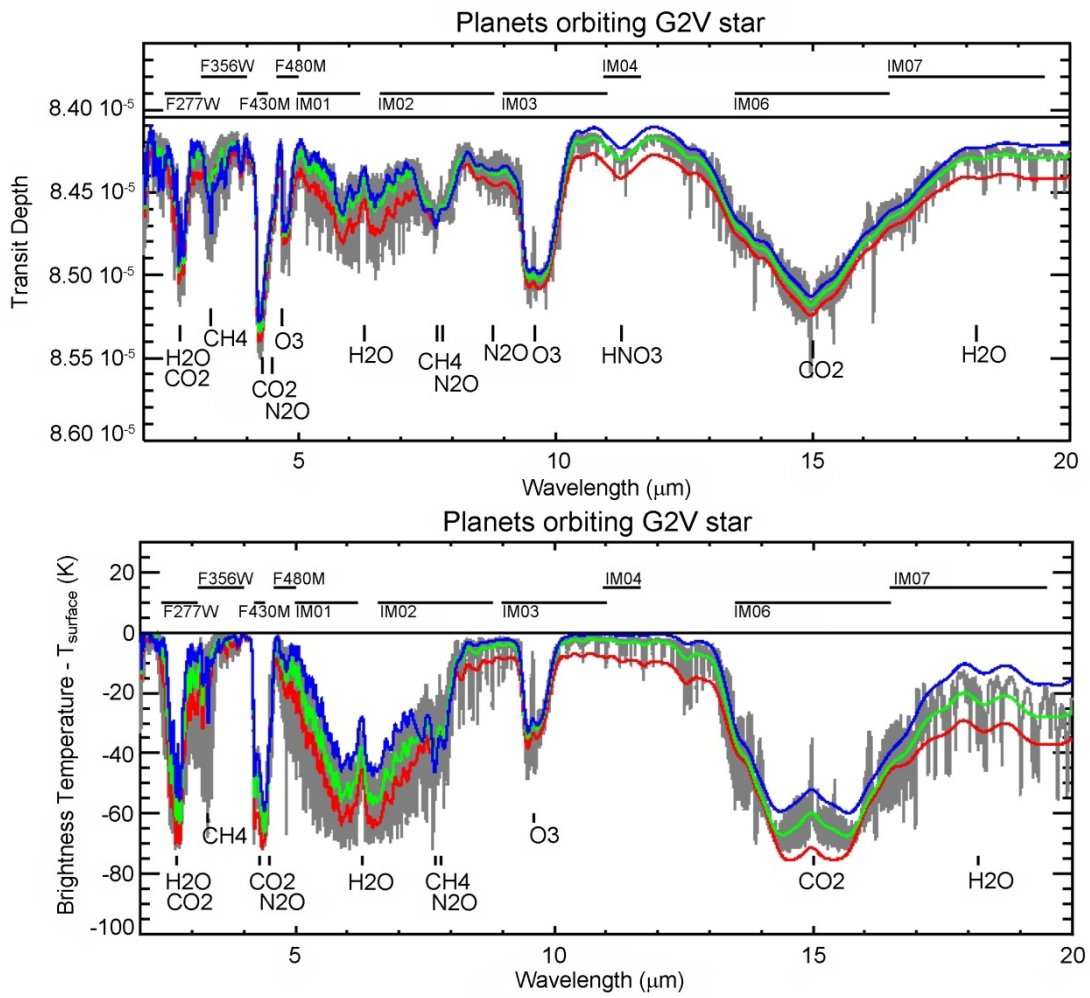

Fig. 4-6: Transit depth spectrum during primary eclipse (upper figure) and brightness temperature difference to model surface temperature during secondary eclipse (lower plot). Spectra shown have been calculated for R=100, except for the grey spectrum, which has been calculated with R=3000. The colors correspond to the orbital position of the planet: Inner HZ (red), center HZ (green) and outer HZ (blue).

To summarize, we have shown for the first time, that photometric filters planned for the JWST or the E-ELT can also be used for the characterization of Earth-like exoplanet atmospheres, although the filter bandpasses have been defined for different scientific purposes. They can be used to characterize a given planetary atmosphere even if they provide only a very low spectral resolution. However, several filters need to be positioned over a broad wavelength range in order to obtain information about different biomarker molecules and surface conditions. In order to obtain information about the surface conditions and to perform a comparative filter analysis as performed here, reference filters need to be chosen carefully in order not to be contaminated by spectral absorption bands.

References

Cassan A., Kubas D., Beaulieu J.-P., et al.: One or more bound planets per Milky Way star from microlensing observations, Nature, 481, 167, 2012

Dole S.H.: Habitable planets for man (New York, Blaisdell Pub. Co. 1964, 1st ed.), 1964

Rauer H., Gebauer S., von Paris P., et al.: Potential Biosignatures in Super-Earth Atmospheres I. Spectral appearance of super-Earths around M dwarfs, Astron. Astrophys., 529, A8, 2011

Schreier F. and Schimpf B.: A New Efficient Line-By-Line Code for High Resolution Atmospheric Radiation Computations incl. Derivatives, in International Radiation Symposium IRS2000: Current Problems in Atmospheric Radiation, ed. W. Smith & Y. Timofeyev (A. Deepak Publishing), 381–384, 2001

4.5 Biomolecules in Astrobiology

M. Meringer, H.J. Cleaves (BMSIS), S.J. Freeland (UHNAI)

Astrobiology is the study of the origin, distribution and future of life in the universe. At the moment we know only one instance of life in the universe, that found on our own planet. However, due to the continuously growing number of discovered extrasolar planets, questions regarding the origins and evolution of life are attracting increasing interest. Another driving force here is the discovery of extremophiles, organisms able to survive under extreme physicochemical conditions, e.g. with respect to temperature, pressure, acidity, etc. These new facts, mainly explored during the past two decades, have led to a re-examination of an age-old question: Is extraterrestrial life possible, does it exist, would it necessarily have to share the same biochemical framework as terrestrial life or could it be organized completely differently?

A key feature of all terrestrial life forms is the genetic code. In simple terms, the genetic code maps information to function. Information about life's composition is stored in DNA, a polymer of nucleotides. Function is realized by proteins. Proteins are polymers of another type of biomolecules, amino acids. Proteins give cells their structure and perform multiple tasks within a living organism's metabolism, such as molecule transport and catalysis of chemical reactions. Interestingly, all known life forms with very few exceptions share the same genetic code, and proteins are built up from a unique but universal set of 20 genetically encoded amino acids.

Important questions arise from this fact: Why did terrestrial life select exactly these 20 amino acids out of a mathematically almost infinite number of possibilities? Is this only a random result of early evolution on Earth, or could there perhaps be universal rules behind this 'choice'? *Philip and Freeland (2011)* came up with some original approaches to asking these questions. They found that the genetically encoded amino acids exhibit a broad, even distribution of some key physicochemical properties, which sets them apart from any alternative set of amino acids drawn randomly from the superset of amino acids that was available for early evolution. This super set comprised about 60 amino acids which were likely available from abiological synthesis.

However, the "chemical space" of possible amino acids is much, much larger, as discussed by *Cleaves (2010*) and illustrated in Fig. 4-7 and 4-8. In order to either prove the hypothesis of Philip and Freeland, or to disprove and improve this approach, it is necessary to generate and examine much larger sets of amino acids. Dedicated computer programs, so-called *structure generators*, use methods from graph-theory, combinatorics, group-theory and algebra to construct virtual chemical compound libraries with given constraints (*Meringer 2010*). In order to define the structural constraints of the required α-amino acids, to code the input for the structure generation software, and to keep the sizes of constructed amino acid libraries and the required computational resources within acceptable limits, a four week on-site cooperation was initiated by the authors and carried out at the University of Hawaii's NASA Astrobiology Institute (NAI), financially supported by NAI's 2012 Director's Discretionary Fund.

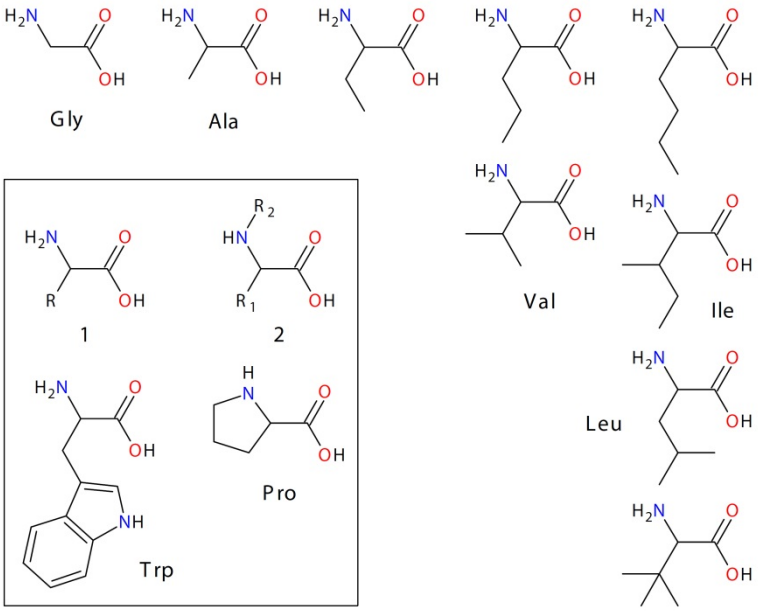

Fig. 4-7: Small aliphatic α-amino acids with up to six carbon atoms. The coded amino acids among them are labelled by their abbreviation (Glycine, Alanine, Valine, Isoleucine, Leucine). Inset: 19 of the 20 coded amino acids are represented by generic structure '1'. R denotes the sidechain. Tryptophane, the largest coded amino acid, includes eleven carbon atoms. Coded amino acid Proline has another generic representation, depicted in structure '2'.

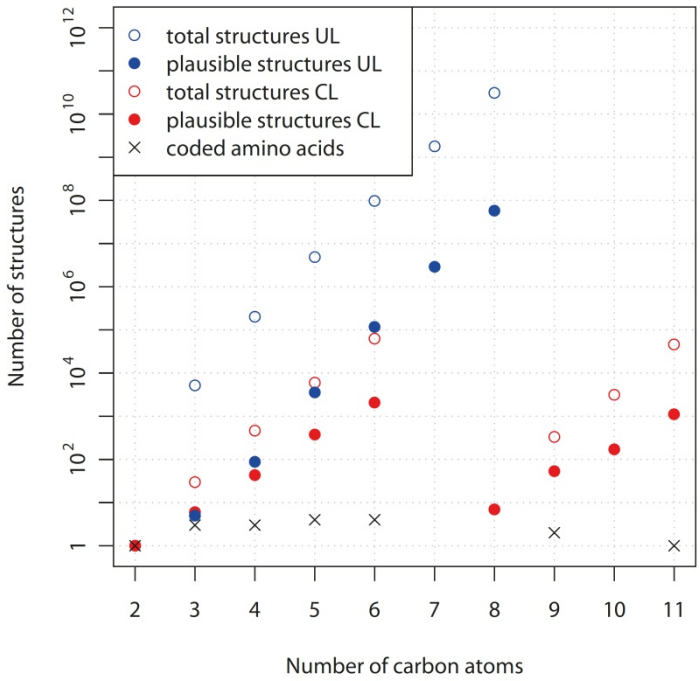

Fig. 4-8: Sizes of α-amino acid libraries calculated during the study. In order to reduce the total set of mathematically possible structures to those structures which are chemically plausible, a list of 156 forbidden substructures was compiled. The plot shows the results of this effort. Compared to the unique library (UL), the combined library (CL) contains also structures of type 2 and structures with a larger number of carbon atoms.

The results include two virtual amino acid libraries that were generated using two different approaches. A large, 'unique' library of 121044 structures limited at an upper bound of six carbon atoms, which covers the space of molecular formulas as completely as possible, and a smaller 'combined' library of 3846 structures, which includes all coded amino acids. Fig. 4-8 shows the composition of these libraries

itemized by the number of carbon atoms. A detailed description of all methods and results is in preparation (*Meringer et al., in preparation*).

References

Cleaves H.J., 2nd: The origin of the biologically coded amino acids. J. Theor. Biol. 263(4): 490-498, 2010

Meringer M.: Structure enumeration and sampling. Handbook of Chemoinformatics Algorithms. Edited by J.-L. Faulon and A. Bender, Chapman & Hall: 233-267, 2010

Meringer M., Cleaves H.J. and Freeland S.J.: Beyond Terrestrial Biology: Charting the Chemical Universe of α-Amino Acid Structures. In preparation.

Philip G.K. and Freeland S.J.: Did evolution select a nonrandom "alphabet" of amino acids? Astrobiology 11(3): 235-240, 2011

5. Documentation

5.1 Books and Book Contributions

Dameris, M., Loyola, D.: Recent and future evolution of the stratospheric ozone layer. In: Atmospheric Physics: Background - Methods - Trends Research Topics in Aerospace, 747-762, Springer, ISBN 978-3-642-30182-7, 2012

Kohlert, D., Schreier, F.: Optimized Implementations of Floating-Point-Polynomials on FPGA-Hardware. In: Informatics Microsystems Information Systems, Hochschule Regensburg and Moscow State Technical University, 89-99, ISBN 978-5-7339-1000-0, 2012

5.2 Journal Papers

Afanas'ev, V.P., Efremenko, D.S., Lubenchenko, A.V.: Determining the applicability boundaries of small-angle approximation to the radiative transfer equation for elastic peak electron spectroscopy. Bulletin of the Russian Academy of Science. Physics, 76 (5), 565-569, DOI 10.3103/S1062873812050036, 2012

Bramstedt, K., Noël, S., Bovensmann, H., Gottwald, M., Burrows, J.P.: Precise pointing knowledge for SCIAMACHY solar occultation measurements. Atmospheric Measurement Techniques, 5 (11), 2867-2880, DOI: doi:10.5194/amt-5-2867-2012, 2012

Budak, V.P, Efremenko, D.S., Shagalov, O.V.: Mathematical modeling of the optical and electronic signals of the remote sensing from space in the presence of broken clouds. News of higher educational institutions, 55(9/2), 148-149, ISSN: 0021-3411, 2012 [in Russian]

Budak, V.P., Efremenko, D.S. and Shagalov, O.V.: Efficiency of algorithm for solution of vector radiative transfer equation in turbid medium slab. Journal of Physics: Conference Series, 369, 012021, doi:10.1088/1742-6596/369/1/012021, 2012

De Smedt, I., Van Roozendael, M., Stavrakou, T., Müller, J.-F., Lerot, C., Theys, N., Valks, P., Hao, N., and van der A, R.: Improved retrieval of global tropospheric formaldehyde columns from GOME-2/MetOp-A addressing noise reduction and instrumental degradation issues. Atmos. Meas. Tech., 5, 2933-2949, doi:10.5194/amt-5-2933-2012, 2012

Doicu, A., Efremenko, D., Trautmann, T.: A multi-dimensional vector spherical harmonics discrete ordinate method for atmospheric radiative transfer. Journal of Quantitative Spectroscopy and Radiative Transfer, dx.doi.org/10.1016/j.jqsrt.2012.12.009, 2012

Doicu, A., Efremenko, D., Trautmann, T.: An analysis of the short-characteristic method for the spherical harmonic discrete ordinate method (SHDOM). Journal of Quantitative Spectroscopy and Radiative Transfer, dx.doi.org/10.1016/j.jqsrt.2012.12.024, 2012

Gottwald, M.: Reisen zu den Planeten. Part 1: Die ersten Schritte. Sterne und Weltraum, 10, 34-45, 2012

Gottwald, M.: Reisen zu den Planeten. Part 2: Die Nachbarn der Erde. Sterne und Weltraum, 11, 44-54, 2012

Gottwald, M.: Reisen zu den Planeten. Part 3: Jenseits des Mars. Sterne und Weltraum, 12, 52-62, 2012 Spektrum der Wissenschaft, Heidelberg.

Grenfell, J.L., Griessmeier, J.M., von Paris, P., Patzer, B., Lammer, H., Stracke, B., Gebauer, S., Schreier, F., Rauer, H.: Response of atmospheric biomarkers to NOx-induced photochemistry generated by stellar

cosmic rays for Earth-like planets in the habitable zone of M-dwarf stars. Astrobiology, 12 (12), 1109-1122. DOI: 10.1089/ast.2011.0682, 2012

Koukouli, M.E., Balis, D.S., Loyola, D., Valks, P., Zimmer, W., Hao, N., Lambert, J.-C., Van Roozendael, M., Lerot, C., Spurr, R.J.D.: Geophysical validation and long-term consistency between GOME-2/MetOp-A total ozone column and measurements from the sensors GOME/ERS-2, SCIAMACHY/ENVISAT and OMI/Aura. Atmospheric Measurement Techniques, 5, 2169-2181, doi: 10.5194/amt-5-2169-2012, 2012

Loyola, D., Coldewey-Egbers, M.: Multi-sensor data merging with stacked neural networks for the creation of satellite long-term climate data records. EURASIP Journal on Advances in Signal Processing, 2012:91, DOI: 10.1186/1687-6180-2012-91, 2012

Marpu, P.R., Pedergnana, M., Dalla Mura, M., Peeters, S., Benediktsson, J.A. and Bruzzone, L.: Classification of Hyperspectral Data Using Extended Attribute Profiles Based on Supervised and Unsupervised Feature Extraction. Int. Journal of Image and Data Fusion, 3(3), 269-298, DOI: 10.1080/19479832.2012.702687, 2012

Pedergnana, M., Marpu, P.R., Dalla Mura, M., Benediktsson, J.A., Bruzzone, L.: Classification of Remote Sensing Optical and LiDAR Data Using Extended Attribute Profiles. IEEE Journal of Selected Topics in Signal Processing 6(7), 856-865, 2012

Rix, M.,Valks, P., Hao, N., Loyola, D., Schlager, H., Huntrieser, H., Flemming, J., Koehler, U., Schumann, U., Iness, A.: Volcanic SO2, BrO and plume height estimations using GOME-2 satellite measurements during the eruption of Eyjafjallajökull in May 2010. Journal of Geophysical Research, 117, D00U19, DOI: 10.1029/2011JD016718, 2012

Schmidt, K., Yurkin, M.A., Kahnert, M.: A case study on the reciprocity in light scattering computations, Optics Express, Vol. 20, 23253-23274, 2012

Schymanski, E.L., Gallampois, C.M.J., Krauss, M., Meringer, M., Neumann, S., Schulze, T., Wolf, S., Brack, W.: Consensus Structure Elucidation Combining GC/EI-MS, Structure Generation, and Calculated Properties. Analytical Chemistry, 84 (7), 3287-3295, American Chemical Society, DOI: 10.1021/ac203471y, 2012

Slijkhuis, S.: Undersampling und das missverstandene Nyquist-Kriterium. SPEKTRUM, 43, 20-26, Pollmann, ISSN 1869-4454, 2012

Van Roozendael, M., Spurr, R., Loyola, D., Lerot, C., Balis, D., Lambert, J.-C., Zimmer, W., van Gent, J., van Geffen, J., Koukouli, M., Granville, J., Doicu, A., Fayt, C., Zehner, C.: Sixteen years of GOME/ERS-2 total ozone data: The new direct-fitting GOME Data Processor (GDP) version 5 – Algorithm description. Journal of Geophysical Research, 117 (D3), DOI: 10.1029/2011JD016471, 2012

Wang, S., Zhou, B., Wang, Z., Yang, S., Hao, N., Valks, P., Trautmann, T., Chen, L.: Remote sensing of NO2 emission from the central urban area of Shanghai (China) using the mobile DOAS technique. Journal of Geophysical Research. 117, D13305, DOI: 10.1029/2011JD016983, 2012

Zenner, L., Gruber, T., Beutler, G., Jäggi, A., Flechtner, F., Schmidt, T., Wickert, J., Fagiolini, E., Schwarz, G., Trautmann, T.: Using Atmospheric Uncertainties for GRACE De-aliasing: First Results. In: Geodesy for Planet Earth International Association of Geodesy Symposia, 136 (2), 147-152, Springer, ISBN 987-3-642-20337-4, 2012

5.3 Conference Proceeding Papers and Presentations

Bovensmann, H., Eichmann, K.-U., Noël, S., Wittrock, F., Buchwitz, M., von Savigny, C., Rozanov, A., Kokhanovsky, A., Lelli, L., Hillboll, A., Vountas, M., Burrows, J.P., Lichtenberg, G., Doicu, A., Schreier, F., Hrechanyy, S., Gimeno García, S., Kretschel, K., Meringer, M., und Hess, M., Gottwald, M., Tilstra, L.G. und Snel, R., Krijger, J.M., Lerot, C., De Smedt, I., Van Roozendael, M., Brizzi, G., Dehn, A., Fehr, T.: Development and Maintenance of SCIAMACHY operational ESA level 2 products: from Version 5 towards Version 6. Proceedings of Advances in Atmospheric Science and Applications (ESA SP-708), ISBN 978-92-9092-272-8, Bruges, Belgium, 2012

Budak, V.P., Efremenko, D.S., Shagalov, O.V.: Efficiency of algorithm for solution of vector radiative transfer equation in turbid medium slab. Proceedings of EUROTHERM 95, Nancy, France, 2012

Budak, V.P., Efremenko, D.S., Shagalov, O.V.: Comparative analysis of common parallel computing features for the radiative transfer solution for a homogeneous slab. Proceedings of EUROTHERM 95, Nancy, France, 2012

Efremenko, D., Doicu, A., Loyola, D., Trautmann, T.: On the implementation of the discrete ordinate method with small-angle approximation for a pseudo-spherical atmosphere. Geophysical Research Abstracts, 14 (EGU2012-10817), European Geosciences Union General Assembly 2012, Vienna, Austria, April 22-27, 2012

Efremenko, D., Doicu, A., Loyola, D., and Trautmann, T.: Accelerations of the discrete ordinate method for nadir viewing geometries. International Radiation Symposium 2012 (IRS2012), Berlin, Germany, 2012

Doicu, A., Efremenko, D.S., Loyola D., Trautmann T.: Generalization of three-dimensional scalar model of the radiation transfer SHDOM on the vector case, 10th Annual All-Russian Open Conference on Actual Problems in Remote Sensing of the Earth from Space, Moscow, Russia, 2012

Gimeno García, S., Schreier, F., und Meringer, M., Lichtenberg, G.: Carbon gas retrievals from SCIAMACHY observations using BIRRA. Proceedings of Advances in Atmospheric Science and Applications (ESA SP-708), ISBN 978-92-9092-272-8, Bruges, Belgium, 2012

Godolt, M., Gebauer, S., Grenfell, J.L., Hedelt, P., Kitzmann, D., Patzer, B., Rauer, H., Stracke, B., von Paris, P.: Spectral appearance and detectability of terrestrial extrasolar planetary atmospheres. Observing Planetary Systems II, Santiago de Chile, Chile, 2012

Gottwald, M.: 50 Jahre Interplanetare Raumfahrt - ein neuer Blick auf unsere Nachbarwelten. Public lecture, Trebur, April 20, 2012

Gottwald, M.: 50 Jahre Interplanetare Raumfahrt - ein neuer Blick auf unsere Nachbarwelten. Public lecture, Munich, December 14, 2012

Grossi, M., Valks, P., Slijkhuis, S., Loyola, D., Aberle, A., Beirle, S., Mies, K., Wagner, T., Gleisner, H., Lauritsen, K.B.: Water vapour column density product from GOME-2: Validation with independent satellite observations. EUMETSAT Meteorological Satellite Conference, Sopot, Poland, 2012

Hao, N., Valks, P., De Smedt, I., Loyola, D., Van Roozendael, M., Zhou, B. and Zimmer, W.: Satellite observation of air quality in the Chinese megacities. Geophysical Research Abstracts, 14 (EGU2012-11168), European Geosciences Union General Assembly 2012, Vienna, Austria, 2012

Hao, N., Ding, A.J., Valks, P., Clerbaus, C., Safieddine, S., Trautmann, T.: Assessment of the impact of the East Asian Summer Monsoon on the air quality over China. Dragon 2 Final Results and Dragon 3 KO Symposium, Beijing, China, 2012

Hao, N., Valks, P., De Smedt, I., Van Roozendael, M., Zhou, B., Loyola, D., Clerbaus, C., Safieddine, S.:

Satellite observations of air quality in the Chinese megacities. 12th IGAC open science conference, Beijing, China, 2012

Meringer, M.: Where Chemoinformatics Meets Astrobiology - A Journey to the Event Horizon of Structure Generation. Astrobiology seminar, Honolulu/Hawaii, US, February 27, 2012

Meringer, M., Cleaves, H.J., Freeland, S.J.: Tools to Explore the Evolution of Life: Construction of Virtual Amino Acid Libraries. Lecture, Honolulu/Hawaii, US, March 9, 2012

Pedergnana, M., Marpu, P.R., Dalla Mura, M., Benediktsson, J.A. and Bruzzone, L.: A novel supervised feature selection technique based on Genetic algorithms. Proceedings of the Geoscience and Remote Sensing Symposium (IGARSS 2012), 60-63, Munich, Germany, 2012

Rother, T.: Probability States, Entanglement and Bell's Experiment in Classical Mechanics. Quantum 2012, Torino, Italy, 2012

Valks P., Hao, N., Loyola, D., De Smedt, I., Delcloo, A., Pinardi, G., Lambert, J.-C., van Roozendael, M., and Zimmer, W.: Tropospheric trace-gas column observations from GOME-2 for air quality applications. European Geosciences Union General Assembly (EGU2012), Vienna, Austria, April 22-27, 2012

Valks, P., Hedelt, P., Hao, N., Loyola, D. and Zimmer, W.: SO_2 column and plume height from GOME-2 measurements. EVOSS 2nd Annual Review Meeting, Paris, France, 2012

Valks, P., Hao, N., Loyola, D., De Smedt, I., Van Roozendael, M., Lambert, J.-C.,Pinardi, G., Delcloo, A. and Zimmer, W.: Tropospheric trace gas column observations from GOME-2/MetOp. Proceedings of Advances in Atmospheric Science and Applications (ESA SP-708), ISBN 978-92-9092-272-8, Bruges, Belgium, 2012

Valks, P., Hao, N., Slijkhuis, S., Grossi, M., Loyola, D., Pinardi, G., De Smedt, I., Van Roozendael, M. and Delcloo, A.: Tropospheric trace-gas column observations from GOME-2. EUMETSAT Meteorological Satellite Conference, Sopot, Poland, 2012

Vasquez, M., Schreier, F., Kitzmann, D., Gimeno García, S., Patzer, B., Rauer, H., Trautmann, T.: High Resolution Infrared Radiative Transfer of Earth-like planets Influenced by Multiple Clouds. 39th COSPAR Scientific Assembly 2012, Mysore, India, 2012

Vasquez, M.: Galileo Mobile Khagol Rath expedition. Astronomy traveling science education in Karnataka state, India, 2-13 July 2012 (www.galileo-mobile.org)

Vasquez, M., Schreier, F., Kitzmann, D., Patzer, B., Rauer, H., Gimeno García, S., Trautmann, T.: Effects of Clouds on High Resolution Thermal Emission Spectra of Terrestrial Exo-Planets. In: Geophysical Research Abstracts, 14 (EGU2012-11168), European Geosciences Union General Assembly 2012, Vienna, Austria, 2012

von Paris, P., Hedelt, P., Selsis, F., Schreier, F., Trautmann, T.: Characterization of potentially habitable planets and their atmospheres. 5th Alliance Week of the HGF Alliance *Planetary Evolution and Life*, Berlin, 2012

Xu, J., Schreier, F., Doicu, A., Voigt, P., Trautmann, T.: Retrieval of Stratospheric Trace Gases from FIR/Microwave Limb Sounding Observations. Proceedings of Advances in Atmospheric Science and Applications (ESA SP-708), ISBN 978-92-9092-272-8, Bruges, Belgium, 2012

Xu, J., Schreier, F., Doicu, A., Voigt, P., Trautmann, T.: Deriving Stratospheric Trace Gases From Balloon-borne Infrared/Microwave Limb Sounding Measurements. International Radiation Symposium (IRS2012), Berlin, Germany, 2012

5.4 Attended Conferences

4th Alliance Week. HGF Helmholtz Alliance Planetary Evolution and Life, Berlin, Germany, 20-24 February 2012

2nd SPARC/IOC/IGACO-O3/NDACC Workshop on Past Changes in the Vertical Distribution of Ozone, Columbia, Maryland, US, 16-18 April 2012

EUROTHERM Seminar No. 95 Computational Thermal Radiation in Participating Media IV, Nancy, France, 18-20 April 2012

European Geosciences Union General Assembly (EGU2012), Vienna, Austria, 22-27 April 2012

Datenrettungskonferenz, Moscow, Russia, 26/27 April 2012

Quantum 2012, Torino, Italy,20-26 May 2012

ATMOS 2012. Advances in Atmospheric Science and Application, Bruges, Belgium, 18-22 June 2012

EVOSS 2nd Annual Review Meeting, Paris, France, 14/15 June 2012

Dragon 3 KO Symposium, Beijing, China, 25-29 June 2012

39th COSPAR Scientific Assembly, Mysore, India, 14-22 July 2012

SCAR Open Science Conference, Portland, Oregon, US, 16-19 July 2012

IEEE International Geoscience and Remote Sensing Symposium 2012 (IGARSS2012), Munich, Germany, 22-27 July 2012

International Radiation Symposium 2012 (IRS2012), Berlin, Germany, 6-10 August 2012

Quadrennial Ozone Symposium 2012, Toronto, Canada, 27-31 August 2012

11th Atmospheric Spectroscopy Applications (ASA) Meeting & 12th Biennial HITRAN Database Conference, Reims, France, 29-31 August 2012

EUMETSAT Meteorological Satellite Conference, Sopot, Poland, 2-7 September 2012

12th IGAC Open Science Conference: Atmospheric Chemistry in the Anthropocene, Beijing, China, 17-21 September 2012

5th Alliance Week. HGF Helmholtz Alliance Planetary Evolution and Life, Berlin, Germany, 29 October 2012 – 1 November 2012

10th Annual All-Russian Open Conference on Actual Problems in Remote Sensing of the Earth from Space, Moscow, Russia, 12-16 November 2012

EUMTRISPEC – First Stakeholder Workshop. Traceable spectral reference line data for atmospheric monitoring, Wolfenbüttel and PTB Braunschweig, Germany, 15/16 November 2012

5.5 Academic Degrees

Habilitation

Doicu, A.: Privatdozent ('venia legendi') in Atmospheric Remote Sensing, Technical University of Munich, Faculty for Civil Engineering and Surveying, February 2012

Diploma and Doctoral Theses

Fischer, P.: Solving Optimization and Search Problems in Remote Sensing by using Evolutionary Algorithms. Master thesis in Geodesy and Geoinformation master course at TUM (Supervisor: Diego Loyola)

Gimeno García, S.: Simulation of solar radiative transfer and comparison with spectro-radiometric measurements. Dissertation, Faculty of Physics and Earth Science, University of Leipzig. (Supervisor: Prof. Dr. Thomas Trautmann)

Köhler, C.H.: Observation and simulation of the longwave radiative effects for Saharan mineral dust plumes. Dissertation, Faculty of Physics and Earth Science, University of Leipzig. (Supervisors: Prof. Dr. Manfred Wendisch, University of Leipzig and Prof. Dr. Thomas Trautmann)

Otto, S.: Optische Eigenschaften nichtkugelförmiger Saharamineralstaubpartikel und deren Einfluss auf den Strahlungstransport in der Erdatmosphäre. Dissertation, Faculty of Physics and Earth Science, University of Leipzig, thesis defence completed in February 2012. (Supervisors: Prof. Dr. Thomas Trautmann and Prof. Dr. Manfred Wendisch, University of Leipzig)

Rix, M.: Observation of volcanic SO_2 plumes based on the satellite-borne GOME-2 instrument. Dissertation, Faculty of Civil Engineering and Surveying, Technical University of Munich, successful thesis defence completed in June 2012. (Supervisors: Prof. Dr. Richard Bamler, Technical University of Munich and Dr. Pieter Valks)

Schüssler, O.: Combined Inversion Methods for UV/VIS Nadir Sounding. Dissertation, Civil Engineering and Surveying, Technical University of Munich. (Supervisors: Prof. Dr. Richard Bamler, Dr. Adrian Doicu and Diego Loyola)

Vasquez, M.: Simulation of the radiation field in planetary atmospheres. Dissertation, Centre of Astronomy and Astrophysics, Technical University of Berlin. (Supervisors: Prof. Dr. Heike Rauer, German Aerospace Center, Institute of Planetary Research and Dr. Franz Schreier)

Xu, J.: Inversion for Limb Infrared Atmospheric Sounding. Dissertation, Civil Engineering and Surveying, Technical University of Munich. (Supervisors: Prof. Dr. Richard Bamler, Dr. Franz Schreier, and Prof. Dr. Thomas Trautmann)

5.6 Seminar Talks

Walter Zimmer: Software-Entwicklung für Wissenschaftler bei MF-AP, 17 January 2012

Mayte Vasquez: Effects of Clouds on High Resolution Thermal Emission Spectra of Terrestrial Exo-Planets, 14 February 2012

Jesus Zendejas (LMU-USM and MPE): Photometry of Terrestrial Planets around M Stars, 13 March 2012

Markus Meringer: An excursion into Astrobiology: How did life select its building blocks?, 28 March 2012

Daniel Kitzmann (ZAA-TUB): Discontinuous Galerkin Finite Element Methods for Radiative Transfer, 18 April 2012

Melanie Coldewey-Egbers: Global long-term ozone trends derived from different observed and modelled data sets, 23 May 2012

David Kappel (Institute for Planetology – Westfälische Wilhelms-Universität Münster und DLR-IPF): Radiative Transfer and Retrieval for Venus Nightside Spectra by VIRTIS/VEX, 12 June 2012

Olena Schüssler: Neuronal Networks and Applications in Remote Sensing, 3 July 2012

Carsten Paproth (DLR – Optical Information Systems, Berlin): SENSOR++: Simulation of remote sensing systems from visible to thermal infrared and some videos, 24 July 2012

Walter Zimmer: Subversion, August 7, 2012 and 18 October 2012

Mareike Godolt (DLR-IPF und TUB-ZAA): 3D climate modeling of Earth-like extrasolar planets orbiting different types of central stars, 4 December 2012

Abbreviations and Acronyms

2D	2-dimensional
3D	3-dimensional
AAIA	Aerosol Absorbing Index Algorithm
AC	Atmospheric Correction
ADM	Atmospheric Dynamic Mission
AIRS	Atmospheric Infrared Sounder
AMIL2DA	Advanced MIPAS Level 2 Data Analysis
AMSOS	Airborne Microwave Stratospheric Observing System
AMSU	Advanced Microwave Sounding Unit
ANX	Ascending Node Crossing
AOP	Announcement of Opportunity Provider
APSM	Aperture Stop Mechanism
ARTS	Atmospheric Radiative Transfer Simulator
ASM	Azimuth Scan Mechanism
ATC	Active Thermal Control
ATCOR	Atmospheric/Topographic Correction for Satellite Imagery
ATP	Atmosphärenprozessoren
AZACM	Azimuth Aperture Cover Mechanism
BIRA	Belgisch Instituut voor Ruimte-Aëronomie
BIRRA	Beer InfraRed Retrieval Algorithm
BMSIS	Blue Marble Space Institute of Science
BRDF	Bidirectional Reflectance Distribution Function
CCA	Communication Area
CCD	Convective-Cloud-Differential
CDOP	Continuous Development and Operations Phase
CHAMP	Challenging Minisatellite Payload
CL0	Consolidated Level 0
COSMIC	Constellation Observing System for Meteorology, Ionosphere and Climate
CSE	Civil and Structural Engineering
CTI	Configurable Transfer Item
DFD	Deutsches Fernerkundungsdatenzentrum
DIMS	Data & Information Management System
DISORT	Discrete Ordinates Radiative Transfer
DLR	Deutsches Zentrum für Luft- und Raumfahrt
DMI	Danish Meteorologic Institute
DMOP	Detailed Mission Operation Plan
DOAS	Differential Optical Absorption Spectroscopy
DOM	Discrete Ordinate Method
D-PAC	German Processing and Archiving Center
E2S	End-to-End Simulator
EADS	European Aeronautic Defence and Space Company
ECV	Essential Climate Variable
E-ELT	European Extremely Large Telescope
ELACM	Elevation Aperture Cover Mechanism
EnMAP	Environmental Mapping and Analysis Program
ENVISAT	Environmental Satellite
EO	Earth Observation
EOC	Earth Observation Center
EOL	End-of-Life
ERS	European Remote Sensing Satellite
ESA	European Space Agency
ESM	Elevation Scan Mechanism
ESOC	European Space Operation Center
ESRIN	European Space Research Institute

EUMETSAT	European Organisation for the Exploitation of Meteorological Satellites
EXV	Experimentelle Verfahren
EVOSS	European Volcano Observatory Space Services
FD	Fast Delivery
FOCC	Flight Operation Control Centre
FOP	Flight Operation Procedure
FTIR	Fourier Transform Infrared
GARLIC	Generic Atmospheric Radiation Line-by-Line Infrared Code
GDP	GOME Data Processor
GLORIA	Global Limb Radiance Imager of the Atmosphere
GMES	Global Monitoring for Environment and Security
GOME	Global Ozone Monitoring Experiment
GPS	Global Positioning Service
HALOE	Halogen Occultation Experiment
HIRS	High Resolution Infrared Radiation Sounder
HITRAN	High Resolution Transmission
HKPU	Hong Kong Polytechnic University
HOAPS	Hamburg Ozean-Atmosphäre-Parameter und Flüsse aus Satellitendaten
HZ	Habitable Zone
I3RC	Intercomparison of 3-dimensional Radiation Code
IASI	Infrared Atmospheric Sounding Interferometer
ICGCR	Institute for Climate and Global Change Research
IECF	Instrument and Engineering Calibration Facility
IMAGES	Intermediate Model of Global Evolution of Species
IMF	Institut für Methodik der Fernerkundung
IOM	Instrument Operation Manual
IPF	Instrument Processing Facility
IT	Informationstechnik
ITCZ	Inter-Tropicaö Convergence Zone
IUP-IFE	Institut für Umweltphysik / Institut für Fernerkundung
JWST	James Webb Space Telescope
KNMI	Koninklijk Nederlands Meteorologisch Instituut
KOPRA	Karlsruhe Optimized and Precise Radiative Transfer Algorithm
L1BP	Level 1b Processor
L2AP	Level 2a Processor
LAB	Laboratoire d'Astrophysique de Bordeaux
LATMOS	Laboratoire Atmosphères, Milieux, Observations Spatiales
LbL	Line-by-Line
LEM	Left Eigenvector Matrix
LEOP	Launch and Early Operation Phase
LLI	Life Limited Item
LoS	Line-of-Sight
MACC	Monitoring Atmospheric Composition and Climate
MCMD	Macrocommand
MERIS	Medium Resolution Imaging Spectrometer
MetOp	Meteorological Operational Polar Satellites of EUMETSAT
MF	Institut für Methodik der Fernerkundung
MHS	Microwave Humidity Sounder
MIAWARA	Middle Atmosphere Water Vapour Radiometer
MIPAS	Michelson Interferometer for Passive Atmospheric Sounding
MIPAS-B	MIPAS for Balloons
MIRART	Modular Infrared Atmospheric Radiative Transfer
MoCaRT	Monte Carlo Radiative Transfer
MODIS	Moderate Resolution Imaging Spectroradiometer
MODTRAN	Moderate Resolution Atmospheric Transmission

MOST	Ministry of Science and Technology
MOZART	Model for Ozone and Related Chemical Tracers
MPH	Main Product Header
MPIC	Max-Planck-Institut für Chemie
MSG	Meteosat Second Generation
MTCDK	Mlawer-Tobin-Clough-Kneizys-Davies
NAI	NASA Astrobiology Institute
NASA	National Aeronautics and Space Administration
NCAR	National Center for Atmospheric Research
NCWM	Nadir Calibration Window Mechanism
NDACC	Network for the Detection of Atmospheric Composition Change
NDFM	Neutral Density Filter Mechanism
NH	Northern Hemisphere
NIR	Near Infrared
NNDEC	Non-Nominal Decontamination
NOAA	National Oceanic and Atmospheric Administration
O3M	Ozone Monitoring
OBM	Optical Bench Module
OCM	Orbit Control Manoeuvre
OCR	Operation Change Request
ODE	Ozone Depletion Event
OMI	Ozone Monitoring Instrument
OSDF	Orbit Sequence Definition File
PBL	Planetary Boundary Layer
PDGS	Payload Data Ground Segment
PDS	Payload Data Segment
PF	Planetenforschung
PRD	Pearl River Delta
RAL	Rutherford Appleton Laboratory
RGT	ROP Generation Tool
RMSE	Root Mean Square Error
RO	Radio Occultation
ROP	Reference Operation Plan
RTE	Radiative Transfer Equation
S4	Sentinel 4
S5	Sentinel 5
S5P	Sentinel 5 Precursor
SAA	South Atlantic Anomaly
SACS	Support to Aviation Control Service
SAF	Satellite Application Facility
SAMUM	Sahara Mineral Dust Experiment
SAR	Synthetic Aperture Radar
SBUV	Solar Backscatter Ultraviolet
SCD	Slant Column Density
SCIAMACHY	Scanning Imaging Absorption Spectrometer for Atmospheric Chartography
SDMOP	SCIAMACHY DMOP
SEU	Single Event Upset
SEVIRI	Spinning Enhanced Visible and Infrared Imager
SHDOM	Standard Harmonic Discrete Ordinate Method
SLS	Spectral Line Source
SMHI	Swedish Meteorological and Hydrological Institute
SMILES	Superconducting Submillimeter-Wave Limb Emission Sounder
S/N	Signal-to-Noise
SODAP	Switch-on and Data Acquisition Phase
SOR	SCIAMACHY Operations Request
SOST	SCIAMACHY Operations Support Team

SPH	Secondary Product Header
SPICI	SCIAMACHY PMD Identification of Clouds and Ice/Snow
SQWG	SCIAMACHY Quality Working Group
SRC	SCIAMACHY Radiant Cooler
SRON	Netherlands Institute for Space Research
SSAG	SCIAMACHY Science Advisory Group
SSM/I	Special Sensor Microwave Imager
SWIR	Short-wave Infrared
TC	Thermal Control
TCWV	Total Column Water Vapour
TELIS	TeraHertz Limb Sounder
TN	Technical Note
TPM	Third Party Mission
TROPOMI	Tropospheric Ozone Monitoring Instrument
TRUE	Tangent height retrieval by UV-B
TUB	Technical University Berlin
TUM	Technical University Munich
UHNAI	University of Hawaii, NASA Astrobiology Institute
UV	Ultraviolet
VCD	Vertical Column Density
VIS	Visible
VOC	Volatile Organic Compound
VSHDOM	Vector SHDOM
VVO	Virtual Volcano Observatory
WLS	White Light Source
YRD	Yangtze River Delta
ZAA	Zentrum für Astronomie und Astrophysik

DLR at a Glance

DLR, the German Aerospace Center, is Germany's national research centre for aeronautics and space. Its research and development work in aeronautics, space, energy, transport, defence and security is integrated into national and international cooperative ventures. As Germany's Space Agency, DLR is tasked with the planning and implementation of Germany's space programme. In addition, two project management agencies have been established to promote DLR's research.

Approximately 7300 people are employed at sixteen locations in Germany: Cologne (headquarters), Augsburg, Berlin, Bonn, Braunschweig, Bremen, Göttingen, Hamburg, Jülich, Lampoldshausen, Neustrelitz, Oberpfaffenhofen, Stade, Stuttgart, Trauen and Weilheim. DLR has also offices in Brussels, Paris, Singapore and Washington, D.C.

Remote Sensing Technology Institute
Institut für Methodik der Fernerkundung

DLR's Remote Sensing Technology Institute (MF) is located in Oberpfaffenhofen, Berlin-Adlershof, and Neustrelitz.

MF carries out research and development for retrieving geo-information from remote sensing data. It conducts basic research on physical principles of remote sensing and develops algorithms, techniques, and operational processing systems for synthetic aperture radar, optical remote sensing, and spectrometric sounding of the atmosphere. The processing systems are in operational use for national, European, and international Earth observation missions.

For preparation and in support of spaceborne missions, MF operates a suite of multi- and hyperspectral optical airborne sensors. The institute contributes its expertise to novel sensor and mission concepts.

The German Remote Sensing Data Center (DFD) and MF form DLR's Earth Observation Center (EOC).

Deutsches Zentrum
für Luft- und Raumfahrt e.V.
in der Helmholtz-Gemeinschaft

Institut für Methodik der Fernerkundung
Oberpfaffenhofen
82234 Weßling

www.dlr.de/eoc